Structural characterization of infectious bovine spongiform encephalopathy prion strains

by

Razieh Kamali Jamil

A thesis submitted in partial fulfillment of the requirements for the degree of

Doctor of Philosophy

Department of Biochemistry
University of Alberta

Abstract

Prion diseases, also termed transmissible spongiform encephalopathies (TSEs), are progressive and fatal neurodegenerative disorders in humans and animals. The condition is associated with spongiform changes in the brain tissue. Bovine spongiform encephalopathy (BSE), commonly known as "mad cow disease," belongs to a group of prion diseases primarily affecting cattle. BSE was first reported in the 1980s in the UK and later spread to other parts of the world, including Canada. The first case of BSE in Canada was detected in Alberta in May 2003. Since then, a total of 19 BSE cases have been detected in Canada. Transmission studies suggest a causal link between BSE and variant Creutzfeldt-Jakob disease (vCJD) in humans. Three BSE strains have been known to cause prion disease in cattle, including classical BSE (C-type) and two atypical strains, named L-type and H-type BSE. These BSE strains exhibit distinct biochemical and histopathological characteristics.

The main pathological hallmark in prion disease is a structural transition from a normal host-encoded prion protein (PrP^{C}) to an infectious and disease-causing isoform (PrP^{Sc}). PrP^{C} is a predominantly α-helical membrane protein that misfolds into a β-sheet rich, infectious state, with a high propensity to self-assemble into amyloid fibrils. Although the high-resolution structure of PrP^{C} has been resolved, despite extensive efforts, the high-resolution structure of infectious PrP^{Sc} molecules has yet remained to be determined, mainly due to its insolubility and tendency to aggregate.

The previous structural studies on different prion strains have provided some insights into the overall architecture of these transmissible agents. However, no structural characterization has been reported for infectious BSE prions. To fill this gap, in this research, I performed structural

characterization of infectious, brain-derived C-, H-, and L-type BSE prions employing transmission electron microscopy (TEM) and image processing approaches. First, I purified BSE prions from transgenic mice brains expressing bovine PrP sequence using phosphotungstate anion (PTA) precipitation and sucrose density gradient purification techniques. I performed morphological characterization of the isolated BSE prion amyloid fibrils on negatively stained electron micrographs and examined whether there are conformational differences between the three BSE strains. In addition, to gain insights into the three-dimensional structure of these fibrils, I employed helical reconstruction and 2D average techniques on the EM micrographs of the purified BSE samples. Afterwards, I developed immunogold labeling methods using various gold-conjugated anti-PrP monoclonal antibodies and Fab fragments to confirm the presence of BSE prions at the ultrastructural level. Bioassay experiments were conducted by intracerebral inoculation of Tg4092 transgenic mice, expressing bovine prion protein, to assess the infectivity of the purified prion samples.

In this study, I presented morphological information and 3D reconstructions of C-, L-, and H-type BSE fibrils. EM analysis of the purified samples of the BSE strains revealed amyloid fibrils exhibiting helical twist, which were morphologically distinguishable between the three strains. Helical reconstruction of the amyloid fibrils provided further insights into the structure of these agents. Our results could establish that the conformational features of different BSE strains dictate their distinct biochemical and phenotypic properties. Our data are compatible with the proposed model of four-rung beta-solenoid for the infectious prion protein structure. The findings of this research may have implications for understanding the relationship between pathological properties and conformations in different prion strains and could provide a basis for

elucidating the 3D structure of other infectious prion strains. Moreover, our findings may facilitate therapeutic interventions against prion disease.

Preface

This thesis is an original work by Razieh Kamali Jamil. Chapter 1 includes the introduction, and Chapter 4 is the overall discussion and future directions.

Chapter 2 of this thesis includes a manuscript under revision in the journal of "*PLOS Pathogens"* as Kamali-Jamil, R., Vázquez-Fernández, E., Tancowny, B., Rathod, V., Amidian, S., Wang, X., Tang, X., Fang, A., Senatore, A., Hornemann, S., Dudas, S., Aguzzi, A., Young, H., Wille, H (2021). The content of Chapter 2 is my original work. Bioassay experiments were conducted by BT and SD.

Chapter 3 of this thesis includes a manuscript prepared for publication in the journal of "*Pathogens"* as Kamali-Jamil, R., Vázquez-Fernández, E., Tancowny, B., Tang, X., Rathod, V., Wang, X., Senatore, A., Hornemann, S., Dudas, S., Aguzzi, A., Young, H., Wille, H (2021). The content of Chapter 3 is my original work. Bioassay experiments were conducted by BT and SD.

Appendix A is my original work and not published anywhere.

All animal studies were carried out in accordance with guidelines set by the Canadian Council on Animal Care and approved by the animal care use committee for Health Sciences 2 (protocol AUP00000884). The BSE transmission experiments were carried out at the Canadian Food Inspection Agency, Lethbridge Laboratory, Lethbridge, Alberta, in accordance with guidelines set by the Canadian Council on Animal Care and approved by the animal care use committee for the CFIA-ADRI Lethbridge Laboratory (ACC#0902).

Dedication

Dedicated to the memory of Elnaz Nabiyi,

lost on flight PS752

Acknowledgements

First and foremost, I would like to express my sincere thanks to my supervisor, Dr. Holger Wille, for his continuous support and guidance throughout my PhD program. Thank you for being a great mentor. Thanks for providing me with an excellent research environment and allowing me to participate in different fascinating collaborative projects. I am really grateful for your kindness, patience, and support.

I would like to thank my supervisory committee members Dr. David Westaway and Dr. Michael Overduin, for their support and valuable advice and suggestions regarding my research project and for supporting my award applications. I would like to thank Dr. Suzette Priola and Dr. Olivier Julien for agreeing to be my external and internal defense examiners.

I would like to thank everyone in the Department of Biochemistry, especially our graduate coordinator, Dr. David Stuart, for accepting my PhD application and for his continuous support and advice. Also, I am thankful to the program advisors Kimberly Arndt, Kelsey Robertson, and Lisa Dublin for their tremendous help and support even before I started my PhD program. I thank Dr. Nicolas Touret for taking part in my candidacy examination and for supporting my awards application.

I would like to thank Dr. Howard Young for teaching me image processing technique and for his helpful advice and constructive suggestions.

I am thankful to all members of Dr. Wille's laboratory, Sara Amidian, Vineet Rathod, Andrew Fang, Dr. Xinli Tang, Brian Tancowny, Dr. Ester Vázquez-Fernández (former member), Dr. Maria Carmen Garza-Garcia (former member), Dr. Xiongyao Wang (former member), Dr. Jose

Flores Fernandez, Shelaine Fleck, Dr. Lyudmyla Dorosh, Dr. Yong Liang Wang, Madeleine Fleming, and Aishwarya Sriraman for their help and support and all great moments that we had together.

I am grateful to everyone at the Centre for Prions and Protein Folding Diseases. I have a lot of enjoyable memories from my work and social gatherings all these years. I would like to thank Dr. Judd Aiken, Dr. Debbie McKenzie, Dr. Ted Allison, Dr. Satyabrata Kar, Anthony Ness for all their support and kindness. I thank Dr. Ghazaleh Eskandari-Sedighi for always being a supportive and caring friend. I never forget the first day you picked me up at the MSB building and showed me everywhere. I also would like to thank my supportive friends, Dr. Hadeel Alyenbaawi, Dr. Serene Wohlgemuth, Klinton Shmeit, Nasim Danaei, Dr. Morteza Seifi, Dr. Mansoore Esmaeili, and Dr. Anamika Singh.

Finally, I would like to thank my family. I acknowledge my mom and dad for their endless dedication and love and for providing me a peaceful home so that I could follow my dreams. I am so grateful to my sister, Raheleh Kamali, for always listening to me patiently whenever I needed to talk to her about my struggles. I thank my brothers Hossein and Hassan Kamali for all their support and kindness.

Lastly, I thank my husband, Payam Delshad Khatibi, for his love, patience, and continually supporting me during my PhD study. Thank you for being a great companion. I am grateful to have you in my life.

List of Abbreviations

2D: Two-dimensional

3D: Three-dimensional

4RβS: 4-Rung β-solenoid

Ab: Antibody

AD: Alzheimer's disease

AFM: Atomic force microscopy

AgNO3: Silver nitrate

AP: Alkaline phosphatase

BSA: Bovine serum albumin

BSE: Bovine spongiform encephalopathy

BovPrP: Bovine prion protein

bp: Base pair

CJD: Creutzfeldt-Jakob disease

CNS: Central nervous system

CO2: Carbon dioxide

C-type BSE: Classical type bovine spongiform encephalopathy

Cryo-EM: Cryo electron microscopy

CWD: Chronic wasting disease

DNA: Deoxyribonucleic acid

DY: Drowsy

E. coli*: Escherischia coli*

EM: Electron microscopy

Fab: Fragment antigen binding

FFI: Fatal familial insomnia

FSE: Feline spongiform encephalopathy

FTIR: Fourier transform infrared spectroscopy

GPI: Glycosyl-photphatidylinositol anchor

GSS: Gerstmann-Sträussler-Scheinker

H/D: Hydrogen/Deuterium

HCL: Hydrochloride

H-type BSE: High type bovine spongiform encephalopathy

HY: Hyper

IgG: Immunoglobulin-G

kDa: Kilodalton

kV: Kilovolts

mAb: Monoclonal antibody

MBM: Meat and bone meal

MD: Molecular dynamics

ME7: Mouse-adapted scrapie prion

nm: Nanometer

NMR: Nuclear magnetic resonance

L-type BSE: Low type bovine spongiform encephalopathy

PCR: polymerase chain reaction

PE: Pronase E

PK: Proteinase K

PIRIBS: Parallel In-Register Beta-sheet

PMSF: Phenylmethylsulfonyl Fluoride

***PRNP*:** Prion gene

PrP: Prion protein

PrP^{C}: Cellular prion protein

PrP^{Sc}: Scrapie prion protein

PrP 27-30: N-terminally truncated prion protein

PTA: Phosphotungstate anion

PVDF: Polyvinylidene fluoride

RML: Rocky mountain laboratory

SAFs: Scrapie associated fibrils

sCJD: Sporadic Creutzfeldt- Jakob disease

SDS: Sodium Dodecyl Sulfate

SDS PAGE: Sodium dodecyl sulfate polyacrylamide gel electrophoresis

SHa: Syrian hamster

SNR: Signal-to-noise ratio

ssNMR: Solid state nuclear magnetic resonance

TBS: Tris-buffered saline

TBST: Tris-buffered saline - tween 20

Tg: Transgenic animal

Tg4092: Transgenic mice expressing bovine PrP

TEM: Transmission electron microscopy

TSE: Transmissible spongiform encephalopathy

vCJD: variant Creutzfeldt-Jacob disease

WB: Western blot

Table of Contents

List of Figures

List of Tables

Chapter 1: Introduction

1.1 Introduction to transmissible spongiform encephalopathy (TSE)

Transmissible spongiform encephalopathies, also called prion diseases, are a group of lethal neurodegenerative disorders of humans and animals. Human prion diseases include Creutzfeldt-Jakob disease (CJD), variant Creutzfeldt- Jakob disease (vCJD), Gerstmann-Straussler-Scheinker disease (GSS), Kuru, and fatal familial insomnia (FFI). Scrapie in sheep, bovine spongiform encephalopathy (BSE) in cattle, and chronic wasting disease (CWD) in deer and elk are examples of TSEs in animals. TSEs are caused by the deposition of PrP^{Sc}, the misfolded, self-propagating, and pathogenic conformer of cellular prion protein (PrP^{C}) in the central nervous system (CNS).

Pathologically, prion diseases may be characterized by neuronal loss, astrogliosis, spongiform changes, and accumulation of PrP^{Sc}-positive amyloids in the brain tissue. The incubation time is long, and some common clinical manifestations may include neurological and cognitive dysfunction (Prusiner and DeArmond 1994, Prusiner 1998, Aguzzi and Calella 2009, Colby and Prusiner 2011).

1.1.1 Historical background of prion diseases

The discovery of prion disease dates back to the 18^{th} century when scrapie in sheep was described (Eklund, Kennedy et al. 1967). In the 1920s, a human neurodegenerative disorder with no clear etiology, later termed Creutzfeldt-Jakob disease, was described by neurologists Gerhard Creutzfeldt and Alfons Maria Jacob (Creutzfeldt 1989). Initially, it was believed that an "unconventional slow" virus was the causative agent of the scrapie in sheep (Zabel and Reid 2015). In the 1950s Kuru, was discovered as a common lethal neurodegenerative disease among the people of the New Guinea tribe, who practiced ritual cannibalism (Gajdusek and Zigas 1957).

In 1959, William Hadlow stated that kuru and scrapie have similar neuropathological characteristics (Hadlow 1959).

Later investigations led to the understanding that these disorders are not caused by conventional infectious agents, such as viruses and bacteria. For example, the CJD prion was found to be resistant to inactivation with UV and ionization radiation (Alper, Cramp et al. 1967). In a vaccination experiment, treatment with a formalin-treated vaccine that was administered to sheep to prevent the louping ill disease failed to destroy the scrapie agent, which was unknowingly present in some vaccines (Gordon 1946). Due to their unusual features, including resistance to experimental procedures used to destroy nucleic acids, it was proposed that these infectious agents are devoid of nucleic acid (Alper, Cramp et al. 1967, Gibbs, Gajdusek et al. 1978, Weissmann 2004). In 1982, Dr. Stanley B. Prusiner hypothesized that an infectious protein was responsible for the scrapie disease and coined the term 'proteinaceous infectious particle' (prion) (Prusiner 1982). Following that, it was identified that it is a host cellular gene encodes prion protein (Chesebro, Race et al. 1985, Oesch, Westaway et al. 1985, Locht, Chesebro et al. 1986).

Prusiner et al. isolated the infectious prion amyloids from sick scrapie-infected Syrian hamster brains (SHa) and observed that these agents were not present in uninfected control animals. The isolated polypeptide was degraded by methods that denature proteins, such as SDS, urea, and guanidinium thiocyanate. The purified prions were identified to be partially resistant to digestion with proteinase K (PK), which later helped distinguish this protein from other proteins during the purification process (Bolton, McKinley et al. 1982, Prusiner, Bolton et al. 1982). While PK treatment completely degrades the normal cellular prion protein (PrP^{C}), PK digestion of PrP^{Sc} results in a PK-resistant N-terminally truncated core. The PK-digested form of prion protein termed PrP 27-30, based on its molecular weight in Western blot (WB), maintains its infectious

properties. PK-treated PrP^{Sc} usually forms three bands in Western blot analysis, corresponding to un-, mono-, and di-glycosylated isoforms of the prion protein (Weissmann 2004, Diaz-Espinoza and Soto 2012). It should be noted that some strains contain a higher sensitivity to treatment with PK compared to others (Kuczius and Groschup 1999). For his discovery of prions, Dr. Prusiner was awarded the Nobel Prize in Physiology or Medicine in 1997 (www.nobelprize.org).

Previously it was found that PrP-knock out mice were protected against prion disease (Bueler, Aguzzi et al. 1993). This observation, as well as the study reporting the formation of recombinant mouse prion protein (recMoPrP) capable of inducing prion disease in transgenic mice (Legname, Baskakov et al. 2004), provided the most compelling evidence for the leading role of PrP protein in prion disease.

1.2 Strains in prions

One notable aspect of prions is the existence of different strains. Initially, strain characteristics in prions were demonstrated by variations in incubation time and the pattern of histopathologic lesions within the brain tissue in a specific host (Collinge 2001). Interestingly, strains in the context of prion diseases are not defined by differences in the primary structure of PrP protein (Weissmann 2004, Collinge and Clarke 2007). Currently, several pieces of evidence suggest that the strain characteristics of prions are based on the conformational variations in the arrangement of PrP^{Sc} molecules that can be faithfully propagated by recruiting native PrP^{C} molecules, leading to the transmission of the particular conformational assembly (Morales, Abid et al. 2007). This definition means that differences in clinical phenotypes can be influenced by differences in the PrP^{Sc} structure, which can consequently lead to variations in biochemical properties, such as resistance to digestion with PK, differences in migration patterns in Western blot experiment

after PK digestion, and glycosylation patterns (Bessen and Marsh 1992, Bessen and Marsh 1994, Collinge, Sidle et al. 1996, Telling, Parchi et al. 1996, Safar, Wille et al. 1998).

1.3 Species barrier

The extent of sequence homology of prion protein between two species plays an essential role in the susceptibility of the host to prion infection (Scott, Foster et al. 1989). Lack of success in earlier attempts at the experimental interspecies transmission of prion agents led to the concept of species barrier. According to this phenomenon, although transmission of a TSE agent may naturally occur from one individual to another within one species, the transmission of prion agents between different species is very unlikely or not efficient. The interspecies transmission has been demonstrated by the failure of prion disease transmission, long incubation time, and incidence of subclinical infection (Beringue, Vilotte et al. 2008). Due to the essential role of PrP protein in the prion disease process, the species barrier is believed to be correlated to variations in the conformation of PrP^{Sc} in different species, as well as the PrP sequence (Gajdusek 1965, Prusiner 1998, Beringue, Vilotte et al. 2008). In terms of prion strains, it is believed that the strain properties of prions play an essential role in the capability of these transmissible agents to cross the species barriers (Huor, Espinosa et al. 2019). For instance, compared to human vCJD, which is transmissible to laboratory mice, the experimental transmission of sCJD in the same mouse line has been found very challenging (Gibbs and Gajdusek 1973, Bruce, Will et al. 1997). BSE agent has been transmitted to different species, including humans, and it is widely believed that vCJD is the result of cross-species transmission of BSE from cattle to humans (Hill, Desbruslais et al. 1997).

1.4 Prion replication

According to the protein-only hypothesis, prion agent replicates by inducing the conversion of the host normal prion protein, PrP^{C}, into a conformation similar to PrP^{Sc}, the exact mechanism of which has not been fully understood (Weissmann 2004). Elucidating the detailed structure of PrP^{Sc} is necessary to gain complete knowledge of the prion replication (Baskakov, Caughey et al. 2019).

Two popular models that have been hypothesized for the conversion of PrP^{C} to PrP^{Sc} as the fundamental event in prion propagation in a host: "the refolding (template-directed) model" (Prusiner 1991) and "seeding polymerization model." In the refolding model, PrP^{Sc}, as the most stable form, by acting as a template, induces the unfolding and refolding of PrP^{C} monomers, leading to the formation of new PrP^{Sc} conformers, which itself acts as a template to convert other PrP^{C} proteins. The converted monomers then polymerize into oligomeric and fibrillar forms (Gajdusek 1988). On the other hand, the seeded (nucleated) model proposes that the spontaneous conversion of PrP^{C} to PrP^{Sc} is in equilibrium with the equilibrium favoring the PrP^{C} conformer. In this model, PrP^{Sc} is only stabilized by incorporating into a seed or aggregate of PrP^{Sc} with a bigger size, like oligomers. The existence of the seed enhances the elongation of the infectious forms and, subsequently, the development of PrP^{Sc} aggregates (Figure 1.1) (Come, Fraser et al. 1993, Jarrett and Lansbury 1993).

A recent MD simulation study, using computational techniques and employing the available experimental data provided a full atomistic model of prion protein based on the 4-Rung β-Solenoid (4RβS) arrangement, as well as a scheme indicating the propagation of the conformational information of the prion protein (Spagnolli, Rigoli et al. 2019). This pathway

includes a cascade of events leading to the complete conformational transition of PrP^{C} into its pathologic isoform (PrP^{Sc}) with a 4RβS structure (Figure 1.2). In this process, the C-terminal rung of PrP^{Sc} with 4RβS structure provides an initial template for the conversion of N-terminus (residues 89-124) of PrP^{C} into a new rung. The newly formed rung then acts as a template for forming the next rungs until the complete transition of PrP^{C} to PrP^{Sc}. Accordingly, the fibrils' ends, as an intermediate structure, could have an active role in the templated prion protein replication. These refolding events of the conversion of PrP^{C} to PrP^{Sc}, visualized by molecular dynamics simulations, could demonstrate the infectious nature of prions (Nicholson, Mo et al. 2002, Spagnolli, Rigoli et al. 2019). It is noteworthy of mentioning that, in most cases, the effective prion replication in a host requires the sequence of the host PrP^{C} and the incoming PrP^{Sc} to be highly similar (Prusiner, Scott et al. 1990, Weissmann 2004), as a single or a few amino acid changes in the sequence of PrP^{C} could have a protective effect against prion replication (Priola and Chesebro 1995).

A

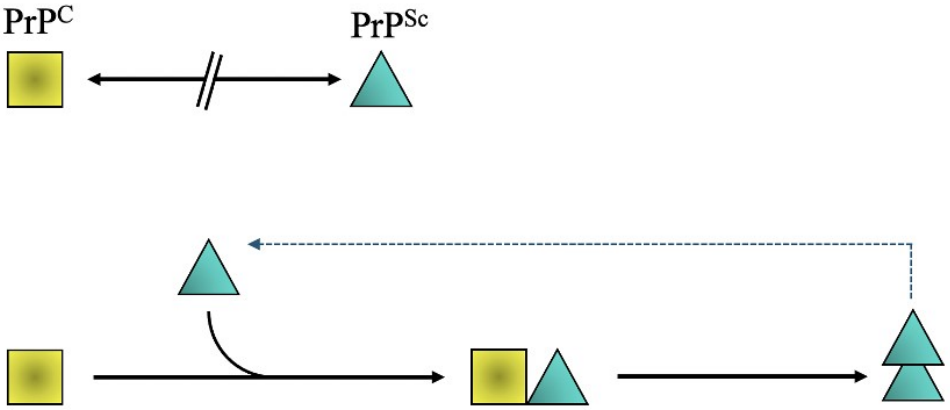

B

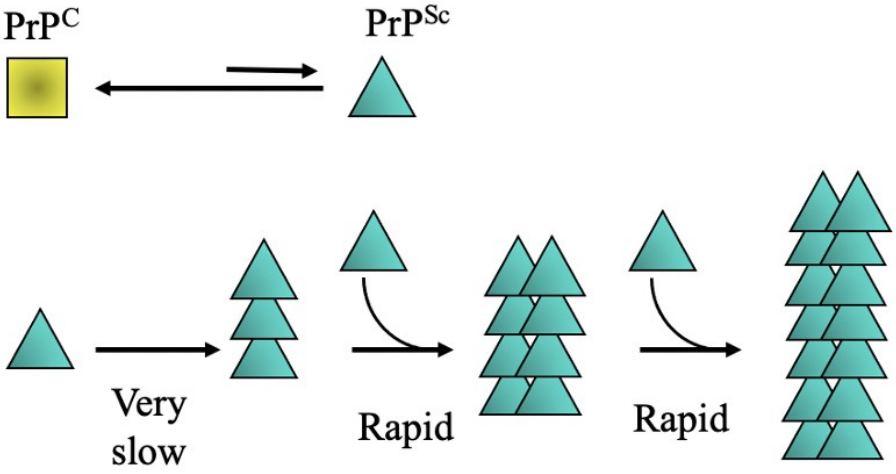

Figure 1. 1 Models for the conversion of PrP^{C} to PrP^{Sc}.

A) The template-directed model. The conformational change is kinetically controlled, a high activation energy barrier preventing spontaneous conversion at detectable rates. Interaction with PrP^{Sc} (green triangle) causes PrP^{C} (yellow square) to undergo an induced conformational change to yield PrP^{Sc}. **B)** The seeding nucleation model. The levels of PrP^{C} (yellow square) and PrP^{Sc} (or a PrP^{Sc}-like molecule), shown as a green triangle, are in equilibrium, with a high preference for the formation of PrP^{C}. PrP^{Sc} is only stabilized when it is recruited to a crystal-like seed or aggregate of PrP^{Sc}. Seed formation is rare; however, once a seed is present, monomer addition ensues rapidly. Figure was adapted from (Weissmann 2004).

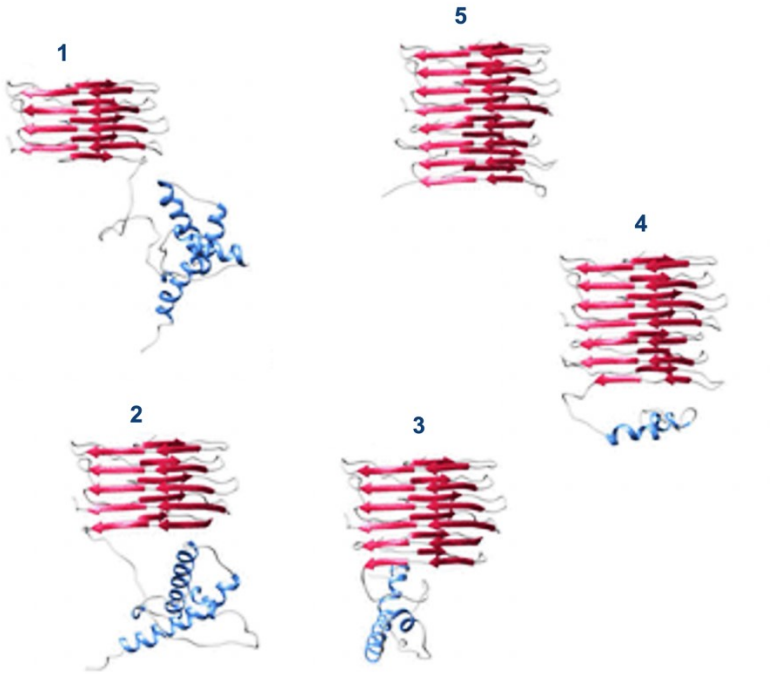

Figure 1. 2 Frames of PrP^{C} to PrP^{Sc} conversation obtained by MD simulation study. Pictures indicate frames extracted from the entire PrP^{C} to PrP^{Sc} conversion simulation. (1) configurations of PrP^{C}-PrP^{Sc} complex. Refolding of PrP^{C} proceeds as follows: (2) residues 89-115; (3) residues 89-151; (4) residues 89-190; (5) residues 89-230. The process highlights the progressive unfolding and refolding of PrP^{Sc} onto the 4RβS template, which initially involves the N-terminal region, followed by the loss of α-helices and a progressive formation of β-sheets. This figure is a modified version of a figure taken from (This figure is in the public domain) (Spagnolli, Rigoli et al. 2019).

1.5 Prion disease in animals

Prion disease affects many non-human mammals, including scrapie in sheep and goats, bovine spongiform encephalopathy in cattle, and chronic wasting disease in deer and elk, transmissible mink encephalopathy, feline spongiform encephalopathy (FSE) in domestic cats as well as wild cats (Bencsik, Debeer et al. 2009, Colby and Prusiner 2011).

1.5.1 Scrapie in sheep and goat

Classical scrapie, a prion disease of sheep and goats, was the first prion disease documented about 300 years ago in the United Kingdom and some European countries (Hourrigan 1979, Greenlee 2019). Sheep scrapie is mostly reported in animals between 2 and 5 years old (Simmons, Simmons et al. 2009). Three major polymorphisms at codons 136, 154, and 171 in PRNP are associated with susceptibility to scrapie prion disease (Goldmann, Hunter et al. 1990, Hunter, Foster et al. 1991, Laplanche, Chatelain et al. 1993, Goldmann, Hunter et al. 1994, Westaway, Zuliani et al. 1994). Infection is mainly caused by oral exposure in contaminated environments (Ryder, Dexter et al. 2004). Within an infected population, both vertical transmission from ewe to offspring with susceptible genotype and horizontal transmission could occur (Touzeau, Chase-Topping et al. 2006). Currently, no evidence indicates that scrapie prion has been transmitted to humans (Brown, Cathala et al. 1987, van Duijn, Delasnerie-Laupretre et al. 1998).

1.5.2 Bovine spongiform encephalopathy (BSE)

BSE is a transmissible spongiform encephalopathy in cattle, which was initially reported in the 1980s in the United Kingdom (Wells, Scott et al. 1987). Compelling evidence indicates that the

practice of feeding animals with the high-protein supplement extracted from other animals, in the form of meat and bone meal (MBM), has caused the BSE epidemic in cattle in the UK (Wilesmith, Wells et al. 1988, Wilesmith, Ryan et al. 1991). Epidemiological studies and biochemical analysis of PrP^{Sc} suggest that BSE has infected humans through ingestion of contaminated food, causing variant Creutzfeldt-Jakob disease in humans, which was first reported in the1990s (Collinge, Sidle et al. 1996, Hill, Desbruslais et al. 1997, Scott, Safar et al. 1997).

In 2004, two atypical BSE strains, called H-type and L-type, were identified in aged and asymptomatic cattle through regular surveillance in Europe (Biacabe, Laplanche et al. 2004, Casalone, Zanusso et al. 2004). The classical and atypical BSE strains differ in their biochemical characteristics, the age of disease onset, lesion profile in the brain, and incubation time (Biacabe, Laplanche et al. 2004, Casalone, Zanusso et al. 2004, Jacobs, Langeveld et al. 2007, Dudas, Yang et al. 2010). Cattle infected with classical and atypical BSE strains share an identical sequence of the PRNP gene (Goldmann, Hunter et al. 1991, Biacabe, Laplanche et al. 2004). It has been suggested that the atypical BSE cases represent sporadic prion disease in aged cattle (Biacabe, Morignat et al. 2008). There has been a successful experimental transmission of BSE prions to sheep and goats (Eloit, Adjou et al. 2005, Jeffrey, González et al. 2006).

1.5.2.1 Classical BSE

Classical BSE was first detected in 1986 in the UK and later spread to other regions of the world (Wells, Scott et al. 1987, Biacabe, Laplanche et al. 2004). The cows with classical BSE condition presented clinical symptoms such as abnormal posture, ataxia and incoordination,

hypersensitivity to external stimuli, aggressiveness and nervousness. The incubation time in cattle with classical BSE infection varies between 2 and 8 years (Costassa, Iulini et al. 2016).

After the start of the outbreak, passive surveillance led to the detection of over 180,000 cases of BSE in the UK. After the start of the screening of slaughter cattle for BSE infection in 2000, more than 5000 cases were reported in European countries (Jacobs, Langeveld et al. 2007). A dramatic reduction was observed in the trend of BSE cases when the control measures banned the feeding ruminant-derived foods (Hoinville 1994). Classical BSE cases are characterized by distinct strain-associated neurological and molecular features compared to the atypical forms affecting older cattle (Bruce, Chree et al. 1994, Jacobs, Langeveld et al. 2007).

1.5.2.2 Atypical BSE strains

Atypical BSE strains are denoted as H-type and L-type BSE due to the higher and the lower position of the unglycosylated PrP^{Sc} band in Western blot analysis compared to classical BSE (Figure 1.3) (Biacabe, Laplanche et al. 2004, Casalone, Zanusso et al. 2004). The approximate PK digestion sites of the classical and two atypical BSE strains have been identified using different anti-PrP monoclonal antibodies against 86-107 region of bovine PrP protein, such as SAF32, P4, 12B2, 9A2 (Biacabe, Jacobs et al. 2007, Jacobs, Langeveld et al. 2007). These BSE prions generally affect older cattle (aged eight years or older) (Jacobs, Langeveld et al. 2007, Costassa, Iulini et al. 2016). To date, the detailed characteristics and the origin of atypical BSE strains are not well characterized, and it is hypothesized that they may have initially emerged in cattle sporadically, similar to sporadic CJD (sCJD) in humans (Costassa, Iulini et al. 2016). Many studies have reported somatic mutation in the *PRNP* gene and indicated the association of these mutations with sporadic human prion diseases (Wadsworth, Hill et al. 2003). With regard

to BSE, in a previous investigation, a point mutation, E211K, was detected in the bovine *PRNP* gene in a cow from Alabama with H-type BSE phenotype, analogous to the E200K mutation in humans with genetic CJD. This mutation in bovine prion protein is associated with atypical BSE disease (Richt and Hall 2008). Recently, the K211 somatic mutation of the bovine prion protein gene was linked to the progression of BSE in cattle (Won, Kim et al. 2020).

L-type atypical BSE was first identified in 2004 in Italy (Casalone, Zanusso et al. 2004), showing different pathological and immunohistochemical phenotypes compared to classical BSE (C-type). Since the neurological feature of L-type BSE involves the deposition of amyloid plaques in the brain, it is also termed bovine amyloidotic spongiform encephalopathy (BASE). Histopathological features of the BASE can be described by a high amount of PrP-positive amyloid plaques associated with L-type BSE that have been detected in the thalamus, subcortical white matter, and olfactory bulb. In addition, unlike classical BSE, which initially involves the brain stem, the L-type strain affects the forebrain region (Casalone, Zanusso et al. 2004).

This atypical variant of BSE and sCJD in humans share some phenotypical features. For example, both BASE and M/V2 sCJD present a similar pattern of intracerebral PrP distribution and amyloid plaque formation (Casalone, Zanusso et al. 2004). One phenotypic characteristic of L-type BSE compared to the classical strain is the decreased mental alertness and muscle atrophy. L-type BSE has been experimentally transmitted to cattle (Lombardi, Casalone et al. 2008, Fukuda, Iwamaru et al. 2009). A previous experiment on humanized transgenic mice inoculated with BSE isolates reported higher transmissibility of L-type BSE to humanized transgenic mice encoding methionine at codon 129 (HuPrP-129M) compared to C-type BSE (Kong, Zheng et al. 2008).

H-type atypical BSE was first reported in 2004 in France in three cattle with BSE disease with distinct molecular features when compared to typical BSE cases (Biacabe, Laplanche et al. 2004). This strain was later detected in other parts of the world, including Europe and North America (Ducrot, Arnold et al. 2008). By Western blot examination following PK digestion, these atypical H-type BSE cases, which were observed in older cows, showed a higher molecular mass of un-glycosylated PrP^{Sc} and strong labeling by P4 monoclonal antibody when compared to the typical BSE cases. Regarding the glycoform ratio, classical BSE showed a stronger molecular mass of di-glycosylated signal when tested with Western blot than atypical samples (Biacabe, Laplanche et al. 2004).

Several experimental transmission tests have been conducted using both atypical BSE strains on different animals, including mice, cattle, macaques, hamsters, and sheep. In a transmission study, multiple passages of H-type BSE prions in bovinized transgenic mice led to the emergence of a new BSE phenotype, termed BSE-SW, with shorter incubation periods in the inoculated mice. This new form of H-type BSE prions, when transmitted to cattle, caused different phenotypes compared to other BSE strains (Masujin, Okada et al. 2016).

In one study, experimental transmission of cattle with L-type or H-type BSE led to the occurrence of nervous disease in all animals with some features similar to classical BSE, with two phenotypic symptoms exhibited at the progressed stage, more dull form and difficulty in rising. The pathology and molecular characteristics of the examined animals were distinguishable from those infected with C-type BSE prions (Konold, Bone et al. 2012). For both H- and L-type atypical BSE cases, some experimental transmission studies have reported the detection of PrP^{Sc} in the CNS tissue, peripheral ganglia and nerve, muscle, adrenal glands and retina (Terry, Marsh et al. 2003, Buschmann and Groschup 2005, Wells, Spiropoulos et al. 2005,

Fukuda, Iwamaru et al. 2009, Balkema-Buschmann, Fast et al. 2011, Hoffmann, Eiden et al. 2011, Stack, Moore et al. 2011, Franz, Eiden et al. 2012, Kaatz, Fast et al. 2012, Fast, Keller et al. 2013, Okada, Miyazawa et al. 2014).

1.5.2.3 Origin of the BSE epidemic

The first case of classical BSE was detected in the UK in 1986 (Wells, Scott et al. 1987); however, it is suspected that the BSE epidemic might have originated around the 1970s (Smith 2003). Although it is clear that the practice of feeding cattle with MBM has caused the BSE outbreak in cattle, it is not known what caused the first BSE case in the United Kingdom (Wilesmith, Wells et al. 1988, Smith 2003). Over the years, several hypotheses have been proposed regarding the origin of BSE (Baron, Biacabe et al. 2007). Initially, it was believed that feeding cattle with bone and meat meal from scrapie-infected sheep might have originated BSE in cattle (Wilesmith, Ryan et al. 1991, Lezmi, Martin et al. 2004).

Another hypothesis is that BSE might have started sporadically in cattle, similar to sporadic CJD, and the tissues from these cattle were transmitted to other cattle through MBM.
The occurrence of atypical BSE cases in 2004 (Biacabe, Laplanche et al. 2004, Casalone, Zanusso et al. 2004) led to the assumption these atypical cases might represent sporadic forms of prion diseases in cattle (Hope 2013). In a previous report, experimental transmission of H-type and L-type atypical BSE cases led to the development of C-type BSE features. These results gave rise to the possibility that the classical BSE disease might have originated from the recycling of atypical L-type and H-type BSE prions. And in this case, the oral route of the acquiring BSE prion infection could account for the different phenotypic and biochemical features of classical BSE compared to the atypical BSE strains (Capobianco, Casalone et al.

2007, Baron, Vulin et al. 2011, Torres, Andreoletti et al. 2011, Nicot, Bencsik et al. 2014, Masujin, Okada et al. 2016). For instance, with regards to L-type BSE, similar PrP deposition and biochemical features were observed between L-type BSE and certain sporadic CJD subgroups (Casalone, Zanusso et al. 2004, Comoy, Casalone et al. 2008). It is speculated that the earlier cases of the atypical BSE strain escaped detection due to the paucisymptomatic characteristics of the initial cases (Capobianco, Casalone et al. 2007). In this regard, according to a previous report, the experimental transmission of cattle with L-type and H-type BSE resulted in two phenotypes of decreased alertness or nervous forms, appeared less clinically extreme than C-type BSE (Konold, Bone et al. 2012).

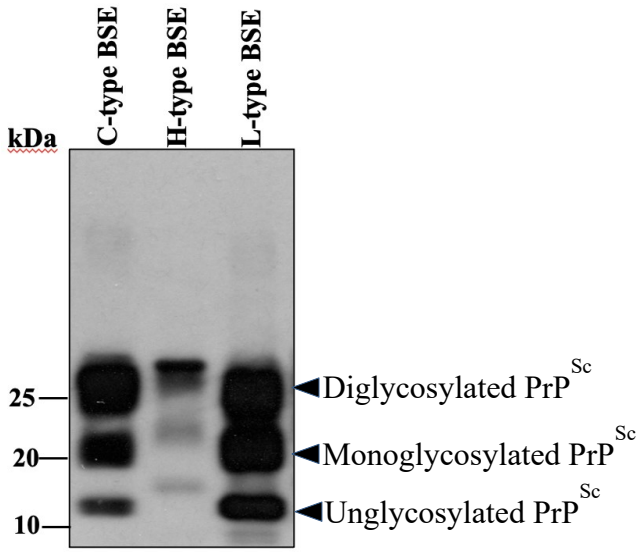

Figure 1. 3 Western blot analysis of classical and atypical BSE prions.

Brain homogenate samples of classical, H-, and L-type BSE prions obtained from BSE-infected bovinized transgenic mice (Tg4092). All three samples were treated with Proteinase K (PK). Western blot examination of the PK digested isolates using D15.15 anti-PrP monoclonal antibody revealed 3 bands corresponding to un-, mono, and diglycosylated PrP 27-30. H-type purified samples are featured by a slightly higher molecular mass of unglycosylated PrP^{Sc} compared to C-type BSE, while L-type samples show a slightly lower molecular mass of unglycosylated PrP^{Sc} compared to classical BSE (Kamali Jamil et al., unpublished data).

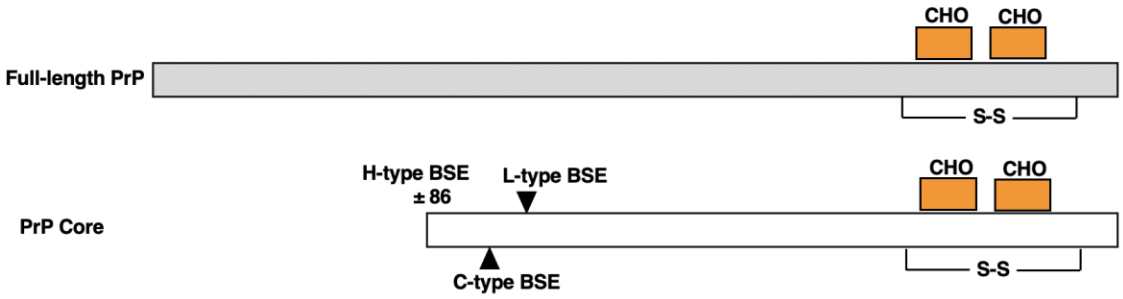

Figure 1. 4 Schematic representation of the approximate PK cleavage sites in PrP^{Sc} for classical and atypical BSE strains.

Approximate protease-resistant core for the different BSE strains based on the immunoreactivity with different anti-PrP monoclonal antibodies. PK-digested C-, H-, and L-type BSE isolates were differentiated based on molecular mass differences and antibody reactivities that detect epitopes within residues 86-107 of bovine PrP using SAF32, 12B2, 9A2, P4 antibodies (Jacobs, Langeveld et al. 2007).

1.5.3 Chronic wasting disease (CWD)

CWD is a highly contagious transmissible spongiform encephalopathy affecting members of the Cervidae family (Rivera, Brandt et al. 2019). CWD has been detected in North America, South Korea, and some European countries, including Norway and Finland. The first case of CWD was reported in North America in 1969 in captive mule deer, which died with the symptoms of weight loss and behavioral changes (Williams and Young 1980). There is growing concern about the potential risk of transmission of CWD prion to humans; however, so far, there is no report of CWD's association with prion diseases in humans (Barria, Balachandran et al. 2014, Houston and Andreoletti 2018, Waddell, Greig et al. 2018). Intracerebral inoculation of humanized transgenic mice with elk CWD isolates has not resulted in CWD disease occurrence in those mice (Kong, Huang et al. 2005). CWD has been transmitted to non-cervid animals under experimental conditions. Laboratory mice, cattle, mink, squirrel, monkeys, cats, sheep and goats have been shown susceptible to experimental transmission of CWD (Bartz, Marsh et al. 1998, Hamir, Cutlip et al. 2001, Belay, Maddox et al. 2004, Gilch, Chitoor et al. 2011).

1.5.4 Transmissible Mink Encephalopathy (TME)

Transmissible mink encephalopathy (TME) is a food-born prion disease that was first detected in 1947 in ranch-raised mink on a farm in Brown County, Wisconsin, USA, with a mortality rate of 100% in adult mink (Hartsough and Burger 1965, Eckroade, ZuRhein et al. 1973). TME affects mink over the age of one, and incubation time is about six months. The clinical signs in mink include behavioral changes and neurological disorders (Barlow 1972). The last TME outbreak was reported in 1985 in Wisconsin (Marsh, Bessen et al. 1991).

TME has been experimentally transmitted to several animals, including ferret, striped skunk, raccoons, Syrian and Chinese hamster, squirrel, macaque monkeys, sheep, and goat with different incubation times (Marsh and Hanson 1969, Kimberlin, Cole et al. 1986, Robinson, Hadlow et al. 1995, Hamir, Miller et al. 2004, Hamir, Kunkle et al. 2006, Hamir, Kehrli et al. 2011). Transmission to Syrian golden hamsters has led to the occurrence of two TME strains, "hyper" (HY) and "drowsy" (DY), which present different biochemical features and clinical symptoms in hamsters. The hyper syndrome is featured by short incubation time, hyperaesthesia and cerebellar ataxia, while the drowsy strain is characterized by lethargy and long incubation time (Bessen and Marsh 1992). The origin of TME is unknown; but, it is hypothesized that TME is linked to feeding BSE-infected cattle to farm mink (Marsh and Hartsough 1988). Cattle inoculated experimentally with TME prions developed transmissible spongiform encephalopathy after 18.5 months incubation time (Marsh, Bessen et al. 1991). TME and L-type BSE prion exhibit a high degree of similarity in molecular and phenotypic features, suggesting that L-type BSE may be a more plausible candidate for the source of TME in mink (Baron, Bencsik et al. 2007).

1.6 Human prion diseases

Human prion diseases can be categorized into three groups: sporadic form, inherited occurrence through autosomal dominant mutations in the PrP gene *PRNP*, and transmissible form acquired from external sources, such as medical equipment, BSE-contaminated meat products, and ritualistic cannibalism (Collinge 2001).

1.6.1 Sporadic human prion diseases

In humans, sporadic prion diseases are more common compared to the genetic and acquired forms and consist of sporadic forms of Creutzfeldt-Jakob disease (CJD) and fatal familial insomnia (FFI) (Collinge 2001). Sporadic Creutzfeldt-Jakob disease (sCJD), the most common prion disease in humans, was the first spontaneously formed human prion disease described in the early 1920s (Creutzfeldt 1989). CJD affects approximately 1-2 individuals per million each year, accounting for about 85% of TSE cases in humans (Aguzzi and Calella 2009, Puoti, Bizzi et al. 2012).

1.6.2 Inherited prion diseases

GSS is a genetic prion disease in humans with mutations in the *PRNP* gene (Masters, Gajdusek et al. 1981), of which the most common mutations are at codons 102, 198 and 117. In contrast to CJD, an earlier age of the disease onset and longer incubation time have been reported in GSS cases. (Hsiao, Baker et al. 1989, Hsiao, Dlouhy et al. 1992). Histopathological examinations have shown the presence of amyloid plaques in the prion tissue (Collins, McLean et al. 2001).

FFI is an inherited prion disease in humans first reported in an Italian family in 1986 (Lugaresi, Medori et al. 1986). The clinical symptoms include severe sleep disturbance leading to death, dysautonomia, cognitive dysfunction and motor disorder (Gambetti, Parchi et al. 1995, Collins, McLean et al. 2001). The average survival time after the initiation of the clinical symptoms is 18 months (Schenkein and Montagna 2006). This prion disease disease is associated with the D178N single gene mutation and polymorphism at codon 129 of the *PRNP* gene (Medori, Tritschler et al. 1992, Gambetti, Parchi et al. 1995). The exact mechanism by which the mutation

elicits prion disease is not well identified; however, it is presumed that these mutations elevate the chance of spontaneous misfolding of cellular prion protein into the abnormal form (Hsiao and Prusiner 1990, Liemann and Glockshuber 1999).

1.6.3 Acquired prion diseases

The acquired forms of prion disease may occur following exposure to infectious resources. Kuru, iatrogenic CJD, and vCJD are examples of the acquired form of prion disease in humans. Kuru was described in the 1950s by V. Zigas and Dr. Gajdusek, in the Fore people of Papua New Guinea tribe that received the infection through practicing ritualistic cannibalism (eating the brains of dead relatives) (Gajdusek and Zigas 1957). Neuropathological changes in Kuru-affected brains were found akin to the typical scrapie lesions when it was experimentally transmitted to chimpanzees (Gajdusek, Gibbs et al. 1966). This disease's occurrence has diminished significantly due to the cessation of cannibalism habits (Collinge, Whitfield et al. 2006). Dr. Gajdusek received the Nobel Prize in Physiology or Medicine in 1976 for his work on this infectious prion agent (www.nobelprize.org).

Variant Creutzfeldt-Jakob disease (vCJD) is an acquired form of CJD, first reported in the United Kingdom. The incidence of this disease is believed to be linked to dietary exposure to infected cattle meat or other products obtained from the nervous tissue of BSE-infected cattle (Will, Ironside et al. 1996). Met/Met homozygosity polymorphism at codon 129 of the *PRNP* gene has been described as a risk factor for this disease (Collinge, Palmer et al. 1991). vCJD differs from sCJD in terms of the age of the disease onset, its neuropathological patterns, and the duration of the disease. vCJD usually affects younger individuals (Will, Zeidler et al. 2000). The typical clinical manifestations of this disease include ataxia, dysphoria, withdrawal, anxiety, and

loss of interest (Spencer, Knight et al. 2002, Prusiner 2004). An experiment on laboratory mice has found that the lesion profile of vCJD is strongly similar to that of BSE (Hill, Desbruslais et al. 1997). Experimental transmission of vCJD and BSE prions to transgenic mice overexpressing bovine PrP resulted in similar biochemical features of PrP^{Sc} (Scott, Will et al. 1999).

The acquired form of prion disease may also happen through iatrogenic transmission. There have been reports of iatrogenic CJD infection from human growth hormone, dura mater graft, and some infected surgical equipment. Some cases of prion disease have also been linked to blood transfusion received from subclinical CJD patients (Wroe, Pal et al. 2006, Turner and Ludlam 2009). Recently a case of vCJD was reported to be likely linked to laboratory exposure to BSE-infected transgenic mice expressing human prion protein (Brandel, Vlaicu et al. 2020).

1.7 The cellular prion protein (PrP^{C})

The cellular prion protein (PrP^{C}) is a monomeric glycoprotein in mammals encoded by the prion protein gene, *PRNP,* and is linked to the cell surface by a glycosylphosphatidylinositol (GPI) anchor (Simonic, Duga et al. 2000). On the cell surface, PrP^{C} is located within lipid rafts and is ubiquitously found in various tissues, including CNS, muscles, heart, kidney, secondary lymphoid organs, lymphocytes and follicular dendritic cells (FDCs) (Manson, West et al. 1992, Aguzzi and Polymenidou 2004). Unlike PrP^{Sc}, PrP^{C} is soluble in detergents and is sensitive to digestion with proteases (Prusiner 2004). In terms of physiological roles, PrP^{C} has been proposed to be involved in different functions, such as cell signalling modulation, neuronal development, neuronal ex stress-protection, and maintaining circadian rhythm (Castle and Gill 2017).

Improvement in the expression of recombinant prion protein allowed the structural characterization of PrP protein from several species. Nuclear magnetic resonance (NMR)

technique was used to determine the structure of mouse and bovine recombinant PrP (Riek, Hornemann et al. 1996, Riek, Hornemann et al. 1997, Lopez Garcia, Zahn et al. 2000). Subsequently, the structure of other prion strains, including human PrP was resolved using NMR and X-ray crystallography techniques (Zahn, Liu et al. 2000, Knaus, Morillas et al. 2001).

Bovine PrP^{C} protein contains 264 amino acids. The structure of recombinant bovine prion protein was resolved using NMR experiment (Lopez Garcia, Zahn et al. 2000). In the following study, Hornemann et al. compared this structure with the bovine prion protein purified from healthy calf brains with glycan moieties and GPI-anchor remained, using circular dichroism (CD) and NMR spectroscopy experiments (Hornemann, Schorn et al. 2004). The obtained data in this research showed that the three-dimensional structure and thermal stability of fully glycosylated, brain-derived and recombinant bovine PrP^{C} are similar. The structure of PrP^{C} contains a globular C-terminal domain consisting of three α-helices and two short anti-parallel beta-strands, and an N-terminal region. The N-terminal region has been previously considered to be structurally disordered; however, it may contain inducible structures to allow interaction of PrP^{C} with other prion molecules and contribute to PrP^{C} to PrP^{Sc} conversion (Castle and Gill 2017). It has been shown that PrP knockout mice are not susceptible to prion disease and are not able to replicate prion protein (Bueler, Aguzzi et al. 1993).

Bovine prion protein has two cysteines at residues 190 and 225 linked by a single disulfide bond that connects α-helices two and three (Lopez Garcia, Zahn et al. 2000). There are two N-linked glycosylation sites at residues 192 and 208 (Figure 1.5). The N-terminal section contains a conserved hydrophobic region with five to six copies of an octapeptide region, which is suggested to be involved in copper binding and also contributing to prion pathogenesis

(Yoshimoto, Iinuma et al. 1992, Brockes 1999). A comparison of amino acid sequence of bovine prion protein with prion protein in other species is shown in Figure 1.6.

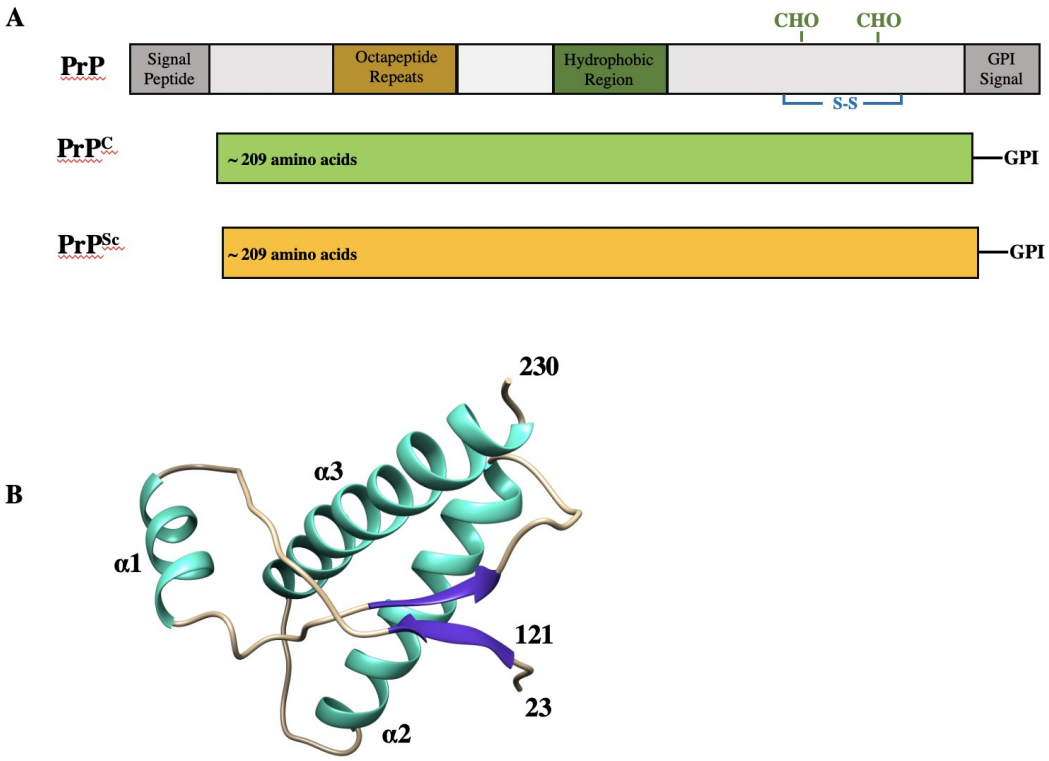

Figure 1. 5 The structure of the prion protein.

A) The primary structure of the prion protein. bovPrP (bovine prion protein) with 264 amino acids is encoded by the PRNP gene. It contains a signal peptide, a GPI (glycosylphosphatidylinositol anchor) signal, five to six octapeptide repeats, a hydrophobic region, and two N-linked carbohydrates (CHO). The GPI signal sequence is necessary for the attachment to membrane raft. PrP^{C} and PrP^{Sc} have identical primary structures. **B)** Cartoon representation of the NMR structure of the recombinant bovPrP (23–230) (Protein Data Bank [PDB] code 1DX0) (Lopez Garcia, Zahn et al. 2000). It contains a flexible disordered N-terminal tail (23–121) and a globular domain, extending around residues 122 to residues 227. The globular domain includes three α-helices (cyan) and a short anti-parallel β-sheet (purple). A single disulfide bond links the α-helices 2 and 3.

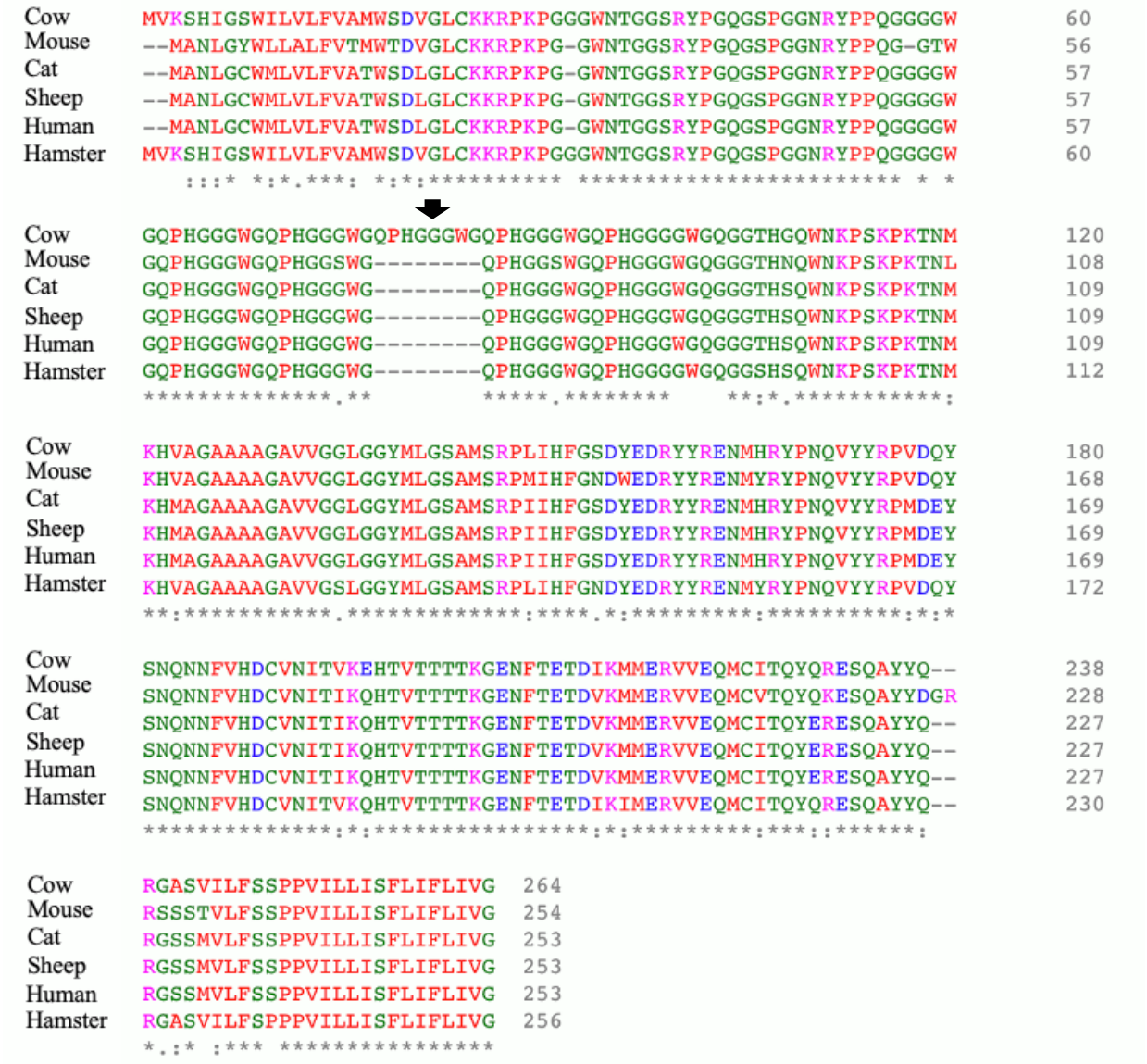
Cow MVKSHIGSWILVLFVAMWSDVGLCKKRPKPGGGWNTGGSRYPGQGSPGGNRYPPQGGGGW 60
Mouse --MANLGYWLLALFVTMWTDVGLCKKRPKPG-GWNTGGSRYPGQGSPGGNRYPPQG-GTW 56
Cat --MANLGCWMLVLFVATWSDLGLCKKRPKPG-GWNTGGSRYPGQGSPGGNRYPPQGGGGW 57
Sheep --MANLGCWMLVLFVATWSDLGLCKKRPKPG-GWNTGGSRYPGQGSPGGNRYPPQGGGGW 57
Human --MANLGCWMLVLFVATWSDLGLCKKRPKPG-GWNTGGSRYPGQGSPGGNRYPPQGGGGW 57
Hamster MVKSHIGSWILVLFVAMWSDVGLCKKRPKPGGGWNTGGSRYPGQGSPGGNRYPPQGGGGW 60
Cow GQPHGGGWGQPHGGGWGQPHGGGWGQPHGGGWGQPHGGGGWGQGGTHGQWNKPSKPKTNM 120
Mouse GQPHGGGWGQPHGGSWG--------QPHGGSWGQPHGGGWGQGGGTHNQWNKPSKPKTNL 108
Cat GQPHGGGWGQPHGGGWG--------QPHGGGWGQPHGGGWGQGGGTHSQWNKPSKPKTNM 109
Sheep GQPHGGGWGQPHGGGWG--------QPHGGGWGQPHGGGWGQGGGTHSQWNKPSKPKTNM 109
Human GQPHGGGWGQPHGGGWG--------QPHGGGWGQPHGGGWGQGGGTHSQWNKPSKPKTNM 109
Hamster GQPHGGGWGQPHGGGWG--------QPHGGGWGQPHGGGGWGQGGSHSQWNKPSKPKTNM 112
Cow KHVAGAAAAGAVVGGLGGYMLGSAMSRPLIHFGSDYEDRYYRENMHRYPNQVYYRPVDQY 180
Mouse KHVAGAAAAGAVVGGLGGYMLGSAMSRPMIHFGNDWEDRYYRENMYRYPNQVYYRPVDQY 168
Cat KHMAGAAAAGAVVGGLGGYMLGSAMSRPIIHFGSDYEDRYYRENMHRYPNQVYYRPMDEY 169
Sheep KHMAGAAAAGAVVGGLGGYMLGSAMSRPIIHFGSDYEDRYYRENMHRYPNQVYYRPMDEY 169
Human KHMAGAAAAGAVVGGLGGYMLGSAMSRPIIHFGSDYEDRYYRENMHRYPNQVYYRPMDEY 169
Hamster KHVAGAAAAGAVVGSLGGYMLGSAMSRPLIHFGNDYEDRYYRENMYRYPNQVYYRPVDQY 172
Cow SNQNNFVHDCVNITVKEHTVTTTTKGENFTETDIKMMERVVEQMCITQYQRESQAYYQ-- 238
Mouse SNQNNFVHDCVNITIKQHTVTTTTKGENFTETDVKMMERVVEQMCVTQYQKESQAYYDGR 228
Cat SNQNNFVHDCVNITIKQHTVTTTTKGENFTETDVKMMERVVEQMCITQYERESQAYYQ-- 227
Sheep SNQNNFVHDCVNITIKQHTVTTTTKGENFTETDVKMMERVVEQMCITQYERESQAYYQ-- 227
Human SNQNNFVHDCVNITIKQHTVTTTTKGENFTETDVKMMERVVEQMCITQYERESQAYYQ-- 227
Hamster SNQNNFVHDCVNITVKQHTVTTTTKGENFTETDIKIMERVVEQMCITQYQRESQAYYQ-- 230
Cow RGASVILFSSPPVILLISFLIFLIVG 264
Mouse RSSSTVLFSSPPVILLISFLIFLIVG 254
Cat RGSSMVLFSSPPVILLISFLIFLIVG 253
Sheep RGSSMVLFSSPPVILLISFLIFLIVG 253
Human RGSSMVLFSSPPVILLISFLIFLIVG 253
Hamster RGASVILFSPPPVILLISFLIFLIVG 256

Figure 1. 6 Sequence alignment the prion protein from different species.

Comparison of the amino acid sequence of PrP protein in cow, human, mouse, sheep, hamster, and cat. The extra octapeptide repeat in cattle PrP is shown using a black arrow. Colors represent the chemical properties of amino acids (blue: acidic; red: small and hydrophobic; magenta: basic; green: hydroxyl, sulfhydryl and glycine).

1.8 Structure of PrP^{Sc}– Experimental data

PrP^{C} and PrP^{Sc} only differ in their conformation; unlike PrP^{C} that is structurally rich in α-helices and has low β-sheet content, PrP^{Sc} appears to be entirely composed of β-sheet (Colby and Prusiner 2011, Wille and Requena 2018, Spagnolli, Rigoli et al. 2019). There is no difference in post-translational modification of PrP^{C} and PrP^{Sc} (Stahl, Baldwin et al. 1993).

Although the high-resolution structure of cellular prion protein has been resolved, the structure of infectious prion protein (PrP^{Sc}) has not been fully determined. Despite various attempts in resolving the structure of PrP^{Sc}, there are still uncertainties about the structural characteristics of this infectious agent (Wille and Requena 2018). Over the years, a combination of structural techniques have been implemented to gain insight into the conformation of this abnormal protein, and different models have been proposed, which are listed below.

1.8.1 FTIR

Fourier transform infrared spectroscopy (FTIR) provides information about the secondary structure of proteins. Earlier FTIR studies on disease-causing prion protein showed that the transformation of PrP^{C} into PrP^{Sc} is accompanied by a diminishing in alpha-helical content and a significant increase in the β-sheet structure. Initially, FTIR was used to analyze PK-digested prion protein, PrP 27-30, which identified that this abnormal conformation contains a high percentage of β-sheet structure (47%) and lower content of α-helices (17%). The remaining 36% was described as turns and random coils, possibly connecting beta-strands. Subsequently, another FTIR report indicated that PrP^{Sc} is composed of 43% β-sheet and 30 percent α-helical structure (Caughey, Dong et al. 1991, Pan, Baldwin et al. 1993).

However, a following hydrogen/ deuterium (H/D) exchange study suggested that PrP^{Sc} is devoid of α-helices, and the infrared band reported earlier as α-helices, in fact, corresponded to turns and loops. At present, it is widely accepted that the structural conformation of abnormal prion protein contains no α-helices and is dominantly composed of β-strands (Smirnovas, Baron et al. 2011, Requena and Wille 2014).

1.8.2 Hydrogen/Deuterium (H/D) exchange

H/D exchange technique can be used to investigate the secondary structure of proteins. In this method, covalently bonded hydrogen ions at backbone amides within the unstructured regions are replaced more rapidly by deuterium ions. However, the exchange rate within the structured regions, including α-helices or β-sheet areas, is relatively slow. In a previous study on a brain-derived PrP^{Sc}, using H/D exchange and mass spectrometry analysis, it was revealed that the region from residues ~80-90 (depending on different species) all the way to the C-terminus shows an extremely low exchange rate, indicating that this region is predominantly composed of beta-sheet structure. The spots for turns and loops within this area exhibited a higher exchange rate (Smirnovas, Baron et al. 2011). This information further reinforces the notion that PrP^{Sc} is devoid of α-helices and predominantly contains β-strands connected by short turns and loops (Requena and Wille 2014).

1.8.3 X-ray fiber diffraction

The repeating nature of prion protein amyloid fibrils has made it possible to investigate the 3D structure of these infectious conformers using the X-ray fiber diffraction technique. In this

technique, structural information is obtained from symmetrical X-ray scattering of fibrillar aggregates of prion protein (Requena and Wille 2014).

This method has been previously used to examine the structure of PrP 27-30 and PrP^{Sc} isolated from the brains of laboratory animals. Initially, applying this method on PrP 27-30 proteins purified from Syrian hamster (SHaPrP 27–30) brains revealed the cross beta diffraction signal at 4.72 Å distance, confirming the fibrillar nature of theses multi-structures (Nguyen, Inouye et al. 1995). Subsequently, the structure of PrP 27-30 samples purified using PTA (Wille, Shanmugam et al. 2009) was investigated by employing synchrotron radiation, which provided further information regarding the structure of PrP 27-30 molecules. This experiment reported a repeating unit of 19.2 Å, representative of the height of each PrP^{Sc} monomer (4 x 4.8 Å), and meridional signals at 4.8 Å, 6.4 Å, and 9.6 Å, which was interpreted to be corresponding to the fourth, third, and second order of the 19.2 Å unit. Some equatorial signals obtained during the purification process, which were attributed to lipids and detergents. According to the revealed diffraction data and the absence of the 10 Å equatorial signal, characteristic of stacked beta-sheet amyloid structure, a beta-solenoid model was suggested for the architecture of PrP 27–30 molecules. Applying the same method on recombinant mouse prion (89-230) or SHaPrP 27–30 (Sc237) revealed a cross-beta diffraction signal at 4.8 Å, as well as a 10 Å equatorial diffraction, characteristic of stacked β-sheet amyloid, indicating a difference in the conformation of infectious brain-derived and recombinant PrP^{Sc} (Figure 1.7) (Wille, Bian et al. 2009). A β-solenoid structure was also proposed later for the conformation of the fungal HET-s (218-289) prions. HET-s is a functional prion protein of the filamentous fungus *Podospora anserina*. HET-s functions in a self/nonself recognition event termed heterokaryon incompatibility that leads to programmed cell death (Maddelein, Dos Reis et al. 2002, Saupe 2007). A solid-state NMR

experiment of HET-s (218-289) prions revealed a two-rung β-solenoid structure for these molecules (Wasmer, Lange et al. 2008, Van Melckebeke, Wasmer et al. 2010). Afterwards, an X-ray fiber diffraction study of recombinant HET-s (218-289) amyloid fibrils demonstrated that at neutral pH HET-s (218-289) forms a β-solenoid conformation and revealed meridian diffractions at 4.8 Å and 9.5 Å, confirming the two-rung β-sheet arrangement (Wasmer, Lange et al. 2008, Wille, Bian et al. 2009, Wan, Wille et al. 2012, Wan and Stubbs 2014). Together, these observations supported the hypothesis that PrP 27-30 adopts a β-solenoid structure (Requena and Wille 2014).

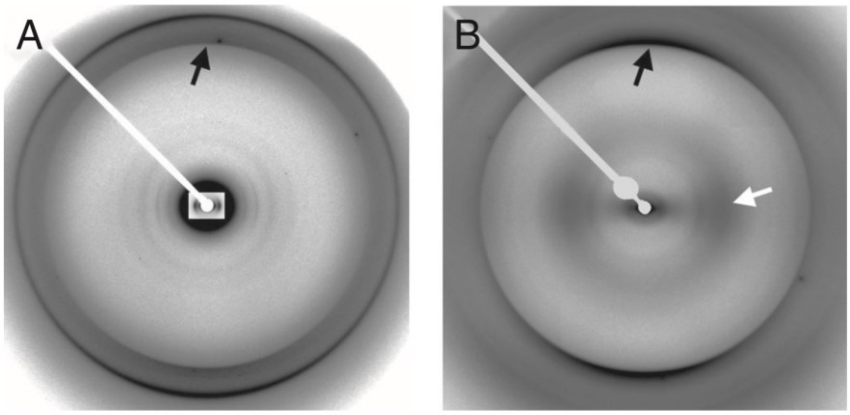

Figure 1. 7 Fiber diffraction patterns from SHaPrP amyloids.

Black arrows indicate cross-beta meridional diffraction at 4.8 Å resolution. A) SHaPrP27-30. B) RecSHaPrP (90–231) amyloid fibrils. The white arrow indicates broad equatorial diffraction at about 10.5 Å resolution, absent in A. Figure was taken from (Wille, Bian et al. 2009), and permission to reuse was obtained from PNAS.

1.8.4 Limited proteolysis

Limited proteolysis has been a useful tool to acquire information about the conformation of PrP^{Sc} and PrP 27-30. Proteinase K (PK) was initially used to gain insight into the structure of prions using this method (Requena and Wille 2014). Treatment with PK showed that PrP^{Sc} is partially resistant to proteolytic cleavage. The unstructured N-terminal region of PrP^{Sc} is cleaved by PK digestion, and a PK-resistant core spanning residue ~ 90-231 remains (Prusiner, Bolton et al. 1982, McKinley, Bolton et al. 1983). Subsequently, other limited proteolysis experiments on PrP^{Sc} strains reported other minor PK-resistant sites, mostly located within the C-terminal region (Kocisko, Lansbury et al. 1996, Zou, Capellari et al. 2003, Zanusso, Farinazzo et al. 2004, Sajnani, Pastrana et al. 2008).

In a previous investigation, digestion of a GPI-less PrP^{Sc} with proteinase K and further analysis based on mass spectrometry on hamster prion protein led to the identification of a complete map of PK-sensitive areas. These areas included the unstructured N-terminal region and some other PK-susceptible spots within the C-terminal region, which were assigned to the loops and turns between beta-strands (Vázquez-Fernández, Alonso et al. 2012). The C-terminal area was found to be highly resistant to digestion with PK, strengthening the idea that this region predominantly contains beta-sheet conformation, given the fact that proteolytic digestion happens more readily within flexible regions such as turns or loops, and with less possibility in α-helices and rarely in regions composed of beta-strands (Hubbard 1998).

1.8.5 Transmission electron microscopy

The first transmission electron microscopy (TEM) study on different scrapie strains from brains of scrapie-affected animals led to the visualization of the fibrillar structure of PrP^{Sc}, which were

named “scrapie associated fibrils” (SAFs) (Merz, Somerville et al. 1981). Following that, 10 to 20 nm wide rod-like polymerized forms of PrP 27-30, designated “PrP rods,” were observed in purified hamster PrP^{Sc} samples using electron microscopy. These prion rods showed green birefringence, typical of amyloid fibrils, after staining with Congo red (Prusiner, McKinley et al. 1983). Electron microscopy micrographs from different murine scrapie strains have been used in several studies to investigate the morphological details of prion fibrils (Merz, Somerville et al. 1981, Sim and Caughey 2009, Wille, Bian et al. 2009, Vazquez-Fernandez, Vos et al. 2016, Terry, Harniman et al. 2019). For example, an electron microscopy study on GPI-anchorless prion fibrils of mouse-adapted ovine scrapie strains, RML, ME7, and 22L, demonstrated that these strains adopt the same fibrillar morphology with differences in their range of periodicity and fibril diameter. The fibrils' width using negative stain electron microscopy examination was reported 4-6 nm (Sim and Caughey 2009). A cryoelectron microscopy study on GPI-anchorless brain-derived murine prions identified amyloid fibrils containing two intertwined protofilaments with an average width of ~ 9 nm (Vazquez-Fernandez, Vos et al. 2016). A plausible explanation for the variety in fibril diameters could relate to the strain-specific features of different prions. In the case of the GPI-anchor less prion protein, the lack of N-linked glycans could account for the smaller width of these fibrils compared to the fully glycosylated ones.

Two-dimensional (2D) crystals of aggregated PrP 27-30 and PrP^{Sc}, which were discovered in the purified prion samples using negative stain electron microscopy, were employed to obtain information about the structural architecture of N-terminally truncated form of infectious prion protein (Wille, Michelitsch et al. 2002, Govaerts, Wille et al. 2004, Wille, Govaerts et al. 2007, Requena and Wille 2014). 2D crystals of infectious PrP 27-30 and a partial deletion mutant of PrP^{Sc} (PrP^{Sc} 106) were examined to gain insight into prion protein structure through electron

crystallography technique. Although this did not provide high-resolution information, image processing and difference map between $PrP^{Sc}106$ and PrP 27-30 enabled visualization of the internal deletions of PrP^{Sc} 106, called miniprion, and revealed the position of N-linked glycans and the internal deletions of PrP^{Sc} 106 (Figure 1.8) (Wille, Michelitsch et al. 2002). The internal deletions were later reported to contribute to beta-sheet structures in PrP 27-30 by FTIR examination (Supattapone, Bosque et al. 1999).

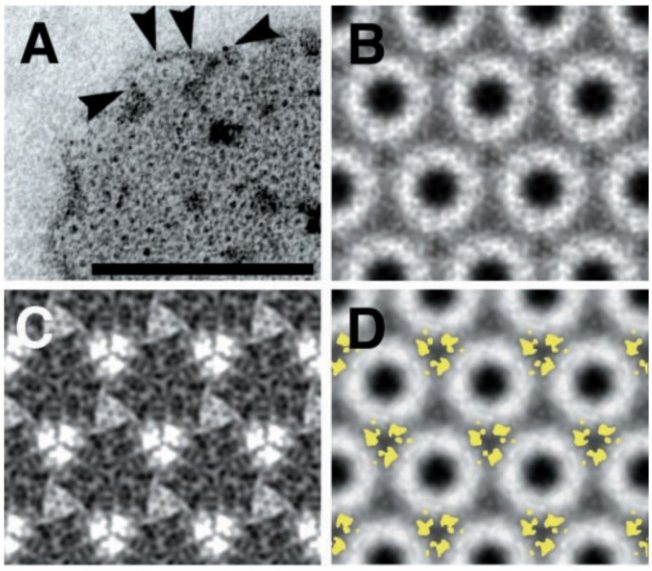

Figure 1. 8 2D crystals of PrP 27-30.

A) Electron microscopy of Nanogold labeled 2D crystal of PrP 27-30 stained with uranyl acetate. Scale bar, 100 nm. **B)** Image processing result of a labeled crystal after correlation mapping and averaging followed by crystallographic averaging. **C)** Subtraction map between labeled and unlabeled crystals showing major differences in lighter shades. **D)** Overlay of the statistically significant differences, corresponding to sugars (yellow), onto a projection map of PrP 27-30. This figure was reprinted with permission from (Wille, Michelitsch et al. 2002). (Copyright (2002) National Academy of Sciences, U.S.A.).

1.9 Proposed structural models of PrP^{Sc}

From extensive research on determining the high-resolution structure of prion protein, two alternative models have been proposed: the Parallel In-Register Intermolecular Beta-Sheet (PIRIBS) (Groveman, Dolan et al. 2014) model and the 4-rung beta solenoid model (Vazquez-Fernandez, Vos et al. 2016, Spagnolli, Rigoli et al. 2019).

1.9.1 The PIRIBS model

The Parallel In-Register Intermolecular Beta-Sheet model was proposed based on the solid-state NMR data of spontaneously formed and initially prion-seeded recombinant PrP amyloid fibrils (Cobb, Sonnichsen et al. 2007, Tycko, Savtchenko et al. 2010, Groveman, Dolan et al. 2014). Consistent with this report, recently, a cryo-EM study of a brain-derived 263K prion strain revealed a Parallel In-Register Intermolecular Beta-Sheet structure for this prion strain. In this report it was indicated that each PrP^{Sc} fibril is composed of one protofilament (Kraus, Hoyt et al. 2021). According to this model, single PrP^{Sc} monomers consisting of eight beta-strands stack on top of each other in-register, providing a 4.8 Å cross beta-sheet distance between them (Figure 1.9).

It should be noted that the 4.8 Å molecule height presented in this structure (Groveman, Dolan et al. 2014) is not compatible with the 19.2 Å repeating units observed in the X-ray fibre diffraction and a following cryo-EM studies on an infectious anchorless prion strain (Wille, Bian et al. 2009, Vazquez-Fernandez, Vos et al. 2016). This assembly forces each monomer to cover the entire cross-section of the amyloid fibril; therefore, the authors state that PrP^{Sc} fibrils contain one

protofilament, and the density, referred to as the gap between two protofilaments in previous studies, is due to stain artifacts (Groveman, Dolan et al. 2014).

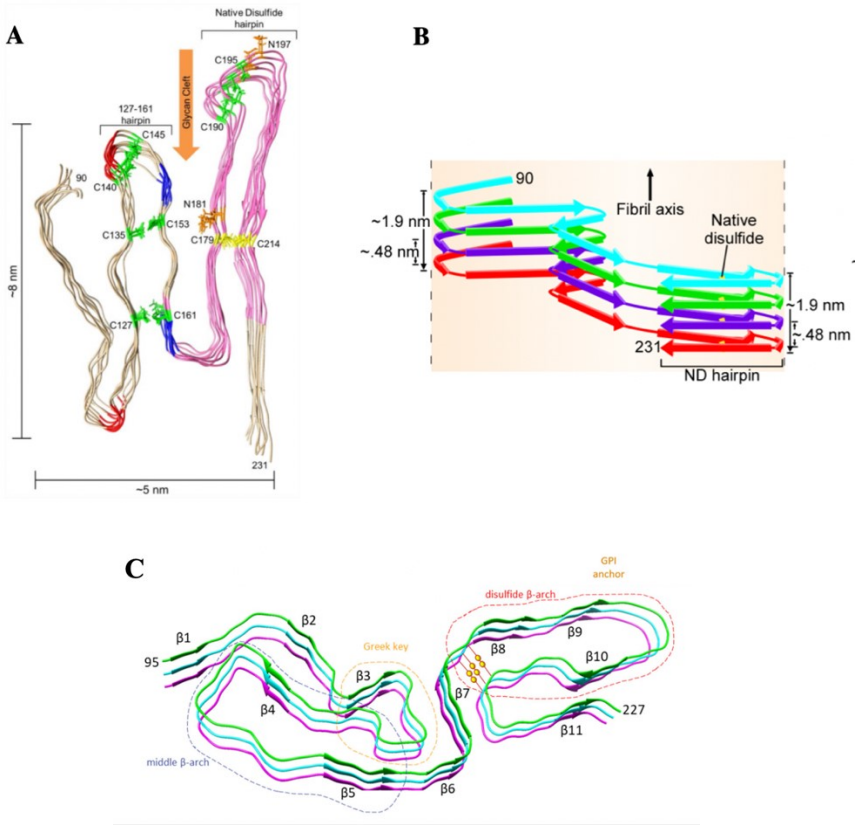

Figure 1. 9 Parallel in-register intermolecular β-sheet model.

A model of an octameric recombinant PrP with parallel in-register intermolecular β-sheet structure. The view is looking down the axis of an energy minimized octamer of mouse PrP 90-231 molecules stacked parallel in-register and with the main hairpins (denoted on the model). The segment that is known to form parallel in-register intermolecular β-sheet in unseeded rPrP amyloid fibrils is pink. PK-cleavage sites (red), Asn-linked glycosylation sites (orange) and the glycan cleft (orange arrow) are also indicated. Size constraints are shown on the outside of the model. **B)** Theoretical diagrammatic Parallel In-Register Intermolecular β-sheet model for residues 90-231 PrP^{Sc} amyloid. This figure was originally published in The Journal of Biological Chemistry (Groveman, Dolan et al. 2014). Copyright the American Society for Biochemistry and Molecular Biology. **C)** A cryo-EM based model of 263K prion strain with Parallel In-Register Intermolecular β-sheet structure. The Figure shows β-sheets in a trimeric segment of the fibril. Structural elements are labeled, and disulfide bond is indicated by pair of yellow spheres. Figure was taken from (Kraus, Hoyt et al. 2021).

1.9.2 The four-rung β-solenoid model

Currently, there is strong evidence suggesting that the PrP^{Sc} molecule adopts a beta helical architecture upon conversion into the infectious state (Wille and Requena 2018, Spagnolli, Rigoli et al. 2019). The β-solenoid or β-helix model was first reported according to the results of the TEM examination of 2D crystals of brain derived PrP 27-30 (Govaerts, Wille et al. 2004).

The 19.2 Å signal revealed by X-ray fiber diffraction analysis of PrP 27-30 prion isolates, corresponding to the height of each PrP^{Sc} monomer, as well as the absence of the prominent stacked beta-sheet signal at 10 Å, provided initial evidence that infectious PrP^{Sc} molecules may adopt a four-rung beta-solenoid model. Subsequently, the data from a cryoelectron microscopy investigation on infectious RML strain further supported the four-rung β-solenoid (4RβS) architecture for the structure of infectious PrP^{Sc} (Figure 1.10). In this study, 4.8 Å repeating units were obtained using Fourier-transform analysis of individual fibrils of cryo-EM micrographs, which was in agreement with the results drawn from a previous X-ray fibre diffraction experiment on prion proteins (Vazquez-Fernandez, Vos et al. 2016). Besides, the four-rung beta-solenoid configuration, by providing 19.2 Å distance, appears to provide simpler accommodation for bulky glycans compared to the PIRIBs model with 4.8 Å intermolecular space (Baskakov and Katorcha 2016). Recently, an atomistic model of PrP^{Sc} was built using molecular dynamics simulation method based on the available experimental data, such as X-ray fibre diffraction results and cryo-EM study of a GPI-anchorless prion protein. This model was shown to be compatible with the four-rung β-solenoid arrangement (Figure 1.11) (Spagnolli, Rigoli et al. 2019).

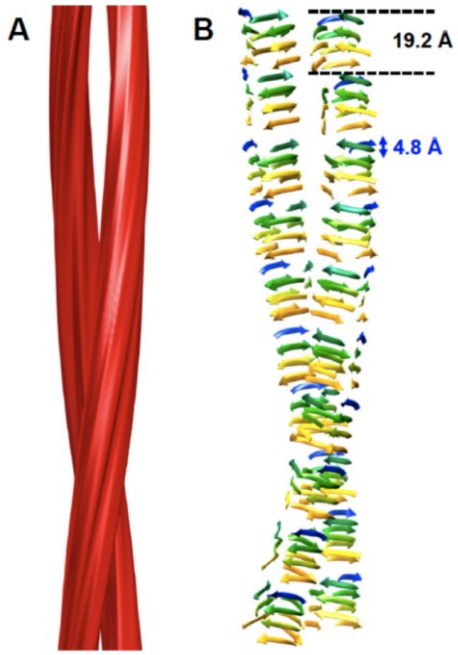

Figure 1. 10 Four-rung β-solenoid architecture of PrP^{Sc}.

(**A**) Three-dimensional reconstruction of a GPI-anchorless mouse PrP^{Sc} amyloid fibril with two protofilaments. (B) Cartoon representation of a four-rung β-solenoid architecture drawn to approximate the 3D reconstruction in (A). The 4.8 Å distance between beta-strands arranged perpendicular to the fibril axis, and the 19.2 Å height of an individual PrP is indicated. This figure was taken from (Vazquez-Fernandez, Vos et al. 2016).

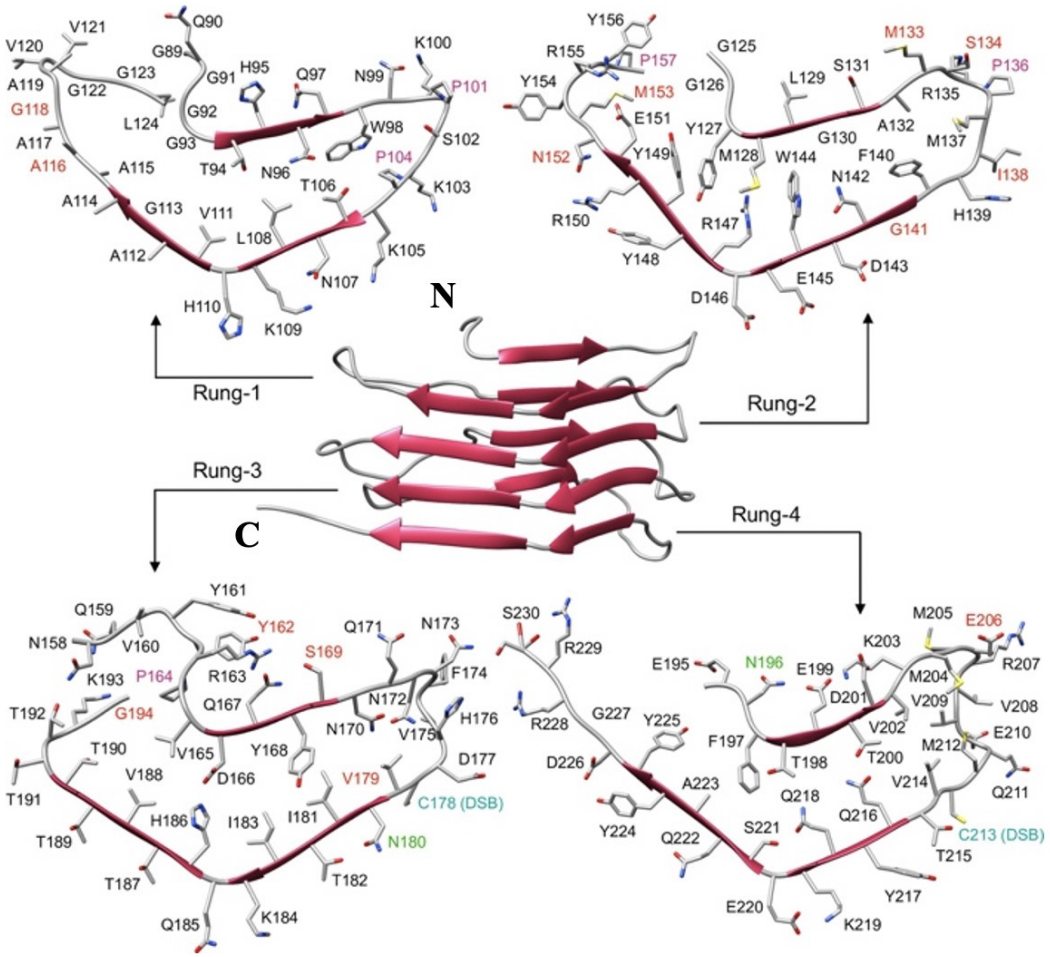

Figure 1. 11 View of the four-rung β-solenoid PrP^{Sc} Model.

The structure of PrP^{Sc} monomer modelled as a 4RβS (β-strands represented as red arrows) obtained by molecular dynamics simulations is shown in the center of the figure. Residues 90-230 are displayed in each individual rung (1–4) with different colors. PK cleavage sites identified by mass spectrometry are colored in red. Glycosylation sites are labeled in green. Proline residues are colored in purple. Cystine is indicated in cyan. This figure was taken from (Spagnolli, Rigoli et al. 2019).

1.10 Research goals

Transmissible spongiform encephalopathies are lethal diseases affecting humans and animals worldwide. Although the feed ban program has considerably reduced the occurrence of classical BSE in cattle (Ducrot, Arnold et al. 2008), emerging atypical cases in European countries, North America, and Alberta have raised concerns about farm animals and human health (Masujin, Okada et al. 2016). The high-resolution structure of infectious BSE prions has not been characterized so far. According to previous findings, the conformation of prion protein plays a vital role in strain characteristics and could determine the susceptibility of a specific host to prion protein infection. Therefore, the overall objective of this thesis was to identify the structural characterization of infectious brain-derived classical and atypical BSE strains using transmission electron microscopy and image processing techniques.

The first part of my project involved a structural investigation of the atypical amyloidogenic strain of BSE, L-type strain. I purified these prions from transgenic mice (Tg4092) brains, genetically engineered mice to express bovine prion protein sequence (Scott, Safar et al. 1997). Following the purification of L-type BSE fibrils, I performed conformational analysis using various techniques, such as TEM, immunogold labeling and three-dimensional reconstruction (Chapter 2). The second part of my thesis was aimed at structural elucidation of the two other BSE strains, C-type and H-type BSE. After purification from transgenic mice brains, I analyzed these two strains in terms of fibril morphology and created three-dimensional models from the EM micrographs. Lastly, I assessed whether there is structural heterogeneity between the three BSE strains (Chapter 3).

This study, for the first time, provides insights into the structural architecture of the three BSE strains. Also, the results of morphological analysis between BSE strains could help better understanding of strains diversity in prions. Finally, these data may help therapeutic interventions.

According to the data in this study and considering previous attempts at the structural elucidation of the prion protein, we hypothesize that infectious BSE prions contain subunits with a four-rung beta-solenoid structural arrangement. In addition, we hypothesize that some conformational variations exist between three BSE strains, which may be responsible for the distinct phenotypic and biochemical features in each strain.

Chapter 2: The ultrastructure of infectious L-type bovine spongiform encephalopathy prions constrains molecular models

2.1 Introduction

Prion diseases, also called transmissible spongiform encephalopathies (TSE), belong to a group of zoonotic, fatal neurodegenerative diseases that cause spongiform changes in the brain (Prusiner 1998). Bovine spongiform encephalopathy (BSE), also known as 'mad cow disease', was first detected in 1986 in the U.K. (Wells, Scott et al. 1987), and later was identified in other European countries and North America (Konold, Bone et al. 2012). So far, BSE is the only prion disease with the confirmed capability of transmission to humans, resulting in the occurrence of variant Creutzfeldt-Jakob disease, an acquired form of prion disease in humans. Thus, BSE was considered an essential human health risk (Wilesmith, Ryan et al. 1991, Nathanson, Wilesmith et al. 1997, Morales 2017). Three BSE strains have been reported to cause prion disease in cattle, including classical BSE (C-type) and two atypical forms termed L-type and H-type BSE, which differ in their neuropathological and molecular phenotypes (Biacabe, Laplanche et al. 2004, Casalone, Zanusso et al. 2004, Jacobs, Langeveld et al. 2007). The disease caused by L-type BSE is also called bovine amyloidotic spongiform encephalopathy (BASE), due to the atypical deposition of amyloid plaques in the brain (Casalone, Zanusso et al. 2004, Dudas, Yang et al. 2010).

The underlying pathogenic event for all prion diseases involves the conversion from the normal, cellular prion protein, PrP^{C}, to an infectious form, known as PrP^{Sc} (Aguzzi, Sigurdson et al. 2008). According to previous nuclear magnetic resonance (NMR) spectroscopic and X-ray crystallographic studies on recombinant PrP, the PrP^{C} structure contains an unstructured N-terminal domain and a C-terminal domain containing three α-helices and two short, antiparallel β-strands (Riek, Hornemann et al. 1996, Lopez Garcia, Zahn et al. 2000, Knaus, Morillas et al.

2001). The unstructured N-terminal domain of bovine PrP^{C} contains five or six octapeptide-repeats, instead of the five repeats that are found in most mammalian species (Goldmann, Hunter et al. 1991). In contrast to PrP^{C}, mammalian PrP^{Sc} is lacking a high-resolution structure due to its insolubility and propensity to aggregate (Requena and Wille 2014). Nevertheless, data obtained from a combination of structural experiments, including Fourier-transform infrared spectroscopy (FTIR), limited proteolysis, X-ray fiber diffraction, cryo electron microscopy (cryo-EM), molecular dynamics simulations, and solid-state NMR spectroscopy (ssNMR), have provided basic insights into the unique arrangements of this incompletely understood conformation (Zweckstetter, Requena et al. 2017, Wille and Requena 2018).

Earlier structural studies reported that PrP^{Sc} has a high β-sheet content and suggested that it retained part of the α-helices that are present in cellular PrP^{C} (Caughey, Dong et al. 1991, Caughey, Raymond et al. 1998, Govaerts, Wille et al. 2004). However, a hydrogen/deuterium (H/D) exchange study demonstrated that the PrP^{Sc} structure is likely devoid of α-helices and predominantly contains β-strands (Smirnovas, Baron et al. 2011). Later, a four-rung β-solenoid model (4RβS) was proposed for the core structure of the infectious prion protein based on an X-ray fiber diffraction study on amyloid fibrils from N-terminally truncated PrP^{Sc}, termed PrP 27-30 (Wille, Bian et al. 2009). The 4RβS arrangement was further confirmed by a cryo-EM analysis and three-dimensional reconstruction experiments on brain-derived and GPI-anchorless mouse prion fibrils (Vazquez-Fernandez, Vos et al. 2016). Recently, an atomistic model for mouse PrP^{Sc} was created based on the 4RβS arrangement and employing results from the previous cryo-EM and X-ray fiber diffraction studies, as well as all other experimental data. Molecular Dynamic (MD) simulations were used to test this model, which was found to be physically stable (Spagnolli, Rigoli et al. 2019). Results of a recent ssNMR study on infectious

recombinant PrP^{Sc} were found to be compatible with the four-rung β-solenoid model (Martín-Pastor, Codeseira et al. 2020). A Parallel In-Register Intermolecular Beta-Sheet (PIRIBS) structure was proposed as an alternative model for the architectures of PrP^{Sc} and recombinant PrP amyloid (Cobb, Sonnichsen et al. 2007). According to this model, monomers of β-structured prion protein stack on top of each other in-register with a 4.8 Å height increase per molecule, requiring the whole cross-section of the fibril to accommodate the full length of the peptide chain (Groveman, Dolan et al. 2014). Although a recent MD simulation study on an octameric PIRIBS amyloid fibril indicated that the incorporation of N-linked glycans in in-register β-sheet structure may not lead to steric clashes (Artikis, Roy et al. 2020), the four-rung β-solenoid arrangement provides more room for the bulky N-linked carbohydrates, including sialylated glycans (Baskakov and Katorcha 2016, Baskakov, Caughey et al. 2019).

While there have been a variety of structural experiments on recombinant and tissue-derived scrapie prion strains, very little is known about the structural characteristics of native BSE prions. It has been previously established that different prion strains may hold variations in their structural conformation and self-replication procedures (Morales 2017, Terry, Harniman et al. 2019). In this regard, we aimed at identifying the structural features of brain-derived infectious $BovPrP^{Sc}$ by purifying BSE prions from transgenic mouse brains and employing electron microscopic approaches, such as image processing and immunogold labeling. For this purpose, we selected L-type BSE prions, as this strain has been demonstrated to be more amyloidogenic compared to the classical and H-type strains (Casalone, Zanusso et al. 2004); therefore, our first goal was to isolate L-type BSE prion fibrils for structural analyses. Here, we provide a first, detailed description of infectious, fully glycosylated, and GPI-anchored BSE prion fibrils. Our study revealed that the infectious BSE prion monomers polymerize into unbranched, long, rod-

like fibrils with one- and two-protofilament morphologies, with the former type being significantly more prevalent. This finding is not compatible with the stacked β-sheet model, as, in this configuration, the fold requires the width of a double-wide amyloid fibril. Therefore, the one-protofilament L-type BSE amyloid fibrils provide independent support for the compact, four-rung β-solenoid model for the structure of PrP^{Sc}.

2.2 Material & Methods

2.2.1 L-type BSE prions

Brain samples from the single L-type BSE affected cow discovered in Canada were confirmed to be BSE positive at the Canadian National BSE Reference Laboratory. The brain tissue from this animal was passaged into two calves. For this purpose, the colliculus tissue was homogenized to 10% (w/v), sonicated, and spun to remove large cellular debris. The supernatant was aspirated into a syringe for subsequent injection into the cranial cavity of two steer calves at approximately 5 months of age (1 mL of 10% homogenate per steer). Prior to inclusion in this project, steers of interest were genotyped to ensure no abnormalities were present in the prion gene. Once confirmed as genetically normal, the steers were moved into the biosafety level 3 containment pens at the CFIA Lethbridge Laboratory. Following challenge, the animals were monitored regularly for the appearance of clinical signs. At 16 months post challenge, both steers began to show mild clinical signs of BSE infection. With noted progression over the next several weeks, the steers were euthanized at 17 and 18 months post challenge, respectively. The brain stem was tested immediately using the Prionics rapid test platform and generated OD values of >8,000 for both animals. The kit lot positive/negative cutoff OD value was 113 with >95% of BSE negative samples giving an OD value of 0 using this kit lot. Both of these sample homogenates were also

strongly positive on a Western blot with three distinct immuno-reactive glycoforms ranging in size from 28 kDa down to 18 kDa.

To type the protease-resistant prions that were found in the central nervous system tissue from the two challenged steers, the homogenate was run on a hybrid Western blot. This assay utilizes mild and stringent protease digestion, a panel of antibodies with different epitopes and molecular weight/glycoform ratios to type BSE samples. Classical BSE PrP^{Sc} has a ~2:1 ratio of di- to mono-glycosylated isoforms when detected on western blot, but the two L-type BSE challenged steer samples had ratios much closer to 1:1; this is commonly seen in atypical BSE. Proteinase K digestion under stringent conditions caused a significant decrease in PrP^{Sc} detected, another consistent characteristic of atypical BSE prions. SDS-PAGE gel separation of the protease resistant core of PrP revealed a subtle 0.5 to 1 kDa molecular weight shift down when compared to the classical BSE control samples. Finally, the PrP^{Sc} from the challenged steers was reactive with core anti-prion antibody 6H4 (Prionics AG, Switzerland) but was not reactive with the slightly more N terminal P4 anti-prion antibody (R-Biopharm AG, Germany). The molecular weight shift and antibody reactivity profile confirmed that the N-terminally truncated PrP^{Sc} detected is L-type atypical BSE. These BSE typing results for the two challenged steers were consistent with the hybrid Western blot results for the Canadian L-type BSE field case used for the challenge.

2.2.2 Transgenic mice and genotyping

Tg4092 mice (Scott, Safar et al. 1997) that overexpress the bovine prion protein were kindly provided by Dr. Stanley B. Prusiner (University of California, San Francisco). Similar to BSE-infected cattle, these transgenic mice have shown to develop vacuolization and astrocytic gliosis

in the brain stem area after inoculation with bovine prion protein (Scott, Safar et al. 1997). The presence of the transgene was identified by PCR using tail-derived genomic DNA, which was amplified using primers, forward 5'.TCGATCCAGAGCCTTTGAATTGAG.3'; and reverse 5'. GGGTGAAATGGTCAGTGCATTACG.3'. PCR thermocycling conditions were as follows: 94°C for 3 min, (94°C for 20 sec, 55°C for 30 sec, 72°C for 90 sec) repeated 35 times, 72°C for 1 min, hold at 4°C, resulting in a 836 bp fragment that was visualized on a 1% agarose gel containing ethidium bromide.

2.2.3 Ethics statement

The BSE transmission experiments were carried out at the Canadian Food Inspection Agency, Lethbridge Laboratory, Lethbridge, Alberta, in accordance with guidelines set by the Canadian Council on Animal Care and approved by the animal care use committee for the CFIA-ADRI Lethbridge Laboratory (ACC#0902). All bioassay experiments in Tg4092 mice were carried out at the Centre for Prions and Protein Folding Diseases (CPPFD), University of Alberta, in accordance with guidelines set by the Canadian Council on Animal Care and approved by the animal care use committee for Health Sciences 2 (protocol AUP00000884).

2.2.4 Bioassays

Tg4092 mice overexpressing the bovine prion protein (Scott, Safar et al. 1997) were inoculated intra-cerebrally with 30 µL of diluted L-type BSE bovine brain homogenate per animal for the primary production of L-type BSE prions. Subsequent bioassay experiments were performed in the same manner, again using Tg4092 mice. The first group of transgenic mice was inoculated intra-cerebrally with 30 µl of 1 % brain homogenate samples from L-type BSE-infected Tg4092 mice. Two other groups were injected separately with 30 µl of 1 % pellet 1, and the final pellet

samples (PK-digested) obtained from the purification experiments. Following inoculation, animals were monitored regularly for the appearance of prion disease clinical symptoms such as weight loss, scruffy coat, loss of appetite, ataxia, and dyspnea. Once the terminal stage of the disease was reached, the animals were euthanized by CO_2 asphyxiation followed by cervical dislocation. The brains were collected and stored at -80°C for future analysis. Prion titers for the L-type BSE samples were determined by measuring the incubation time intervals from inoculation to the onset of neurological illness and calculated as $LogID_{50}$/ml units based on a standard curve relating C-type BSE incubation times to prion dose (Safar, Scott et al. 2002).

2.2.5 Isolation of BSE prions

Infectious L-type BSE prions were isolated from the brains of terminally sick L-type BSE-infected Tg4092 mice using a previously developed protocol (Safar, Wille et al. 1998). First, all brains were pooled and homogenized at 20% concentration (w/v) in phosphate-buffered saline (PBS). Four to ten brains were used in separate purification experiments. The 20% brain homogenate was then clarified at 500 × g for 5 minutes, and the supernatant was collected and added to a new tube with an equal volume of 4% Sarkosyl in PBS to make 10% w/v brain homogenate. Then, the sample was aliquoted into 1 mL screw-cab microcentrifuge tubes and subjected to digestion with PK (50 μg/ml) at 37°C for 1 hour. The PK treatment reaction was stopped with the addition of 10 mM Phenylmethylsulfonyl Fluoride (PMSF). The process continued by adding 2% sodium phosphotungstic acid (PTA, pH 7.2) (SIGMA P-6395) to the aliquots and overnight (16 hours) incubation at 37°C. Afterwards, the samples underwent centrifugation at 16,000 × g for 30 minutes and the P1 pellet fraction was obtained and resuspended with 0.2% Sarkosyl in PBS. Subsequently, 2% Sarkosyl in PBS and 2% PTA were

added to the resuspended pellets, and the samples were centrifuged again at 16,000 × g for 30 minutes to obtain the final pellet. The final pellet was resuspended with 0.2% Sarkosyl in PBS. Samples collected from different steps of the purification were stored at -80°C for future analyses.

In order to generate highly purified L-type BSE prion isolates suitable for structural examination, we combined the PTA-precipitation protocol with a sucrose step-gradient centrifugation. In this method, the standard PTA purification was performed until the first pellet (P1) was obtained, and after resuspension with 0.2% Sarkosyl in PBS, the pellet 1 was loaded onto a sucrose-step gradient of 40% and 80% sucrose and subjected to ultracentrifugation at 115,000 × g at 4 °C for 16 hours (overnight). Following centrifugation, 500 µL fractions were collected from the top of the ultracentrifugation tube. The bottom of the tube was washed with 100 µl of sucrose buffer (10 mM Tris HCl pH 7, 1mM NaN_3, 0.2% Sarkosyl) to recover pelleted proteins and labeled as 'pellet wash'. All collected samples were stored at -80°C for SDS-Page, silver staining and TEM studies.

2.2.6 Western blotting

Samples were mixed with a gel-loading buffer (Bio-Rad) containing 2% (w/vol) SDS and heated at 100°C for 10 minutes before electrophoresis. The proteins were separated by SDS-PAGE gel electrophoresis using 12% acrylamide gels (Bio-Rad), run for 1 hour at 150 volts and blotted onto a polyvinylidene difluoride (PVDF) membrane (Millipore) at 100 volts for 1 hour. The blotted membranes were blocked with 5% (w/v) BSA in Tris buffered saline solution containing 0.05% Tween 20 (v/v) (TBST), overnight, at 4 °C and incubated with anti-PrP antibody, D15.15 at a 1:5,000 dilution, for 1 hour, at room temperature, followed by washing three times for 5

minutes with TBST. Next, the membranes were incubated with alkaline phosphatase conjugated anti-mouse IgG (Bio-Rad) at a 1:10,000 dilution in TBST for one hour and washed three times for 5 minutes in TBST. Prion protein signals were developed by adding ~1 ml alkaline phosphatase (AP) substrate (Bio-Rad) and detected by chemiluminescent visualization using ImageQuant (GE Life Science).

2.2.7 Silver staining

Samples from the purification were loaded on 12% polyacrylamide gels (Bio-Rad) and run for 60 minutes at 150 volts. The gels were then incubated for 30 minutes at room temperature in fixing solution (50% methanol, 12% acetic acid) and afterwards incubated in SDS removal solution (10% ethanol, 5% acetic acid) for 30 minutes at room temperature. Next, the gels were transferred to Farmer's solution to enhance PrP staining (containing: 0.15 g potassium ferricyanide, 0.3 g sodium thiosulfate, 0.05 g sodium carbonate) for 2 minutes, and then washed three times in distilled water. Next, the gels were treated with 0.2% (w/v) $AgNO_3$ for 20 minutes and rinsed briefly in distilled water, followed by 100 ml developing solution (15 g sodium carbonate and 250 microL 30% formaldehyde stock solution). Finally, the development stopped by addition of a solution of 0.2% acetic acid (Wille, Shanmugam et al. 2009).

2.2.8 Negative stain electron microscopy

10-µl drops of purified samples were adsorbed onto freshly glow-discharged 400 mesh carbon-coated copper grids (Electron Microscopy Sciences) for 1 minute and washed in 1-3 drops of (50 µl) 0.1 M and 0.01 M ammonium acetate solutions each. Then, the grids were stained using a freshly filtered 2% solution of uranyl acetate and air-dried after removing the excess stain with filter paper. The stained samples were examined with a Tecnai G20 transmission electron

microscope (FEI Company) operating at an acceleration voltage of 200 kV. Electron micrographs were recorded with an Eagle 4k x 4k CCD camera (FEI Company). Defocus levels of 1-2 µm were applied for recording the images.

2.2.9 Width measurements

Width measurements were performed on L-type BSE fibrils using EMAN's boxer (Ludtke, Baldwin et al. 1999). For each fibril, the maximum diameter between two crossover regions was determined.

2.2.10 Immunogold labeling

Immunogold labeling of the L-type BSE fibrils was performed using a combination of anti-PrP antibodies, including Fab fragments Fab 69 and Fab 29, and monoclonal antibody YEG mAb Sc-G1, detecting prion protein epitopes at different positions. The Fab fragments were selected from a phage display library. Fab 69 and Fab 29 react with epitopes within residues $_{100}$GWGQGGTHGQW$_{110}$ and $_{227}$TQYQRESQAYY$_{237}$ located at N- and C-terminal regions of the bovine prion protein, respectively (Senatore, Frontzek et al. 2020). The Fabs were expressed in *E.coli* (BL21(DE3)) as a His-tagged, soluble, and functional protein. The Fab fragments were purified via IMAC chromatography, following lysis of the bacterial cells. Next, the fragments were eluted using imidazole buffer, desalted, and further assessed for purity and activity (Rathod *et al*., unpublished data). The YEG mAb Sc-G1 monoclonal antibody was produced in-house and recognizes a discontinuous epitope in native PrP^{Sc} only (Fang et al., manuscript in preparation).

Based on a previously published immunogold labeling protocol (Wille, Govaerts et al. 2007), 7 µl of purified L-type BSE samples were adsorbed onto glow discharged formvar/carbon-coated

nickel grids (Ted Pella, Inc.) for ~5 minutes, and washed using three drops (50 µl) of 0.1 M and 0.01 M ammonium acetate buffer pH 7.4. Samples used for labeling with Fab 69 and Fab 29 antibodies, were treated with 50 µl of 3 M urea for 10 minutes, to increase the epitope accessibility. Following the washing steps, the grids were stained with 2 drops of freshly filtered 2% sodium phosphotungstic acid (PTA), pH 7.2, then blocked for 60 minutes with 0.3% bovine serum albumin (BSA) in Tris buffered saline (TBS: 50 mM Tris-HCl, pH 7.4; 150 mM NaCl). Next, all grids, except for the control samples, were incubated on 50 µl drops of primary antibodies YEG mAb Sc-G1, Fab 69, and Fab 29 for 2.5-3 hours, followed by 5 washes in 1% BSA. The grids that were treated with Fab 69 and Fab 29 were transferred onto droplets of goat F(ab')2 anti-human IgG F(ab')2 (Abcam ab98531) for 2 hours, followed by washing steps, incubated with a 5-nm-gold-conjugated rabbit anti-goat IgG (Abcam ab202670) for 2 hours and rinsed 5 times in 0.1% BSA. For the YEG mAb Sc-G1 antibody, incubation with the primary antibody and washes in 1 % BSA, followed by treatment with 50 µl droplets of the gold-conjugated secondary antibody, 6 nm goat anti-mouse IgG (Abcam ab39614), diluted 1/50 in blocking buffer, for 2.5 hours and 5 washes in 0.1% BSA. Finally, the grids were rinsed with TBS solution and water, and placed onto two drops of 2% PTA for final staining, air-dried, and stored for EM analysis. The control experiments were conducted similarly except for the omission of the primary antibodies. The samples were analyzed with a Tecnai G20 transmission electron microscope (FEI Company) operating at an acceleration voltage of 200 kV. Electron micrographs were recorded with an Eagle 4k x 4k CCD camera (FEI Company).

2.2.11 2D class averaging

Two-dimensional classification is a computational tool performed on electron micrographs to enhance the signal-to-noise ratio (SNR) of the images. This involves the alignment and grouping

of the dataset into classes based on morphological similarities (Ohi, Li et al. 2004). Reference-free 2D class averaging was performed by applying boxes with a size of 200 by 200 pixels and a 50% overlap along the fibrils' axis between two crossovers using EMAN's boxer program (Ludtke, Baldwin et al. 1999). Classification and averaging were implemented on a total of 532 segmented particles of one-protofilament fibrils and 297 segmented particles of two-protofilament fibrils for a total of n= 3 classes.

2.2.12 3D helical reconstruction

For helical reconstructions, we selected representative isolated fibrils with an apparent helical twist from among hundreds of electron micrographs, all previously examined visually for the width measurements. For this method, individual fibrils were segmented along the fibril axis covering at least two crossovers into overlapping boxes with the size of 300 by 300 pixels, and 95% to 99% overlap between adjacent segments using EMAN's boxer software (Ludtke, Baldwin et al. 1999, Vazquez-Fernandez, Vos et al. 2016). All segments were aligned, and the angular orientation of each box was calculated based on the fibril's repeat distance, followed by generation of a preliminary 3D map by back-projection of all boxed 2D projections using the image processing software SPIDER (Frank, Radermacher et al. 1996). Next, the reconstruction was low-pass filtered to 20 Å, and the corresponding symmetry was imposed (no symmetry for the one-protofilament fibrils and two-fold symmetry for the two-protofilament fibrils). Afterwards, the initial model underwent further refinements, including alignment of the reconstruction to other reconstructions of the same fibril with different segmentation overlaps (Glaves, Gorski et al. 2013), which continued by averaging aligned 3D volumes through an iterative process of alignment and averaging.

Extended helical reconstruction: This approach was implemented on the final reconstructions in order to eliminate the rippling artifacts from the overlapping boxes (Vazquez-Fernandez, Vos et al. 2016). Briefly, the refined reconstructed volume was sliced across the yz plane, following 90° rotation around its x-axis direction, which yielded a set of 2D projections of the fibril's cross-section. Then, the stack of 2D projections underwent alignment and averaging processes iteratively. Next, the IMAGIC software was used to center and replicate the final 2D averaged image (van Heel, Harauz et al. 1996). Finally, rotation angles were applied to the set of replicated averaged 2D cross-sections according to the helical repeat, and a 3D map was built using IMAGIC software (van Heel, Harauz et al. 1996). All 3D reconstructions were visualized in UCSF Chimera (Pettersen, Goddard et al. 2004).

2.3 Results

2.3.1 Propagation of L-type BSE prions in transgenic mice expressing bovine PrP

In Canada a total of 19 BSE field cases have been detected since May 2003; one of them was typed as an L-type, atypical BSE case (Dudas, Yang et al. 2010). This animal was a Hereford pure breed heifer that was 13.7 years old when it was euthanized and tested positive for L-type BSE. Brain samples from this case were confirmed BSE positive at the Canadian National BSE Reference Laboratory. Western blot typing identified that the BSE prions in the brain of this heifer were consistent with L-type BSE. As a field case animal, the tissue condition was poor, and the amount of brain available was limited. In order to generate better quality tissue for follow up studies, brain tissue from the Canadian L-type BSE field case was passaged into 2 calves. At 16 months post inoculation, brain homogenate samples from these L-type BSE affected cows were used for intracerebral inoculation of transgenic mice overexpressing bovine

PrP (Tg4092) (Scott, Safar et al. 1997). Brains from terminally sick Tg4092 mice were used for the purification and subsequent ultrastructural characterization of L-type BSE prions.

2.3.2 Isolation of L-type BSE prions

Digestion with proteinase K (PK) has been employed as a standard approach to diagnose prion formation for many years (Prusiner, McKinley et al. 1983, Prusiner 1998, Leffers, Wille et al. 2005), and it has been shown that proteolysis with PK does not alter the self-replication and disease-causing capability of the resulting PK-digested prions (Wang, Wang et al. 2018, Vanni, Pirisinu et al. 2020). Here, we used the PK digestion method to eliminate PrP^{C} and other proteins from the purified samples. The purification procedure also included PTA, as this agent has been demonstrated to facilitate selective precipitation of PrP^{Sc} and PrP 27-30 compared to PrP^{C} (Safar, Wille et al. 1998, Wille, Shanmugam et al. 2009). Following the isolation of L-type BSE prions using PK and PTA, the quality and purity of the samples were analyzed using Western blots and silver stained SDS gels. The latter showed signals in the pellet fraction (Figure 2.1A) that matched the bands in the Western blot (Figure 2.1B), indicating the relative purity of the final pellet samples. Western blots of samples collected during the purification indicated the stepwise enrichment of the prion protein. The final pellet showed the typical three bands corresponding to non-, mono-, and diglycosylated PrP 27-30 when detected using the anti-PrP monoclonal antibody D15.15 (Figure 2.1B).

We also implemented a modified purification procedure, including a sucrose step-gradient centrifugation to remove bound lipids, which interfere with the ultrastructural analysis using electron microscopy. For this purpose, the semi-purified P1 pellet from the PTA purification was loaded onto a layered sucrose gradient cushion (40% and 80% sucrose), which separates the

prion protein from the lipid components and PTA according to their densities. The prion protein with a density of 1.2 g/ml was expected to migrate to the interface between 40% and 80% sucrose, with 1.1 g/ml and 1.4 g/ml solution densities, respectively. After ultracentrifugation, fractions were collected from the top and examined by immunoblotting and silver stain SDS gels (Figure 2.1C-D). As predicted, Western blots showed strong PK-resistant PrP 27-30 signals in the middle fraction compared to the fractions from higher and lower density areas. The top fractions and the bottom fractions showed relatively weak PrP 27-30 signals only. On the other hand, the pellet-wash fraction that was recovered once all fractions were collected, contained a high intensity PrP 27-30 signal (Figure 2.1D), which can be explained by the pelleting of prion aggregates complexed with PTA, resulting in a particle density in excess of 1.4 g/ml (Levine, Stohr et al. 2015).

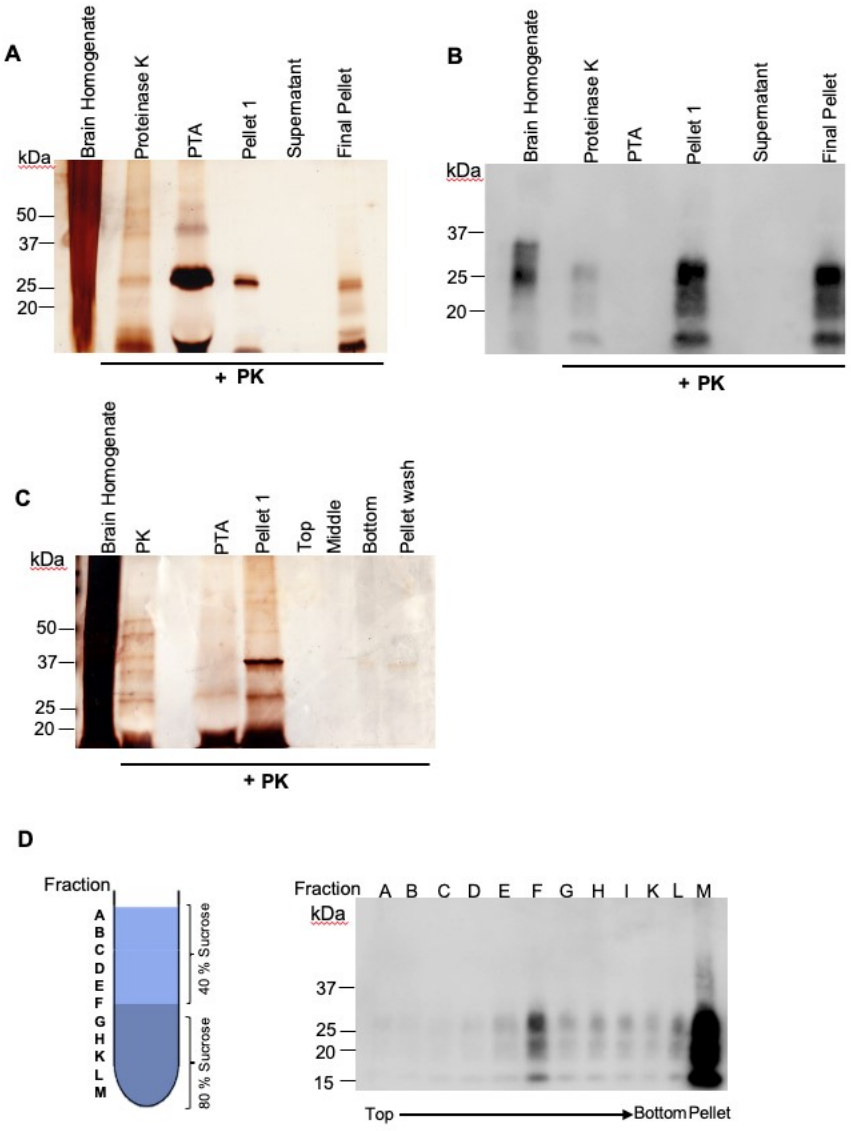
A
Brain Homogenate
Proteinase K
PTA
Pellet 1
Supernatant
Final Pellet
kDa
50
37
25
20
+ PK
B
Brain Homogenate
Proteinase K
PTA
Pellet 1
Supernatant
Final Pellet
kDa
37
25
20
+ PK
C
Brain Homogenate
PK
PTA
Pellet 1
Top
Middle
Bottom
Pellet wash
kDa
50
37
25
20
+ PK
D
Fraction
A
B
C
D
E
F
G
H
K
L
M
40 % Sucrose
80 % Sucrose
Fraction A B C D E F G H I K L M
kDa
37
25
20
15
Top
Bottom
Pellet

Figure 2. 1 Purification of L-type BSE prions.

Silver stain SDS-PAGE gel of samples taken at different steps of the PTA purification. (**B**) Western blot of the L-type BSE prion purification samples using the D15.15 anti-prion monoclonal antibody. The PK-digested pellet 1 and the final pellet show the typical three bands of the bovine prion protein corresponding to di-, mono- and non-glycosylated forms. (**C**) Silver stain SDS-PAGE gel of samples from the sucrose step gradient centrifugation. The samples from the top, middle, bottom, and the pellet wash fractions demonstrate the purity of the samples, even though the prion protein signal is weak. (**D**) Western blot of the sucrose step gradient fractions. After ultracentrifugation through 40% and 80 % sucrose, all fractions were separated based on their densities from top to bottom (A-L). The pellet-wash fraction (M) was obtained by washing the tube with 100 µl of sucrose buffer. The Western blotting was developed using the D15.15 antibody. As expected, the middle fraction (F) shows a stronger signal compared to the top (40%) and the bottom fractions (80%). The pellet-wash fraction (M) also showed a high yield of L-type BSE prions.

2.3.3 Transmission electron microscopy of L-type BSE fibrils

Following the successful purification of the L-type BSE prions from the Tg4092 mouse brains, we sought to examine the morphology of the infectious protein samples using TEM. We performed negative stain electron microscopy tests on all fractions from the sucrose gradient purification as well as the P1 pellet sample of the PTA precipitation step, which was obtained before loading onto the sucrose gradient column (Figure 2.1). The P1 pellet was very crowded with amyloid fibrils as well as amorphous aggregates and lipid containing particles when observed by electron microscopy, indicating the need for additional purification steps (Figure 2.13). Only a few amyloid fibrils were observed in the samples from the top and the bottom fractions, which yielded weak bands in the Western blot (Figure 2.1D), while the remaining fractions displayed no or only rare amyloid fibrils. Predominantly, fibrils were found in the negatively stained samples of the middle and the pellet-wash fractions. However, the micrographs of the pellet-wash fraction revealed a significantly higher yield of amyloid fibrils, in good correlation with the signal intensity in the Western blot. As expected, electron micrographs of samples from the sucrose gradient ultracentrifugation showed better purity compared to the pre-spin P1 sample and contained more clean, non-overlapping isolated fibrils and fewer amorphous aggregates or lipid particles. A more extensive examination of the samples revealed some non-fibrillar particles along with the fibrils (Figure 2.2), including small two-dimensional (2D) crystals (Wille, Michelitsch et al. 2002).

2.3.4 One- and two-protofilament L-type BSE fibrils

Overall, the L-type BSE fibrils were found to be morphologically heterogeneous when studied by EM. We found two main populations of amyloid fibrils: two-protofilament fibrils displaying two fibrillar densities with a gap between them (Figure 2.3A) and thinner single-protofilament fibrils (Figure 2.3B). Both fibrillar types exhibited helical properties. The one-protofilament fibrils, accounting for ~73% of the total fibril population, were significantly more abundant compared to the two-protofilament fibrils, which were identified in ~27% of the fibrils (Table 2.1). In contrast, in a previous study of a GPI-anchorless prion, the sample contained only helical fibrils containing two protofilaments (Vazquez-Fernandez, Vos et al. 2016). While the two-protofilament morphology is in agreement with the conclusions drawn from previous studies on other prion strains (Sim and Caughey 2009, Wille, Bian et al. 2009, Vazquez-Fernandez, Vos et al. 2016, Wang, Zhao et al. 2020), here, for the first time, we observed the single protofilament fibrils as the dominant structure of infectious L-type BSE prion fibrils. This unique quaternary structural arrangement had not been observed before.

By analyzing hundreds of electron micrographs, we discovered a few interesting images in which the fibrils transitioned between one- and two-protofilament morphologies (Figure 2.4). Each of the three representative electron micrographs contains a long L-type BSE fibril that on one end consists of two protofilaments (white arrowheads), while the other end is split into two one-protofilament fibrils (black arrows). This finding appears to indicate the interaction of two separate single-protofilament fibrils to form a two-protofilament fibril. Moreover, the presence of two distinct and separable protofilaments in these images contradicts the PIRIBS model, which proposed an in-register stacking of PrP^{Sc} monomers covering the full width of a "two-protofilament" structure (Groveman, Dolan et al. 2014). These micrographs preclude the

possibility that stain artifacts contribute to the observed gap between the protofilaments, as the protofilaments separate into distinct fibrils. In this context, a recent study demonstrated that the negative staining process or stain artifacts do not substantially alter the dimensions and overall conformation of amyloid fibrils based on the observation that the morphology of mouse-adapted prion fibrils in a negative stain experiment were in agreement with cryo-EM and atomic force micrographs of the same samples (Terry, Wenborn et al. 2016, Terry, Harniman et al. 2019).

As shown in Figure 2.5, from a selection of 867 fibrils, the average diameter of the two-protofilament fibrils at their widest part was 22.5 ± 3.4 nm, which resembles the width of the double-helical fibrils of infectious RML prion fibrils published in a recent study using cryo-EM and AFM microscopies (Terry, Harniman et al. 2019). The average width of one-protofilament L-type BSE fibrils was 10.6 ± 1.7 nm at the widest region of the fibrils. It is notable from the histogram (Figure 2.5) that the width of the two-protofilament fibrils is about twice that of one-protofilament fibrils, plus the gap between the two protofilaments can account for the slightly larger values for these thicker fibrils. In a previous cryo-EM study, the two-protofilament fibrils of GPI-anchorless mouse PrP^{Sc} had a maximum width of ~10 nm (Vazquez-Fernandez, Vos et al. 2016). The underglycosylated and GPI-anchorless PK-resistant PrP^{Sc} fragment was found to migrate as a single band with a mass of ~17 kDa (Chesebro, Trifilo et al. 2005), while the PK-resistant fragments of L-type BSE PrP 27-30 migrated between 30 and 17 kDa, depending on their glycosylation (Figure 2.1B and Figure 2.1D). The mass difference between these two prion variants can easily explain the apparent difference fibril widths. The helical pitch for one- and two-protofilament fibrils were 82 nm and 102 nm, respectively. These values were both in the range that was reported for the distance per half turn for hamster-adapted scrapie associated fibrils (SAFs) (Sim and Caughey 2009). We also measured the length of the fibrils to find out

whether there is a difference in both morphologies. The negatively stained two-protofilament fibrils had an average length of 598 nm, and the single-filament fibrils were on average 387 nm in length. The greater length for the first group appears to be due to a reduced sensitivity of these thicker (wider) fibrils to breakages (Table 2.1).

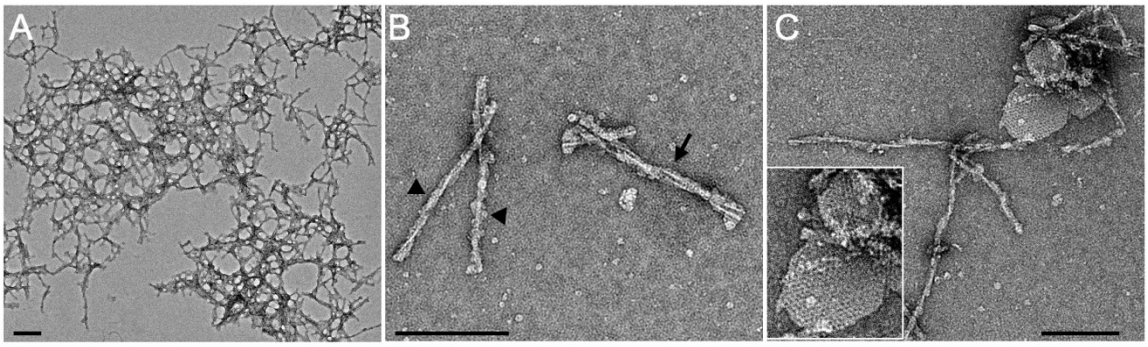

Figure 2. 2 Negative stain electron micrographs of purified L-type BSE samples showing heterogeneous morphologies.

Representative electron micrographs of the final pellet obtained through sucrose gradient purification. (**A**) large PrP 27-30 aggregates, (**B**) isolated forms of both single (arrowheads) and double (arrow) protofilament fibrils, and (**C**) 2D crystals along with amyloid fibrils. Grids stained with 2% uranyl acetate. Scale bar = 100 nm.

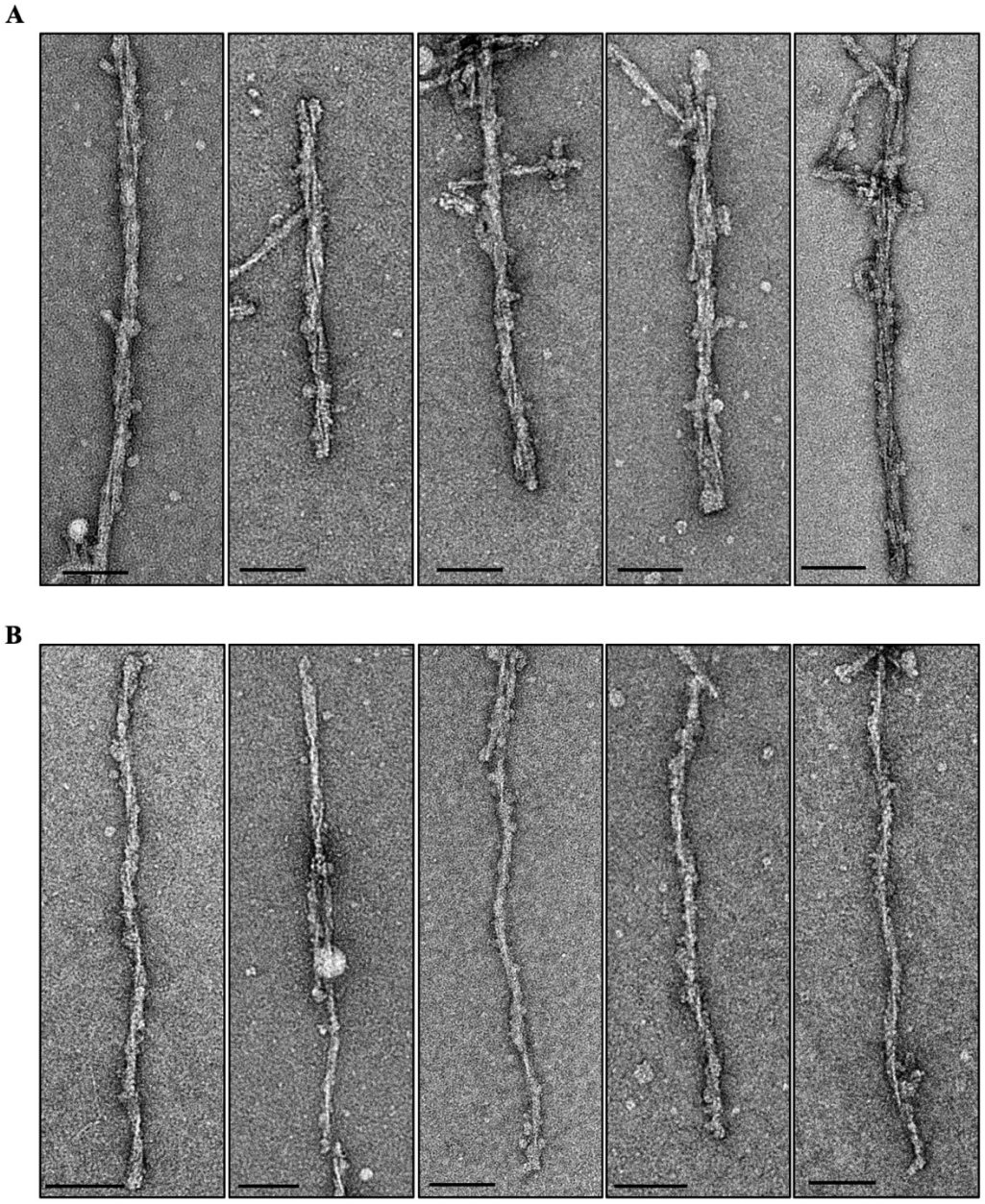

Figure 2. 3 Gallery of negative-stained L-type BSE fibrils.

Representative electron micrographs from the final pellet sample of the sucrose gradient purification of L-type BSE fibrils. Fibrils exhibit distinct morphologies, including two- (**A**) and one-protofilament (**B**) fibrils. Grids stained with 2% uranyl acetate. Scale bar = 100 nm.

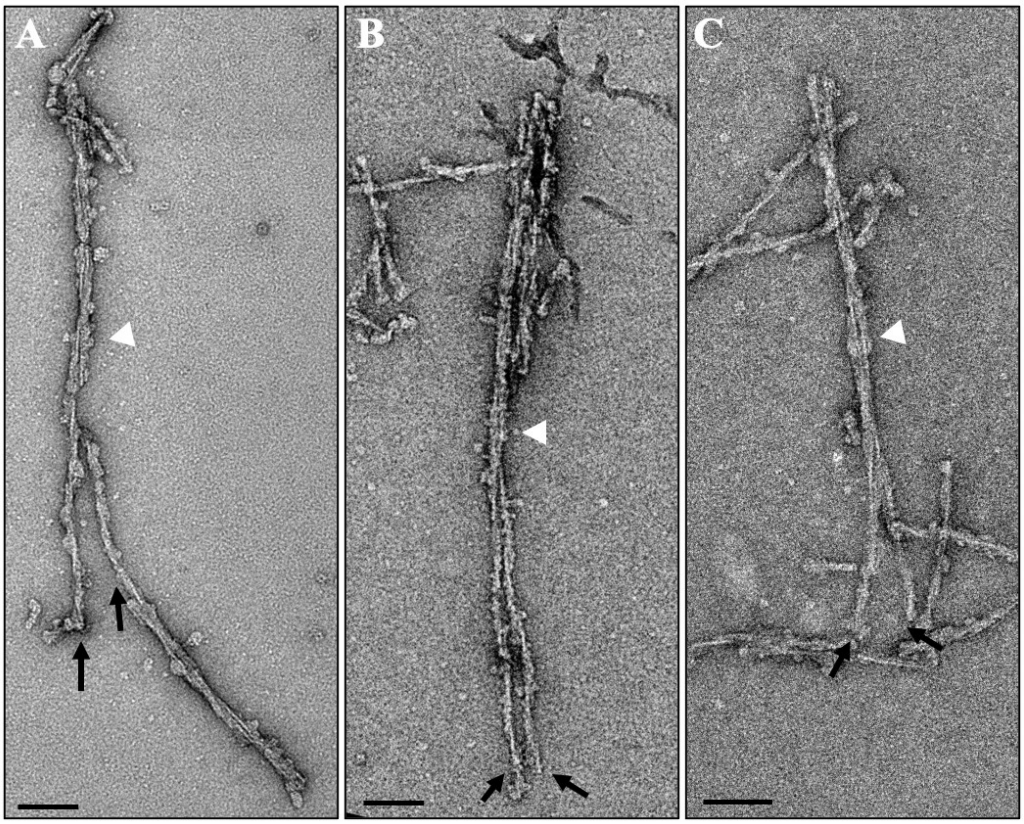

Figure 2. 4 Side-by-side comparisons of the one- and two-protofilament fibrils.
(**A-C**) Negative stain electron micrographs of the final pellet obtained through sucrose gradient purification showing the two distinct morphologies of L-type BSE fibrils side-by-side. (**A**) A negative-stained electron micrograph showing a long, isolated fibril composed of two protofilaments (white arrowhead), which appears to be broken and split into two one-protofilament fibrils towards its lower end (black arrows). (**B, C**) Two long, L-type BSE amyloid fibrils showing a two-protofilament fibril at one end (white arrowheads) and two one-protofilament fibrils at the other end (black arrows). Scale bar = 100 nm.

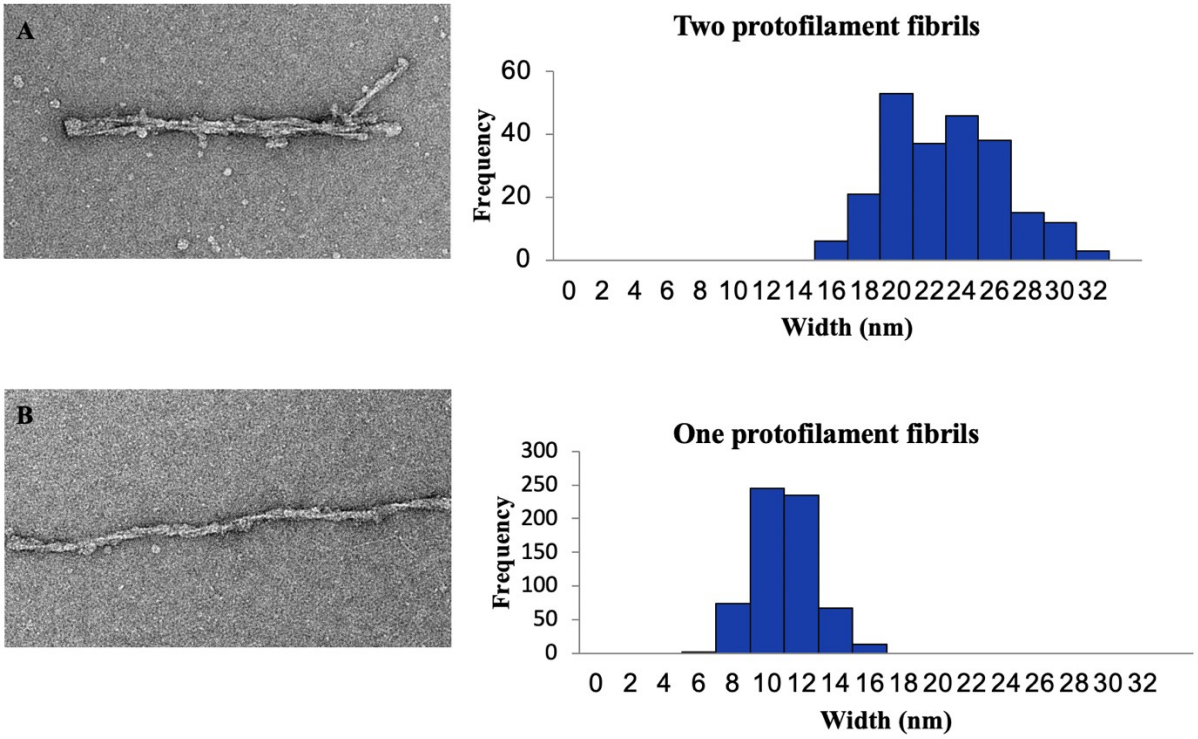

Figure 2. 5 Width distribution of L-type BSE fibrils.

(**A**) A sample electron micrograph and histogram of the maximum width of 231 two-protofilament L-type BSE fibrils. (**B**) A sample electron micrograph and histogram of the maximum width of 636 one-protofilament L-type BSE fibrils. The width measurements were performed using EMAN's boxer program.

Morphology	Number of fibrils	Width Mean ± SD (nm)	Helical Pitch Mean ± SD (nm)	Length Mean ± SD (nm)
Two-protofilament	n= 231 fibrils	22.5 ± 3.4	102.3 ± 16.9	598.2 ± 268.5
One-protofilament	n= 636 fibrils	10.6 ± 1.7	89.3 ± 15	387.5 ± 155.4

Table 2. 1 Fibril dimensions of negatively stained brain-derived infectious L-BSE fibrils

The measurements were performed using EMAN' boxer image software.

2.3.5 Image processing and 3D reconstruction

In order to decipher the ultrastructure of L-type BSE prions, we applied image processing techniques on representative negative-stain electron micrographs. The quality and good yield of isolated, non-overlapping L-type BSE fibrils observed enabled us to employ image processing and 3D reconstruction strategies on individual amyloid fibrils, which provided insightful results.

The first approach was to generate 2D class averages from hundreds of short image sections from isolated fibrils, which were treated as "single particles" during the image processing. The class averages on a group of 2D images contain higher signal-to-noise ratio compared to a single raw image, further intensifying the features in the object of interest, which aid the interpretation of the images (Ohi, Li et al. 2004). Reference-free class averaging was performed independently on each group of one- and two-protofilament fibrils. In a segmentation procedure, boxes of 200 by 200 pixels with a 50% overlap were applied along the fibril axis, and the resulting segmented particles were separately averaged and sorted into different classes according to structural similarity. As depicted in Figure 2.6A-C, class averages obtained from the thicker, two-protofilament fibrils revealed two fibrillar densities with an apparent, stain-filled space between them. Given that the particles were sorted into classes based on structural similarities, class C appears to be related to the crossover section of the helical fibrils. The same approach on the thinner fibrils revealed class averages exhibiting a helical fibril with one protofilament only (Figure 2.6D-F), that are also characterized by the narrower fibril width and the lack of a separating gap as seen in Figure 2.6A-C.

The helical nature of L-type BSE fibrils allowed us to perform three-dimensional (3D) helical reconstructions on individual fibrils. We performed this technique on fibrils with an apparent

helical twist covering at least one half helical turn (180°), following an earlier protocol (Vazquez-Fernandez, Vos et al. 2016). The 3D maps showed two distinct morphologies of the reconstructed fibrils, including fibrils with two intertwined protofilaments twisting around the fibril axis (Figure 2.7A) and single protofilament fibrils (Figure 2.7B). In the process of extended helical reconstructions, reconstructed fibrils were rotated and averaged along the fibril axis to generate an average cross-section of the fibril. The averaged cross-section densities of the first group contain two apparent densities corresponding to two protofilaments (Figure 2.7A 5), whereas the 2D projection of the averaged cross-section of the second group includes only one fibrillar density, i.e. one protofilament (Figure 2.7B 5). This observation confirms the existence of both distinct morphologies, which had been inferred from the fibril diameters (Figure 2.5 and Table 2.1) and individual micrographs (Figures 2.3 and 2.4). Contour maps and contour density maps of both reconstructions (Figure 2.7A 6-7 and 2.7B 6-7) provided us with more information about the ultrastructural arrangements of these amyloid fibrils. The density distribution revealed distinct densities in both morphologies, which could correspond to the different components of the protein (peptide, glycans, GPI-anchor).

We collected about 700 electron micrographs of L-type BSE fibrils, which enabled us to produce a panel of 3D helical reconstructions on isolated two- (Figure 2.8A-B) and one-protofilament fibrils (Figure 2.9A-B). Comparing the panel of separate 3D reconstructions provided further evidence regarding the heterogeneity and quaternary structural arrangements of these amyloid fibrils. The cross-sections of all 3D reconstructed fibrils, although of low resolution, adopted triangular or roughly oval morphology, similar to the shape of cross-sections of other β-solenoid proteins (Kajava and Steven 2006, Flores-Fernández, Rathod et al. 2018). Superimposition of the recent 4RβS model combined with N-linked glycans (Vazquez-Fernandez, Vos et al. 2016,

Spagnolli, Rigoli et al. 2019) with cross-sections from our 3D reconstructions representing the average width of the fibrils, as indicated in Table 1, showed that these reconstructions fit well with the 4RβS model (Figure 2.10).

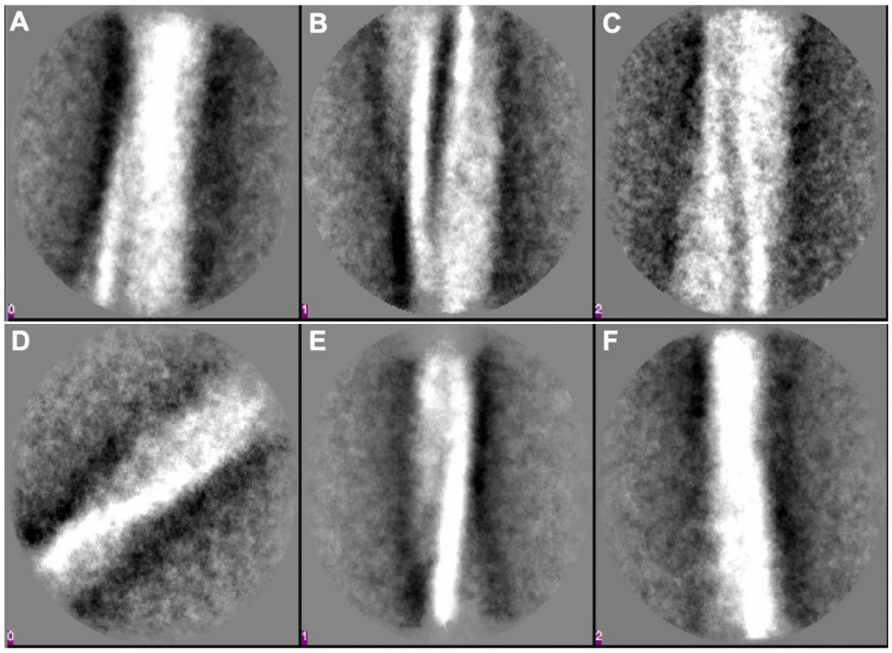

Two-Protofilament BSE Fibrils

One-Protofilament BSE Fibrils

G

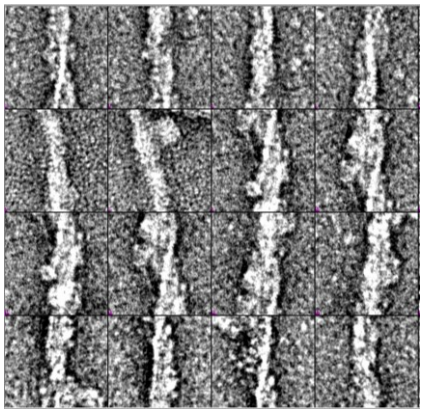

H

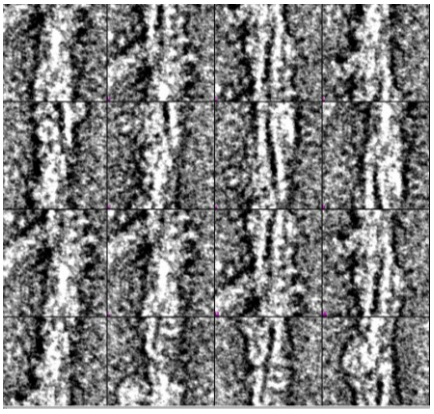

Figure 2. 6 Alignment, classification and averaging of L-type BSE fibrils.
(**A-C**) Reference-free alignment and classification of particles of two-protofilament L-type BSE fibrils. Class averages of 297 segmented particles exhibiting different regions of the fibrils, including the crossover region (**C**), showing two intertwined protofilaments with an apparent, stain-filled gap between them. (**D-F**) Class averages from the reference-free alignment of 532 particles of one-protofilament L-type BSE prion fibrils. All three class averages show a single helical filament only. Representative images of aligned fibril segments of one- (**G**) and (**H**) two-protofilament fibrils before classification.

A

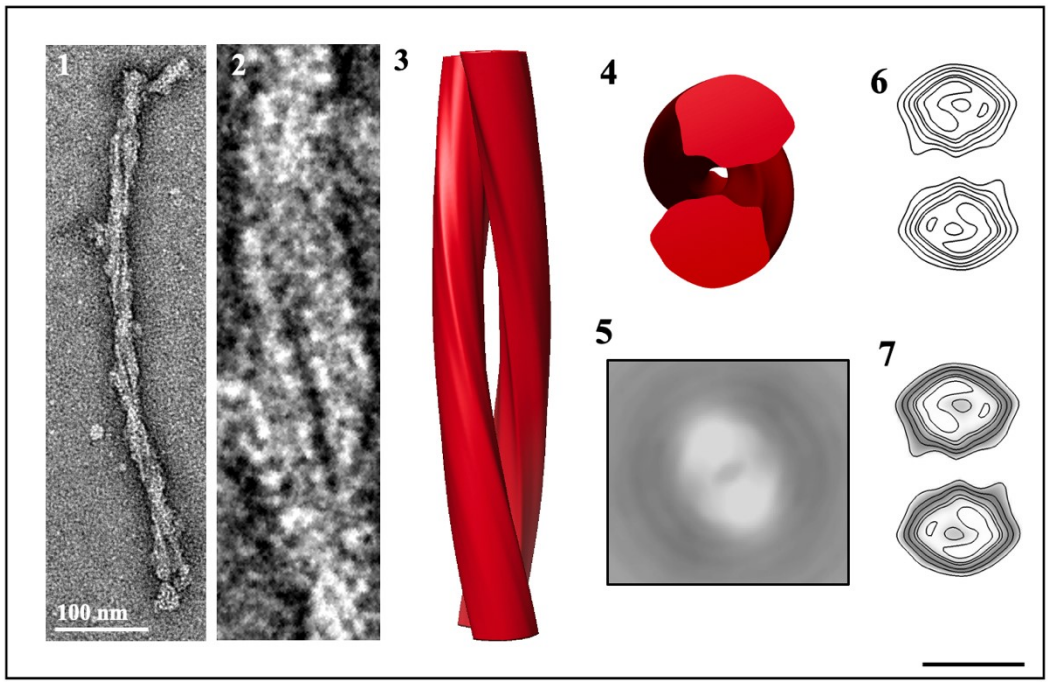

B

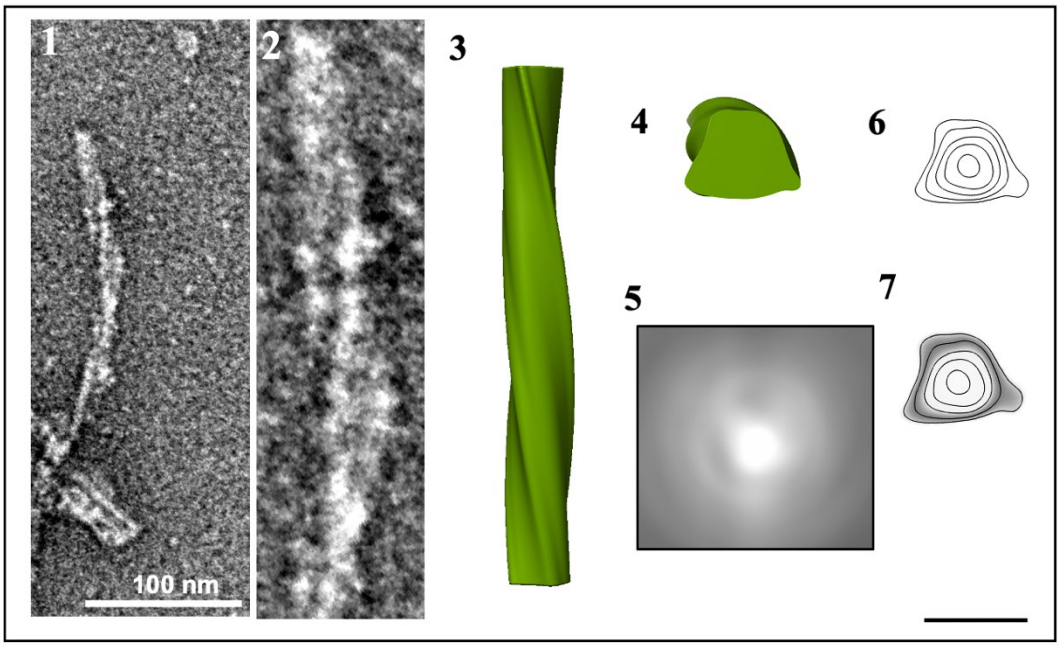

Figure 2. 7 Three-dimensional reconstructions of BSE prion fibrils.

(**A**) A 3D reconstruction of a two-protofilament fibril. (**1**) A negatively stained electron micrograph of a L-type BSE fibril, and (**2**) magnified view of the selected fibril section used for generating the 3D reconstruction. (**3**) A surface view of the 3D reconstruction showing two intertwined helical protofilaments. (**4**) Cross-section of the reconstruction. (**5**) The corresponding 2D projection of the averaged view of the cross-section region. (**6**) A contour map of the cross-section. (**7**) A contour density plot of the cross-section obtained by superimposition of the contour map onto a cross-section from the 3D volume. (**B**) A 3D reconstruction of a one-protofilament fibril. (**1**) A negatively stained electron micrograph of a L-type BSE fibril, and (**2**) enlarged view of the selected fibril. (**3**) Surface view of the 3D reconstruction. (**4**) Cross-section of the reconstruction. (**5**) The corresponding 2D projection of the averaged view of the cross-section region. (**6**) A contour map of the cross-section. (**7**) A contour density plot of the cross-section. The 3D reconstructions were low-pass filtered to 20 Å resolution. Scale bar = 10 nm.

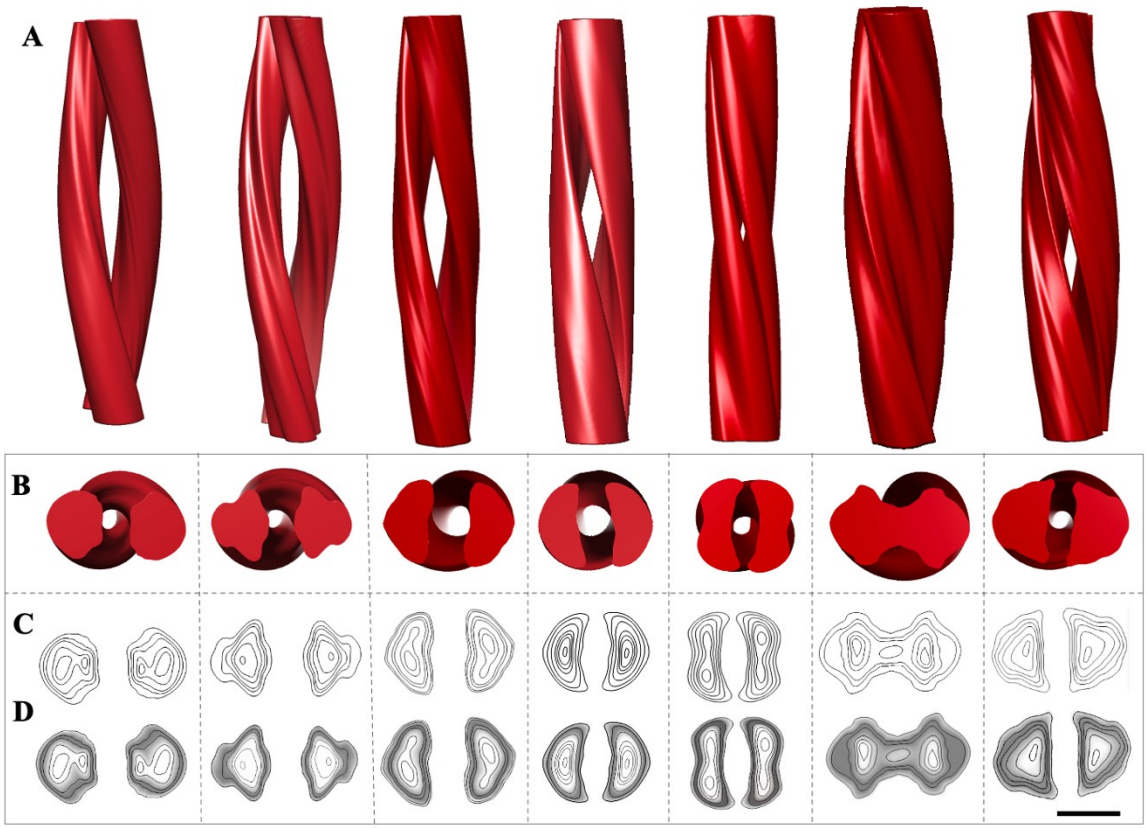

Figure 2. 8 Gallery of independent, 3D reconstructions of two-protofilament L-type BSE fibrils.

(**A**) 3D volumes of different two protofilament L-type BSE fibrils. (**B**) Cross-section views of the helical reconstructions. (**C**) Contour maps and (**D**) density maps of the reconducted volumes. Scale bar = 10 nm.

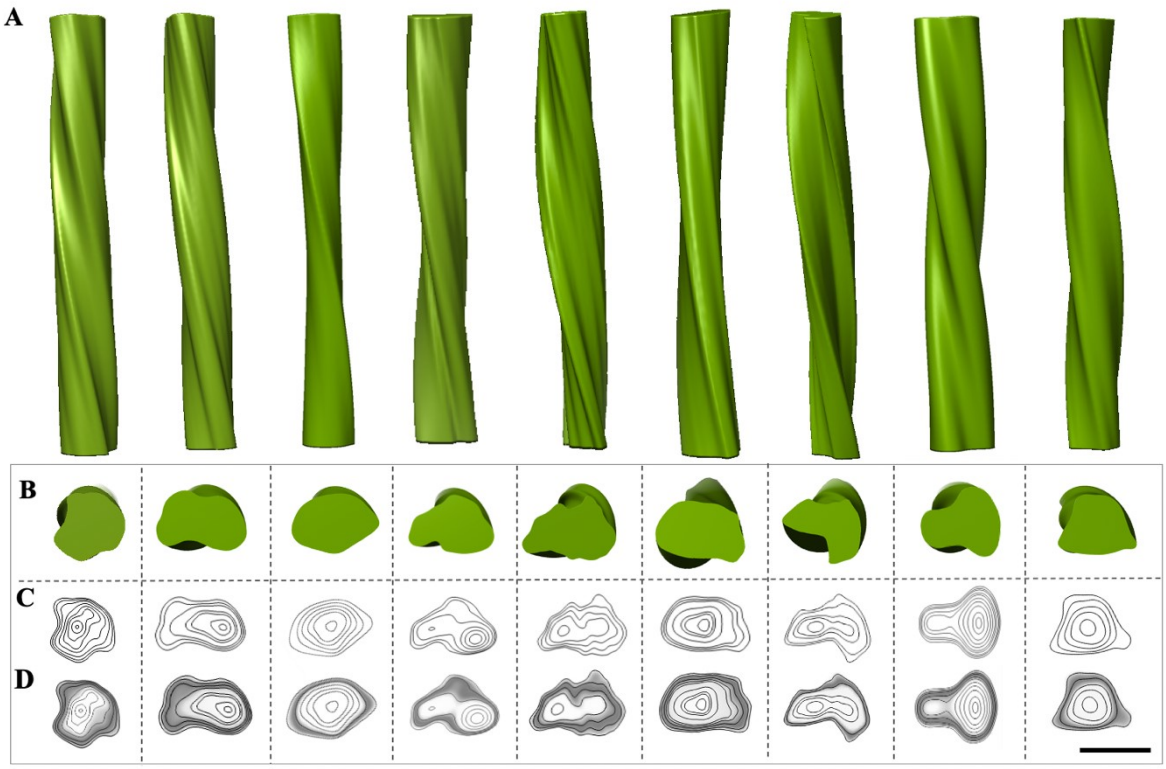

Figure 2. 9 Gallery of independent, 3D reconstructions of one-protofilament L-type BSE fibrils.

(**A**) 3D volumes of various thin, one-protofilament L-type BSE fibrils. (**B**) Cross-section views of the helical reconstructions. (**C**) Contour maps and (**D**) density maps of the reconstructed volumes. Scale bar = 10 nm.

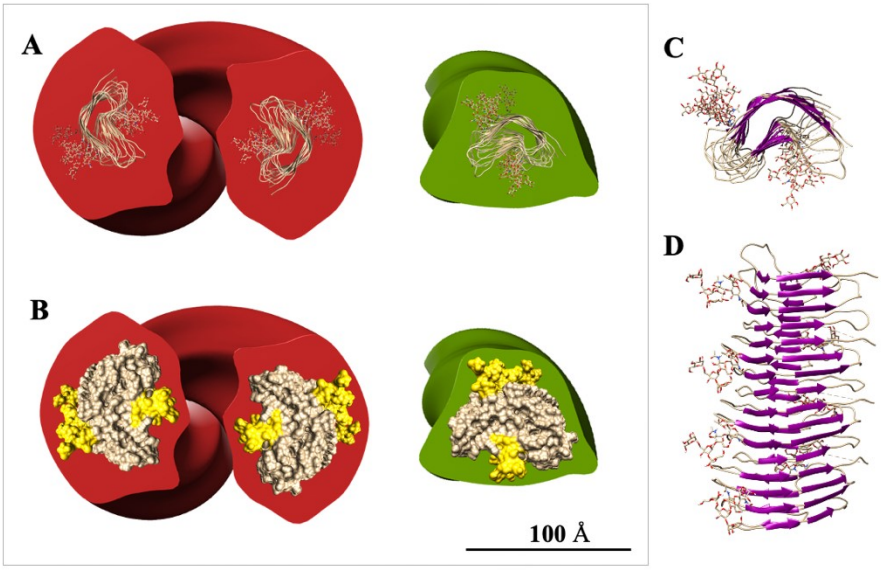

Figure 2. 10 Superimposition of the 4RβS PrP^{Sc} model and the 3D L-type BSE fibril reconstructions.

(**A**) A representative view of the 4RβS model of PrP^{Sc} (residues 90-230) with attached N-linked glycans superimposed onto the cross-section view of 3D reconstructions of a two-protofilament (red) and a one-protofilament (green) L-type BSE fibril with diameters of 200 Å and 100 Å, respectively. The size of the 4RβS model (50 Å x 30 Å) was set based on the previous cryo-EM and molecular dynamics simulation studies (Vazquez-Fernandez, Vos et al. 2016, Spagnolli, Rigoli et al. 2019). (**B**) A surface view of the 4RβS PrP^{Sc} model carrying glycans superimposed onto the cross-section view of 3D reconstructions of a two-protofilament (red) and a one-protofilament (green) L-type BSE fibril. (**C**) Top and (**D**) side views of a representative tetrameric version of the 4RβS PrP^{Sc} model containing glycans (Spagnolli, Rigoli et al. 2019).

2.3.6 Immunogold labeling for N- and C-terminal epitopes

To determine whether the fibrils contain PrP 27-30 or more truncated forms of the prion protein, we performed immunogold labeling experiments using different anti-PrP Fab fragments and monoclonal antibodies targeting epitopes located in different regions of the prion protein, including N-terminal and C-terminal epitopes. For this purpose, we first employed two recombinantly produced antibody fragments: Fab 69, which detects an epitope within residues $_{100}$GWGQGGTHGQW$_{110}$ near the N-terminus of truncated bovine PrP 27-30, and Fab 29, which binds an epitope within residues $_{227}$TQYQRESQAYY$_{237}$ near the very C-terminus of bovine PrP (based on the numbering of six octapeptide-repeat PrP). The best immunogold labeling was achieved when the purified samples were pre-treated by a denaturing procedure with urea, suggesting a reduced accessibility of these epitopes in the native state. Both one- and two-protofilament fibrils were decorated by the Fab fragments, followed with a secondary anti-Fab antibody and a tertiary antibody carrying 5 nm gold particles (Figure 2.11). Control experiments were run concurrently without use of the primary Fab fragments, which showed no or very rare presence of gold particles, demonstrating the specificity of the immunogold labeling (Figure 2.11D and 2.11H).

In another attempt at immunogold labeling we used YEG mAb Sc-G1, a novel monoclonal antibody that recognizes a conformational against a conserved epitope on native PrP^{Sc} only (Fang et al., manuscript in preparation). By using this monoclonal antibody and a secondary antibody conjugated with 6 nm gold particles, we were able to label L-type BSE prions in their native form (Figure 2.12A-B). In contrast, no antibody decoration occurred in the control samples (Figure 2.12C), indicating the specificity of the labeling. Successful labeling of the fibrils in the purified L-type BSE samples allowed us to conclude that our isolated L-type BSE

fibrils contain native PrP 27-30. In addition to the two Fab fragments that detect epitopes at both N- and C-terminal regions, respectively, the positive immunogold labeling result with YEG mAb Sc-G1 confirms that the observed L-type BSE fibrils are generated by polymerization of PrP 27-30 monomers.

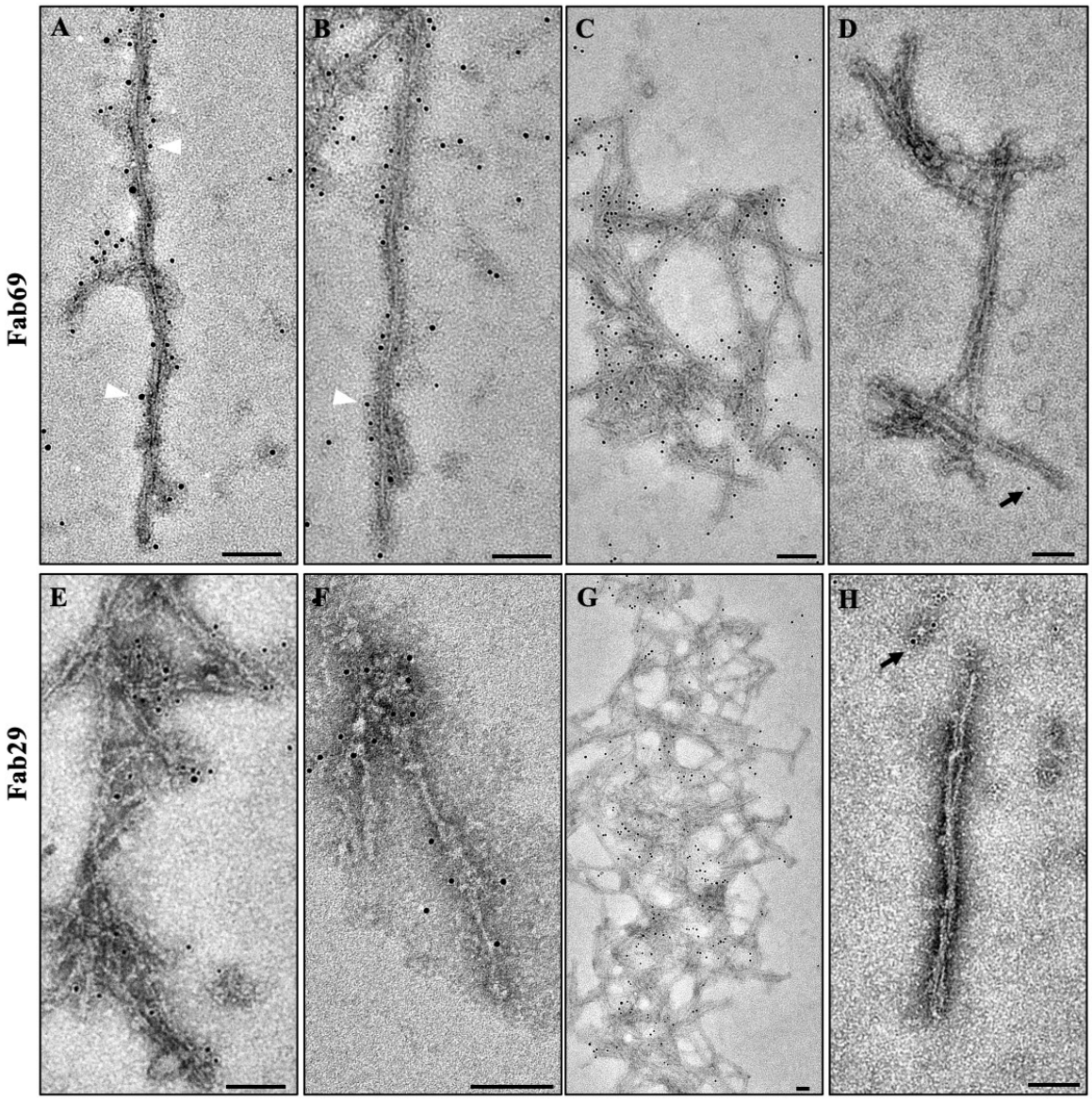
Fab69
Fab29
A
B
C
D
E
F
G
H

Figure 2. 11 Immunogold electron microscopy of purified L-type BSE fibrils.
Decoration of different fibrillar assemblies, including (**A**) two-protofilament, (**B**) one-protofilament, and (**C**) fibrillar aggregates, with Fab 69 and a 5 nm gold-conjugated ternary detection system. White arrowheads highlight a few gold particles along the fibrils. (**D**) Grids that were incubated without primary antibody showed only rare gold particles (black arrow), demonstrating the specificity of the Fab 69 labeling. Immunogold labeling of **(E)** two-protofilament, **(F)** one-protofilament, and **(G)** aggregates of L-type BSE fibrils with Fab 29 and a 5 nm gold-conjugated ternary detection system. (**H**) No specific labeling was observed in the grids with no primary antibody. Scale bar = 100 nm.

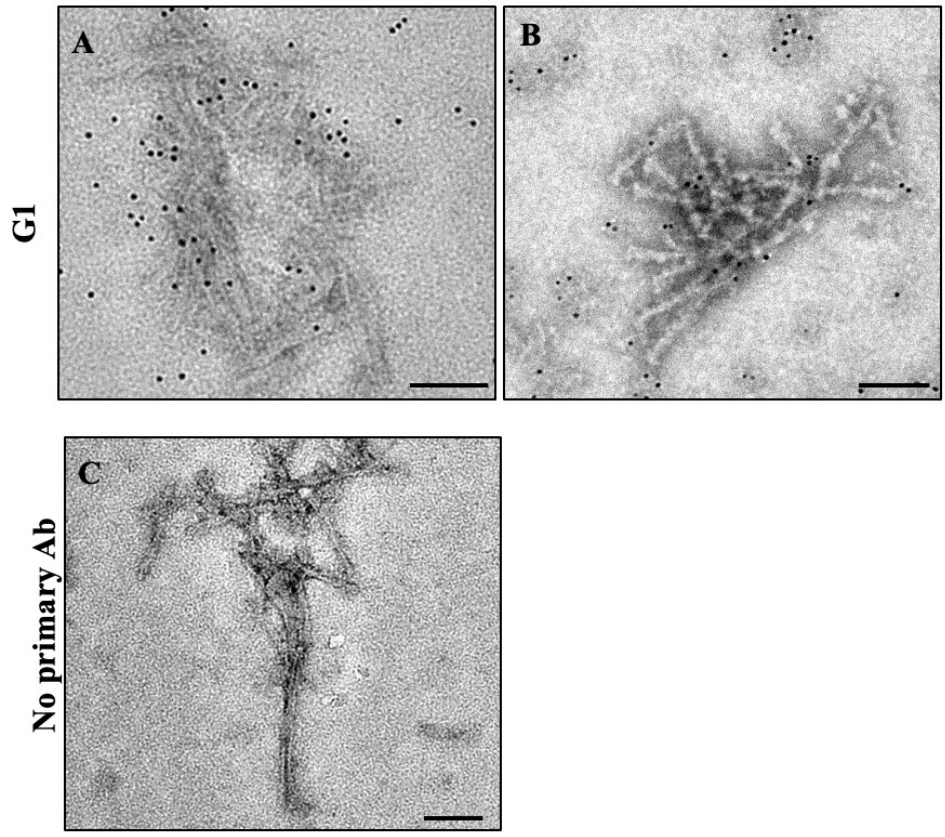

Figure 2. 12 Immunogold labeling of purified L-type BSE fibrils with a conformation-dependent monoclonal antibody.

(**A & B**) Represents L-type BSE fibrils from the final pellet sample labeled with the YEG mAb Sc-G1 monoclonal antibody and a secondary antibody conjugated with 6 nm gold particles. The YEG Sc-G1 monoclonal antibody recognizes a discontinuous epitope on native PrP^{Sc} only. (**C**) Control grid that underwent the same treatment except for the omission of the primary antibody, showing no gold labeling. Scale bar = 100 nm.

2.3.7 Infectivity of purified BSE prions

To confirm whether the purified L-type BSE samples are infectious, we intracerebrally inoculated Tg4092 mice that overexpress bovine PrP^C (Scott, Safar et al. 1997) with samples from the pellet 1 and the PK-treated final pellet. One group of transgenic mice was also inoculated with 1% brain-homogenate without PK treatment. L-type BSE-infected Tg4092 mice were euthanized upon developing clinical symptoms. In all three groups, we observed clinical symptoms of prion disease, confirming that these preparations contain infectivity. Moreover, as shown in Table 2.2, the mice inoculated with the final pellet showed the shortest incubation period of about 206 days compared to those inoculated with the semi-purified P1 pellet and the brain homogenate, which caused disease in 240 days and 227 days, respectively. By using a standard curve that relates incubation period to prion titer we were able to calculate the $LogID_{50}$/ml units for each of these samples (Safar, Scott et al. 2002). Therefore, we were able to conclude that the isolated samples contain infectious L-type BSE prions and that the purification protocol and digestion with PK did not destroy the infectivity.

Mouse Line	Sick/Total	BSE Strain	Inoculum	Incubation Time (Days ± SEM)	Prion Titers ($LogID_{50}$/ml)
Tg4092	11/11	L-type	Brain homogenate	227 ± 15	7.31
Tg4092	5/5	L-type	Pellet 1	240 ± 1.6	6.92
Tg4092	12/12	L-type	Final pellet	206 ± 3.4	8.06

Table 2. 2 Infectivity of the purified L-type BSE samples.

Intracerebral inoculation of transgenic mice with the BSE prion samples obtained during purification experiments.

There were no significant differences between the incubation periods in the two groups that received brain homogenate and the final pellet samples. However, the difference of the incubation times between the mice inoculated with the final pellet and those who received pellet 1 was found to be statistically significant ($p=0.000089$). However, the final pellet showed a higher infectivity titer than the brain homogenate. The infectivity titers in $LogID_{50}$/ml units were calculated from a standard curve relating incubation time to prion dose that was obtained using a C-type BSE (Safar, Scott et al. 2002).

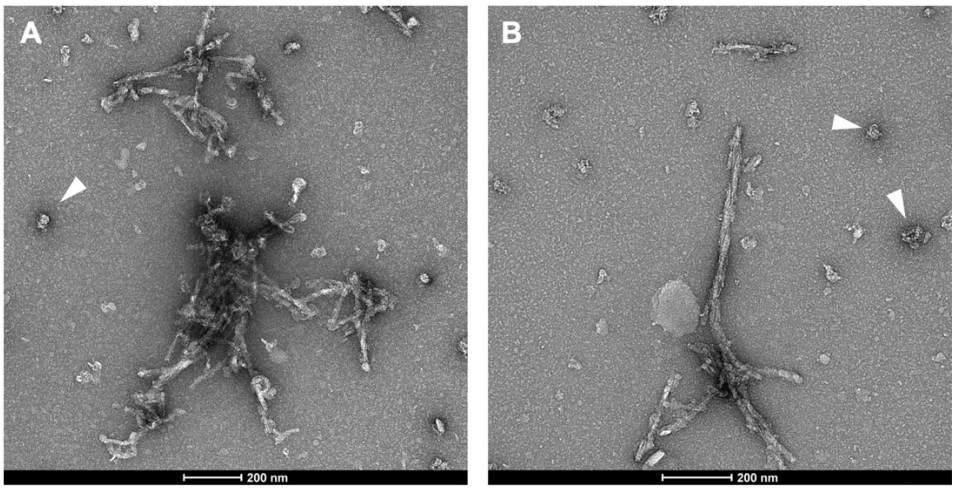

Figure 2. 13 Two representative EM micrographs of semi-purified pellet 1 L-type BSE samples.
The pellet 1 sample was taken before the sucrose gradient ultracentrifugation. Both micrographs show L-type BSE fibrils; however, they contain more amorphous material (some are shown with white arrowheads) compared to the final pellet after sucrose gradient purification.

2.4 Discussion

In this study, we employed electron microscopy and image processing techniques to analyze infectious, brain-derived L-type BSE amyloid fibrils, which included the typical posttranslational modifications: N-linked glycans and a GPI-anchor. We discovered that the L-type BSE prions present as long amyloid fibrils, which matches with previous pathological studies that indicated the increased amyloidogenicity of this strain when compared to the classical (C-type) BSE strain (Casalone, Zanusso et al. 2004). The purified samples presented different conformational states of the infectious prion protein, such as small amorphous aggregates, 2D crystals, isolated amyloid fibrils, and clumps of fibrillar aggregates. Intracerebral inoculation of the purified samples into Tg4092 mice produced clinical prion disease symptoms, confirming that the purified bovine PrP 27-30 maintained its infectious property and is capable of converting normal PrP into its abnormal disease-causing conformer.

Our purification protocol allowed the isolation of a high yield of L-type BSE prion fibrils, which proved to be morphologically heterogeneous when examined by transmission electron microscopy. The observed heterogeneity is consistent with previous works on amyloid fibrils of prions or other proteins (Meinhardt, Sachse et al. 2009, Vazquez-Fernandez, Vos et al. 2016, Scheres, Zhang et al. 2020). The novel finding of our study was the discovery of two distinct morphological populations of L-type BSE amyloid fibrils. The majority of fibrils were observed to be single-protofilament fibrils, with an average width of 10.6 nm. These single-protofilament fibrils accounted for ~73 % of the total fibril population. The second group included thicker two-protofilament fibrils with an average diameter of 22.5 nm, which is about twice the width of the single-protofilament group.

The two-protofilament morphology was consistent with the previous cryo-EM and image processing study on GPI-anchorless RML prion rods, in which each PrP 27-30 fibril was comprised of a twisting pair of intertwined protofilaments (Vazquez-Fernandez, Vos et al. 2016). Previous negative stain EM and cryo-EM studies of other prion strains, such as ME7, 22L, and RML, also reported the presence of two-protofilament fibrils (Sim and Caughey 2009, Wille, Bian et al. 2009, Terry, Wenborn et al. 2016, Terry, Harniman et al. 2019). However, we discovered that mature L-type BSE fibrils are composed of one-protofilament and two-protofilament fibrils in the same samples. We verified this finding by 2D class average and 3D reconstruction techniques. Furthermore, immunogold labeling experiments using Fab fragments that detect epitopes within residues $_{100}$GWGQGGTHGQW$_{110}$ and $_{227}$TQYQRESQAYY$_{237}$ demonstrated that both ends of cattle PrP 27-30 are present in the one- and two-protofilament fibrils.

Previously, PrP (127-147) peptide fragments from elk, bovine, and hamster were examined utilizing electron microscopy and image processing. The resulting bovine PrP (127-157) fibrils, when studied by negative stain electron microscopy, displayed helical morphologies similar to what we have seen in our infectious bovine fibrils. The maximum fibril width for bovine peptide fibrils was found to be 17.0 nm (Glaves, Gorski et al. 2013), which is close to the width of our two-protofilaments fibrils of bovine PrP 27-30 prions. It can be speculated that the peptide fibrils may have adopted a PIRIBS like structure (Glaves, Gorski et al. 2013), similar to recent cryo-EM structures of non-infectious prion protein amyloid fibrils (Glynn, Sawaya et al. 2020, Wang, Zhao et al. 2020). To understand the differences in more details, an atomic-resolution structure of infectious bovine PrP^{Sc} would be required.

An abundance of experimental evidence indicates that the core structure of the infectious prion contains a 4RβS fold (Wille and Requena 2018, Baskakov, Caughey et al. 2019). The conformational differences between prion strains are believed to be related to minor variations in the amino acid sequence of the PrP^{Sc} monomers, more localized in the connecting loops and less affecting the β-strands. Consequently, the cross-sections of the L-type BSE fibril reconstructions (Figures 2.8B-D and 2.9B-D) strongly resemble the ones observed for the GPI-anchorless PrP^{Sc} fibrils (Vazquez-Fernandez, Vos et al. 2016). Also, a recent MD simulation study suggested that the 4RβS arrangement is flexible enough to allow such variations and explain the occurrence of different prion strains (Silva, Vázquez-Fernández et al. 2015, Vazquez-Fernandez, Vos et al. 2016, Spagnolli, Rigoli et al. 2019, Martín-Pastor, Codeseira et al. 2020). Thus, the variations in the quaternary structure of bovine PrP^{Sc}, as compared to previously studied strains, could provide insights into the prion strain phenomenon. From the two main models for prion structure, our findings are compatible with the β-solenoid model only, as we identified both one- and two-protofilament fibrils in our samples of purified L-type BSE prions (Groveman, Dolan et al. 2014, Vazquez-Fernandez, Vos et al. 2016, Wille and Requena 2018). Moreover, our image processing results showed that the average cross-section density of each protofilament from the one- and two-protofilament fibrils adopts a triangular or elliptical shape, which is akin to the cross-section of amyloids from β-solenoidal proteins (Kajava and Steven 2006, Flores-Fernández, Rathod et al. 2018).

In conclusion, our structural analysis of infectious, brain-derived L-type BSE fibrils provided novel insights about the biochemical and conformational characteristics of atypical BSE prions. The presented data offered insights into the quaternary structure of BSE amyloid fibrils, provided a framework for new hypotheses on how prion proteins interact, assemble into amyloid fibrils,

and encrypt prion strains. Investigating strain-specific features of BSE prions could help to resolve the structure of these pathogens and accelerate the development of prion vaccines and other countermeasures.

Chapter 3: Quaternary structure differences among bovine spongiform encephalopathy prion strains

3.1 Introduction

Transmissible spongiform encephalopathies (TSEs) or prion diseases are a group of neurodegenerative conditions caused by pathogenic infectious agents composed of the misfolded and multimeric form (PrP^{Sc}) of a normal cellular protein (PrP^{C}) (Prusiner 1998, Collinge 2001). BSE belongs to a group of transmissible spongiform encephalopathies in cattle, which was first detected in the UK in the 1980s and then spread to other parts of the world, including many European countries, Japan, the US, and Canada. Compelling evidence suggests that the BSE agent has crossed the so-called "species barrier" and transmitted to humans or adapted to other mammals (Casalone, Zanusso et al. 2004). Initial research indicated that a single BSE strain caused prion disease in cattle; however, in 2004, two atypical forms of BSE, termed H-type and L-type BSE, were detected as the causative agents of prion disease in cows (Casalone, Zanusso et al. 2004, Biacabe, Jacobs et al. 2007). These BSE strains can be distinguished by differences in their disease phenotype, electrophoretic mobility in Western blot (WB), and lesion profile in the brain (Biacabe, Laplanche et al. 2004, Casalone, Zanusso et al. 2004). Although BSE incidence is diminishing worldwide, mostly due to an effective feed ban program (Ducrot, Arnold et al. 2008), the emergence of atypical variants has raised significant concerns regarding the disease crossing the species barrier and future human and animal health impacts (Masujin, Okada et al. 2016, Huang, Forshee et al. 2020).

During the pathogenesis of prion disease, the misfolded version of the host-encoded normal prion protein, PrP^{Sc}, induces the conversion of the normal prion protein, PrP^{C}, to its infectious conformer. These proteinaceous agents are partially proteinase K-resistant and can eventually assemble into amyloid fibrils. Although the structure of PrP^{C} is well understood, the

conformation and the exact mechanisms underpinning the transformation of PrP^{C} to PrP^{Sc} remain poorly defined (Wang, Wang et al. 2017, Requena 2020). As the discovery of DNA structure allowed the understanding of its replication mechanisms, characterization of the detailed conformation of PrP^{Sc} is essential to unravelling the mechanism of its folding and propagation (Diaz-Espinoza and Soto 2012, Wille and Requena 2018).

Over the last several decades, extensive structural studies on recombinant and brain-derived prion strains led to the proposing of several models for PrP^{Sc}. However, little global consensus exists regarding the three-dimensional (3D) structure of prions. Currently, two alternative models exist for the structural arrangement of prion fibrils: the Parallel In-Register Intermolecular Beta-Sheet (PIRIBS) assembly (Groveman, Dolan et al. 2014) and the 4-rung β-solenoid (4RβS) model (Wille, Bian et al. 2009, Vazquez-Fernandez, Vos et al. 2016). In the PIRIBS model, PrP^{Sc} monomers stack on top of each other in register perpendicular to the fibril axis, meaning that each amino acid is exactly on top of the same residue in the beta-strand below. Previously, recombinant prion proteins and the smaller fragments of PrP amyloids have been reported to adopt the PIRIBS organization. The 4RβS model, by contrast, is based on the β-solenoid fold, in which each PrP monomer winds around itself. The stacking of β-strands in this configuration is not in-register (Requena 2020). The data from a previous cryo-EM investigation on infectious GPI-anchorless mouse prions were identified consistent with the 4RβS structure (Wille, Bian et al. 2009, Vazquez-Fernandez, Vos et al. 2016). A recent atomistic model developed by Molecular Dynamics (MD) simulation, as well as a solid-state nuclear magnetic resonance (NMR) spectroscopy on infectious recombinant PrP^{Sc}, suggested that the 4RβS structure is a plausible model for the structure of PrP^{Sc} protein (Spagnolli, Rigoli et al. 2019, Martín-Pastor, Codeseira et al. 2020).

One feature of TSEs is the existence of different strains, which could lead to various phenotypes within the same host (Prusiner 1998, Safar, Wille et al. 1998, Castilla, Morales et al. 2008, Collinge 2016). This feature was initially noticed by detecting different migration patterns in Western blot between different prion strains (Bessen and Marsh 1992). In a previous investigation on eight prion strains passaged in Syrian hamsters, each strain was found to have a unique PrP^{Sc} conformation when analyzed using a conformation-dependent immunoassay (Safar, Wille et al. 1998). Additionally, the transmission of different prion strains to mice and hamsters has led to the occurrence of prion diseases with different characteristics, such as banding patterns of Proteinase K (PK)-treated prion protein (PrP^{Sc}), incubation times, phenotypic features, and brain lesion profiles. These differences could indicate the relevance of conformation of prion protein and its clinicopathologic features (Telling, Parchi et al. 1996, Kuczius, Haist et al. 1998, Baron and Biacabe 2001, Baron, Crozet et al. 2004, Biacabe, Jacobs et al. 2007).

Previous reports indicate that the substructural variation of PrP^{Sc} amyloid fibrils may encode the strain specific transmission properties of prions (Wang, Wang et al. 2017, Terry and Wadsworth 2019). However, insufficient evidence supports the significant role that PrP^{Sc} conformation plays in strain properties of prions, partly due to an absence of a detailed structure of PrP^{Sc} (Prusiner 1991, Cohen, Pan et al. 1994, Morales, Abid et al. 2007). Understanding the 3D structure of different prion strains could provide valuable insights into the strain-specific features of various prion strains and their transmissibility.

Although several reports describe the biochemical characteristics and pathology of classical and atypical BSE strains (Biacabe, Laplanche et al. 2004), the detailed knowledge of the conformational aspects of these fatal agents is lacking due to their highly insoluble nature and

aggregation tendency. To our knowledge, no structural analysis has been reported on BSE prions to date. Therefore, in this study, we sought to investigate the structural features of fully glycosylated brain-derived BSE prions.

Our recent study discovered novel features of the more amyloidogenic atypical BSE strain, called L-type BSE (Kamali-Jamil et al., unpublished manuscript). Here, we extended our structural investigation by studying the conformational structure of the infectious, brain-derived prion assemblies of C-type and H-type, two other BSE strains, utilizing electron microscopy and image processing. We generated three-dimensional maps of C- and H-type BSE fibrils and analyzed whether there are morphological differences between these strains. Furthermore, we report the ultrastructural localization of C-type and H-type BSE prions by employing immunogold labeling using monoclonal anti-PrP Fab fragments. Our findings represent the first insights into the quaternary structure of classical and H-type atypical BSE prions and supports the four-rung beta-solenoid model for the structure of infectious prion protein. These findings could also help to identify the relationship between pathology and structural features among different strains.

3.2 Material & Methods

3.2.1 Canadian C-type and H-type BSE prions

The brain tissues from 2 H-type and 2 C-type BSE challenged Canadian cattle were used to inoculate Tg4092 transgenic mice. Of the 19 BSE cases detected in Canada, one was typed as H-type BSE, and 17 cases were C-type BSE. The H-type BSE Canadian field case animal was a Charolis/Hereford cross breed heifer that was 16.5 years old when it was sacrificed and tested.

Brain samples from this case were confirmed BSE positive using histology, immunohistochemistry and molecular methods at the Canadian National BSE Reference Laboratory. Brain tissue from this H-type BSE field case was used to challenge 2 steer calves in 2009. The two classical BSE steers used for structural analysis were challenged with brain material from the 2nd and 3rd Canadian BSE field cases. The 2nd case was a Holstein heifer that was euthanized and tested at 8.2 years of age. The 3rd case was an Angus/Charolis cross breed heifer the was 6.8 years of age when it was euthanized and tested. Both of these cases were confirmed as classical BSE positive at the Canadian National and BSE Reference Laboratory using histology, immunohistochemistry and western blot.

To passage the Canadian BSE field cases, colliculus tissue was homogenized to 10% (w/v), sonicated, spun to remove large cellular debris. The supernatant was aspirated into a syringe for subsequent injection into the cranial cavity of steer calves at approximately 5 months of age (1mL of 10% homogenate per steer). Prior to inclusion in this project, steers of interest were genotyped to ensure no abnormalities were present in the prion gene. Once confirmed as genetically normal, the steers were moved into the biosafety level 3 containment pens at the Canadian Food Inspection Agency (CFIA) Lethbridge Laboratory. Following the challenge, the animals were monitored regularly for the appearance of clinical signs. At 16 months post-challenge, both of the H-type BSE challenged steers began to show clinical signs of BSE infection. With noted progression over the next several weeks, the steers were sacrificed at 17.3 and 17.6 months post challenge. The 2 C-type BSE challenged steers incubated for almost 2 years before showing clinical signs of diseases. At 24 and 27 months post challenge, the steers challenged with C-type BSE field case 2 and case 4, respectively, were euthanized. Brain stem from each of the animals was tested immediately on the Prionics rapid test platform with OD

values of 4400 or greater for all 4 animals. The kit lot positive/negative cut-off OD value was 113 with >95% of BSE negative samples giving an OD value of 0 using this kit lot. Sample homogenates were also strong positive on Western blot with 3 distinct immuno-reactive glycoforms.

To type the protease-resistant prions present in the central nervous system tissue of BSE challenged steers, the homogenate was run on a hybrid Western blot. This assay utilizes mild and stringent protease digestion, a panel of antibodies with different epitopes and molecular weight/glycoform ratios to type BSE samples. The PrP^{Sc} from the 2 steers challenged with C-type BSE field case brain homogenate is extremely resistant to protease digestion and has glycoform ratios (~2:1 ratio of di- to mono-glycosylated isoforms), molecular weights (28.5 kDa/22 kDa/18.5 kDa) and immuno-reactivity profiles (6H4 (Prionics AG, Switzerland) P4 (R-Biopharm AG, Germany) (N terminal Ab)) consistent with classical BSE. When brain homogenate from the H-type BSE challenge steers was digested and tested, the results were distinctly different. The H-type BSE challenged steer PrP^{Sc} also has a 2:1 di- to monoglycosylated immuno-reactive protein ratio, but when digested under stringent protease conditions, the H-type BSE PrP^{Sc} was significantly degraded. The PrP^{Sc} from these 2 steers was also reactive with both 6H4 and P4 antibodies, indicating that this protein fragment contains more of the N terminal portion of the PrP protein than C-type and L-type BSE PrP^{Sc}. These BSE typing results were consistent with the hybrid Western blot results for the Canadian BSE field case used for challenge and confirmed that the biochemical characteristics of the PrP^{Sc} were maintained following intra-species passage.

3.2.2 Mice

Transgenic mice overexpressing bovine prion protein, termed Tg4092 (Scott, Safar et al. 1997), were kindly provided by Dr. Stanley B. Prusiner (University of California, San Francisco). Experimental C-type BSE and H-type BSE isolates, obtained from the Canadian Food Inspection Agency CFIA, Lethbridge, were used for intracerebral inoculation of the transgenic mice.

3.2.3 Genotyping assay

The genotyping experiments were performed as described previously (Kamali-Jamil et al., unpublished manuscript).

3.2.4 Purification of Classical and H-type BSE strains from transgenic mice brains

BSE fibrils were prepared from the brains of two groups of terminally sick Tg4092 mice infected with C- and H-type BSE prions using a PTA purification protocol (Safar, Wille et al. 1998). For each group, the isolation experiment started with 4 brains from BSE-infected transgenic mice. Brain tissues were then homogenized at 20% concentration (w/v) in phosphate-buffered saline (PBS) and centrifuged for clarification at 500 × g. Next, the supernatants were collected and mixed with 4% Sarkosyl in PBS. Then, the samples were treated with PK (50 μg/ml) for 1 hour. Following the termination of the reaction with Phenylmethylsulfonyl Fluoride (PMSF), the samples were incubated with 2% phosphotungstic acid (PTA, pH 7.2) (SIGMA P-6395) at 37°C. The first pellets were obtained by centrifugation of the samples at 16,000 × g for 30 minutes after PTA incubation. The pellets were resuspended using 0.2% Sarkosyl in PBS and spun at 16,000 × g for 30 minutes after adding 2% Sarkosyl in PBS and 2% PTA. Afterwards, the final pellets were obtained and resuspended in 0.2% Sarkosyl in PBS. The samples were stored at -80°C for

immunoblot and TEM analyses. To increase the final yield, we performed further purification experiments using 8 brains from C-type and H-type BSE-infected mice. As this preparation contained the ideal fibrillar yield; therefore, the following purifications were performed using eight mice brains, and these samples were used for TEM investigations.

3.2.5 Western blot and silver staining

An equal volume of gel-loading sample buffer (Bio-Rad) containing 2% SDS was added to all samples, and each heated at 100°C for 10 minutes before loading on 12% acrylamide gel (Bio-Rad). Samples were run for 1 hour at 150 volts and blotted electrically onto a polyvinylidene difluoride (PVDF) membrane (Millipore) at 100 volts for 1 hour. Blocking was performed using 5% (w/v) BSA in tris buffered saline solution containing 0.05% Tween 20 (v/v) (TBST). The anti-PrP monoclonal antibody D15.15, a 1:1000 dilution, was used for immunodetection. Next, the membranes were incubated for 1 hour in alkaline phosphatase-conjugated anti-mouse IgG (Bio-Rad) at a 1:10,000 dilution in TBST. Following the washing steps, development was performed using alkaline phosphatase (AP) substrate (Bio-Rad). The results were detected by chemiluminescent visualization using ImageQuant (GE Life Science).

Silver staining was performed according to a previously described protocol (Merril, Dunau et al. 1981, Wille, Shanmugam et al. 2009) as follows: the samples were mixed with an equal volume of sample buffer and were loaded on 12% polyacrylamide gels and run for 60 minutes at 150 volts. The gels were then incubated in fix solution (50% methanol, 12% acetic acid) for 30 min. Next, the samples were transferred to the SDS removal solution (10% ethanol, 5% acetic acid) for 30 minutes at room temperature. Following 2 minutes incubation in Farmers solution (containing: 0.15 g potassium ferricyanide, 0.3 g sodium thiosulfate, 0.05 g sodium carbonate)

and washing steps, the gels were added to 0.2% (w/v) AgNO3 solution for 20 minutes and rinsed briefly in distilled water. Developing solution (15 g sodium carbonate and 250 microL 30% formaldehyde stock solution) was added until the signals appeared, and the process stopped with 0.2% acetic acid.

3.2.6 Bioassay

C-type and H-type BSE purified samples were inoculated into two separate groups of Tg4092 mice. 30 µl volume of 1% brain homogenate and final pellet samples from the purification experiments were used for inoculation. For each sample, at least 5 animals were assigned for intracerebral inoculation. The mice were examined regularly for the onset of prion disease neurological signs. Terminally sick animals were euthanized by CO_2 asphyxiation followed by cervical dislocation. The brains were collected and stored at -80°C for future analysis. Prion titers for the C-type and H-type BSE samples were determined by measuring the incubation time intervals from inoculation to the onset of neurological illness and calculated as $LogID_{50}$/ml units based on a standard curve relating C-type BSE incubation times to prion dose (Safar, Scott et al. 2002).

3.2.7 Ethics Statement

The BSE transmission experiments were carried out at the Canadian Food Inspection Agency, Lethbridge Laboratory, Lethbridge, Alberta, in accordance with guidelines set by the Canadian Council on Animal Care and approved by the animal care use committee for the CFIA-ADRI Lethbridge Laboratory (ACC#0902). All bioassay experiments were carried out at the Centre for Prions and Protein Folding Diseases (CPPFD), University of Alberta, in accordance with

guidelines set by the Canadian Council on Animal Care and approved by the animal care use committee for Health Sciences 2 (protocol AUP00000884).

3.2.8 Negative staining

The specimen preparation for TEM involved absorbing 10-µl of the purified samples onto freshly glow-discharged 400 mesh carbon-coated copper grids (Electron Microscopy Sciences), allowed to adsorb for 1 minute. Then, the grids were washed in 1 drop of (50 µl) 0.1 M and 0.01 M ammonium acetate solutions each and stained twice with 50 µl freshly filtered 2% solution of uranyl acetate. The grids were air-dried and explored using a Tecnai G20 transmission electron microscope (FEI Company) operating at an acceleration voltage of 200 kV. Electron micrographs were recorded with an Eagle 4k x 4k CCD camera (FEI Company). Applied defocus levels for recording the images were in the range of 1-2 µm.

3.2.9 Width measurement

Width measurements were performed on C-type and H-type BSE fibrils using EMAN's boxer program. For each fibril, the maximum diameter between two crossover regions was considered for measurement.

3.2.10 Immunogold labeling

The pellet samples from purified C-type and H-type BSE prions were used for electron microscopy immunogold labeling. For this method, Fab 69 anti-prion monoclonal Fab, selected from a phage display library reacting with an epitope within amino acid residues $_{100}$GWGQGGTHGQW$_{110}$ of bovine prion protein, was utilized for immunodetection (Senatore, Frontzek et al. 2020). Fab 69 was expressed in *E.coli* BL21(DE3) as a soluble and functional

protein. Following bacterial cell lysis, his-tagged Fab fragments were isolated using IMAC chromatography. (Rathod *et al*., unpublished data).

The immunogold labeling experiment was carried out according to a previous protocol (Wille, Govaerts et al. 2007). First, ~7 µl of C- and H-type BSE final pellet samples were placed onto glow discharged formvar/carbon-coated nickel grids (Ted Pella, Inc.) for ~5 minutes. After three times wash using 50 µl 0.1 M and 0.01 M ammonium acetate buffer (pH 7.4), samples were incubated with 3M urea for 10 minutes and washed three times. Next, two drops (50µ) of freshly filtered 2% sodium phosphotungstic acid (PTA) (pH 7.2) was used for staining. Samples were blocked using 0.3% bovine serum albumin (BSA) in Tris buffered saline (TBS: 50 mM Tris-HCl, pH 7.4; 150 mM NaCl) for ~ 1 hour. After blocking, the grids were treated for 2 hours with Fab 69 primary antibody. This step was omitted for the control grids of C- and H-type BSE samples. After 5 times washes in 0.1% BSE, all grids were incubated with goat F(ab')2 anti-human IgG F(ab')2 (Abcam ab98531) for 2 hours. Then, the samples were transferred to droplets of 5-nm-gold-conjugated rabbit anti-goat IgG (Abcam ab202670) for 2 hours. The grids were washed using 0.1% BSA, TBS solution, and water and underwent final staining in 2% PTA. Finally, the samples were air-dried and examined using a Tecnai G20 transmission electron microscope (FEI Company) operating at an accelerating voltage of 200 kV. Electron micrographs were recorded with an Eagle 4k x 4k CCD camera (FEI Company).

3.2.11 2D classification

Three C-type BSE fibrils showing subunit repeats were selected for 2D classification. A reference-free 2D classification was performed by applying boxes of sizes of 200 by 200 pixels with a 50% overlap along the fibrils' axis between two crossovers using the EMAN's boxer

program. Class averages were produced by alignment and classification of the particles obtained from fibril segmentation, and the classes were generated using EMAN's boxer startnrclasses program (Ludtke, Baldwin et al. 1999).

3.2.12 Reconstruction of the 3D maps

EM micrographs from the pellet samples of C-type and H-type prions presenting isolated, non-overlapping amyloid fibrils were picked for image processing approaches. The process started with segmenting the fibrils utilizing EMAN's boxer program. The selected fibrils were windowed into individual images using a pixel size of 300 × 300 or 200 × 200 and about 5% to 10% inter-box size distance (Ludtke, Baldwin et al. 1999, Vazquez-Fernandez, Vos et al. 2016). For each fibril, following assigning angles based on the helical repeat, an initial 3D model was generated utilizing the SPIDER program (Frank, Radermacher et al. 1996). The initial reconstructions were refined and low-pass filtered to 20 Å (Glaves, Gorski et al. 2013).

To further refine the 3D volume, an extended reconstruction approach was conducted (Vazquez-Fernandez, Vos et al. 2016), in which the reconstructed volume was rotated 90° about the z-axis and sliced along the yz plane. The stack of images then was aligned and averaged through iterative processes, and centred, replicated, and corresponding symmetry was applied. The final 3D map was generated using the IMAGIC program (van Heel, Harauz et al. 1996). UCSF Chimera software was used for visualization of the 3D reconstructions (Pettersen, Goddard et al. 2004).

3.3 Results

3.3.1 Propagation of C-type and H-type prions in transgenic mice

A total of 19 BSE field cases have been detected in Canada since May 2003; of these cases, one has been typed as H-type BSE, one has been typed as L-BSE, and the rest were classical BSE (C-type BSE). Brain tissue from all of these animals was collected and retained following confirmation, but numerous factors have resulted in less than optimal tissue quality. In order to generate additional, good quality tissue, brain homogenate from several of the Canadian BSE field case has been passaged in cattle. Passage has been completed for H-type atypical BSE cases as well as the first 3 cases of classical BSE detected in Canada. Brain tissue from the 2 H-type BSE and 2 C-type BSE challenged cattle were used for intracerebral inoculation of transgenic mice that overexpress bovine PrP (Tg4092) (Scott, Safar et al. 1997). Brain tissues from terminally sick transgenic mice were extracted and used for structural analyses of C- and H-type BSE prions.

3.3.2 Isolation and biochemical characterization of C-type and H-type BSE prions

C- and H-type BSE prions were isolated from the brains of terminally sick transgenic mice overexpressing bovine prion protein (Tg4092). The first step involved the purification and biochemical characterization of C-type and H-type BSE prions from infected mice brains. For this purpose, purifications using 4 to 8 brains were performed. The purification protocol involved treatment with Proteinase K (PK) and phosphotungstic acid (PTA), with two centrifugation rounds. Samples were taken from each step of the purification procedure and analyzed by SDS PAGE followed by Western blotting or silver staining. Western immunoblot of C-type (Figure 3.1A) and H-type BSE (Figure 3.1C) preparations using a monoclonal anti-PrP antibody,

D15.15, showed the apparent molecular weight of the N-terminally truncated form of PrP^{Sc} (PrP 27-30) in the final pellet, confirming the successful isolation of the BSE prions. The SDS-PAGE and silver stain gels for C-type (Figure 3.1B) and H-type (Figure 3.1D) BSE isolations showed no signal in the supernatant. The bands observed in the lanes corresponding to the final pellets were also detected with the anti-prion antibody D15.15 in the Western blot examination.

In a separate experiment, we used Western blot analysis as a molecular tool to detect the differences in the migration pattern of the PK-resistant PrP^{Sc} between the BSE strains. Brain homogenate samples from C-, H-, and L-type BSE-affected Tg4092 mice were treated with 50 μg/ml PK and examined using Western blot with anti-PrP D15.15 monoclonal antibody. As expected, the three PK-digested BSE isolates exhibited a relatively distinct banding pattern in Western blot, resembling previous reports on C-, H-, and L-type BSE strains (Biacabe, Laplanche et al. 2004, Casalone, Zanusso et al. 2004, Jacobs, Langeveld et al. 2007). For example, as previously described, compared to classical BSE, atypical H- and L-type BSE showed a higher and lower molecular mass of unglycosylated prion protein in Western blot, respectively (Figure 3.2A).

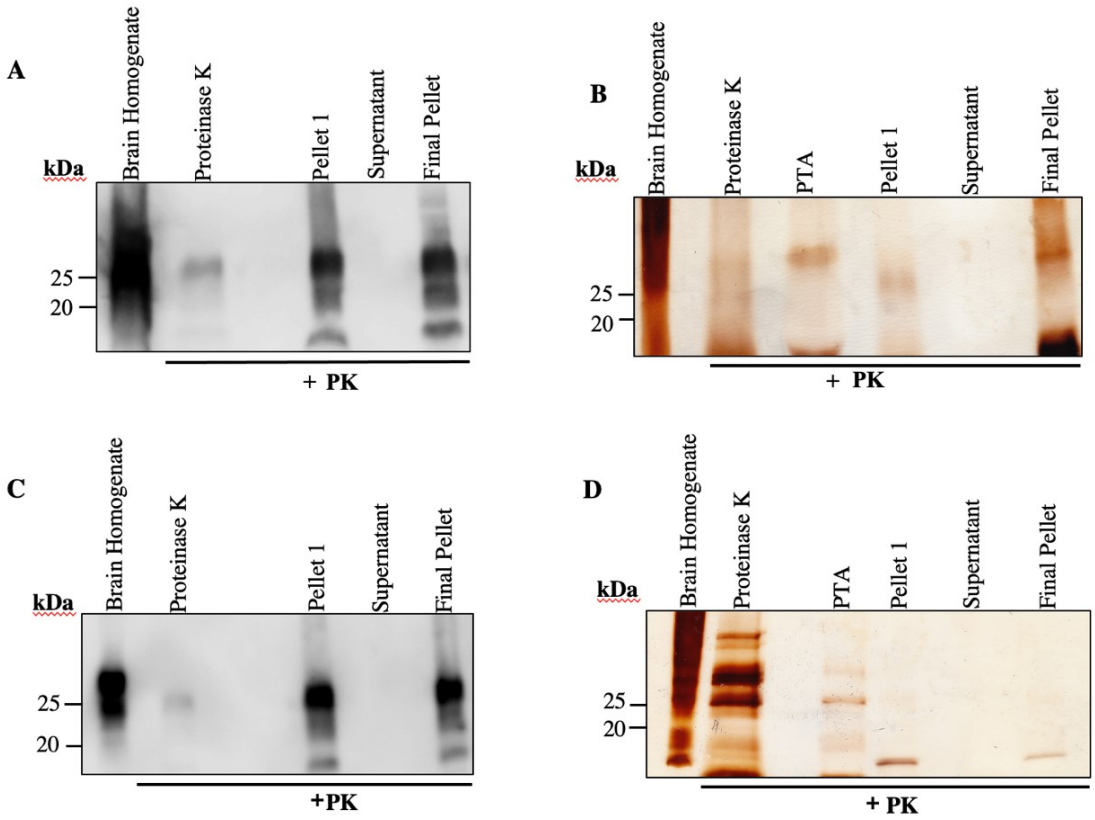

Figure 3. 1 Biochemical characterization of purified C-type and H-type BSE prions.
(**A**) Western-blot detection of purified C-type BSE preparations. Samples were resolved on SDS-PAGE, and prion protein was detected using D15.15 anti-PrP monoclonal antibody. The PK-digested purified pellet 1 and the final pellet show the typical three bands of PrP 27-30 corresponding to un-, mono- and diglycosylated prion protein. (**B**) Silver stain SDS-PAGE gel of C-type BSE representing samples taken at different steps of PTA purification. (**C**) Western-blot examination of purified H-type BSE samples using D15.15 anti-prion monoclonal antibody. The PK-digested purified pellet 1 and the final pellet show the typical three bands of bovine PrP 27-30. (**D**) Silver stain SDS-PAGE gel of C-type BSE representing samples obtained at different steps of PTA purification.

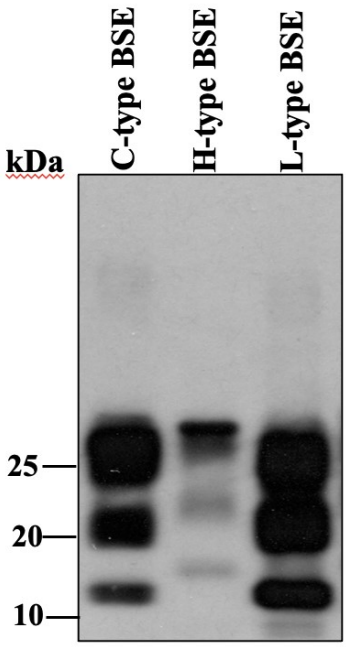

Figure 3. 2 Electrophoretic analysis of classical and atypical BSE prions.

Western blot detection of PrP^{Sc} in PK-treated brain homogenates of C-, H- and L-type BSE prions. Signals were detected using D15.15 monoclonal antibody. In atypical BSE isolates, the electrophoretic migration of the unglycosylated PrP^{Sc} is slightly higher (H-type) or lower (L-type) than classical BSE (C-type).

3.3.3 Morphological analysis of C-type and H-type BSE fibrils

Having confirmed the isolation of C-type and H-type BSE prions using biochemical analysis, we sought to investigate the presence of amyloid fibrils in the isolated BSE samples to analyze whether there are morphological differences between the two BSE strains. We examined the negatively stained samples employing transmission electron microscopy (TEM). The fibrils were morphologically distinguishable between the two BSE strains, while slight heterogeneity existed within each strain (Figure 3.3A-B). This phenomenon seems to support the previous view that structural heterogeneity not only exists between prion strains but also could be manifested within a specific prion population (Angers, Kang et al. 2010, Igel-Egalon, Bohl et al. 2019). Furthermore, the abundance of C-type BSE fibrils was found to be relatively lower than the H-type fibrils, which raises interesting questions if other forms of C-type BSE prions (e.g. amorphous aggregates) might be more prominent. However, compared to the results drawn from our previous study on L-type BSE fibrils (Kamali-Jamil et al., unpublished manuscript), a significantly lower yield of fibrils was found in C- and H-type BSE samples, which is not surprising given the more amyloidic nature of L-type BSE prions (Casalone, Zanusso et al. 2004).

The widths of C-type and H-type BSE fibrils were measured 20.3 ± 6.8 nm and 24.5 ± 4.8 nm on average, respectively (Table 3.1), comparable to that of two-protofilament L-type BSE fibrils of our previous work (22.5 nm) (Kamali-Jamil et al., unpublished manuscript). The widths obtained for C- and H-type BSE fibrils are in range with the results of the previous investigations on ex vivo infectious PrP^{Sc} amyloid fibrils measured ~20 nm, studied by cryo-EM and negative staining (Terry, Wenborn et al. 2016, Terry, Harniman et al. 2019). However, our two-protofilament BSE fibrils are much wider compared to the ~10 nm fibrils detected in the

previous cryo-EM study of an infectious GPI-anchorless mouse prion strains with no N-linked oligosaccharides (Vazquez-Fernandez, Vos et al. 2016). Overall, the width differences between our BSE fibrils and previous studies on other prion strains could be explained by factors such as strain differences, polymorphic nature of amyloid fibrils, or the experimental conditions of sample preparation, like removing surface glycans (Wang, Zhao et al. 2020).

The overall architecture of C-type BSE fibrils. The purification approach using PK and PTA yielded dispersed, isolated, non-overlapping C-type BSE fibrils, appropriate for our structural analysis purpose. Negative stain electron microscopy examination involved the adsorption of the purified samples to carbon-coated EM grids and staining with 2% uranyl acetate. EM analyses of the final pellet of C-type BSE samples revealed relatively short fibrils (Figure 3.3A) with an apparent helical twist. The lengths of the fibrils were measured between 80 nm and 474 nm, with a mean value of 193 ± 72.0 nm. The average distance between two crossovers in C-type BSE fibrils was 158.8 ± 43.1 nm (Table 3.1).

By TEM analysis, we were able to discern two dominant morphologies of C-type BSE amyloid fibrils with respect to the number of protofilaments: one- and two-protofilament fibrils. In contrast to our previous observation on atypical L-type BSE, in which the total number of one-protofilament fibrils was significantly higher than the two-protofilament ones, the majority of the C-type fibrils, accounting for 79% of the total population, consisted of two protofilaments. A smaller group, corresponding to 21% of the fibrils, appeared to have one protofilament (Figure 3.3A-5), with approximately half the thickness (~9 nm) of the two-protofilament ones (~ 20 nm). When we quantified the distinguishable single and two-protofilament fibrils, the C-type BSE sample was found to contain the lowest number of fibrils in comparison to H-type BSE and the L-type isolates from our previous work (Figure 3.4).

The overall architecture of H-type BSE fibrils. The EM investigation of several negative stain micrographs from H-type BSE samples revealed heterogeneous fibrils twisted around each other. The length of the fibrils varied between approx. 100 and 1000 nm, with an average of 315.1 ± 169.1 nm. The distance between the two crossovers or helical pitches was obtained 137 ± 33.2 nm on average (Table 3.1). Occasional bundles of fibrils containing more than two filaments were observed. Fibrils from H-type BSE isolates displayed greater heterogeneity as compared to the other two BSE strains (Figure 3.3B). No single protofilament fibrils were observed in the EM study of this BSE strain. Based on the fibril diameters mentioned above, the H-type fibrils were wider compared to the other two BSE strains.

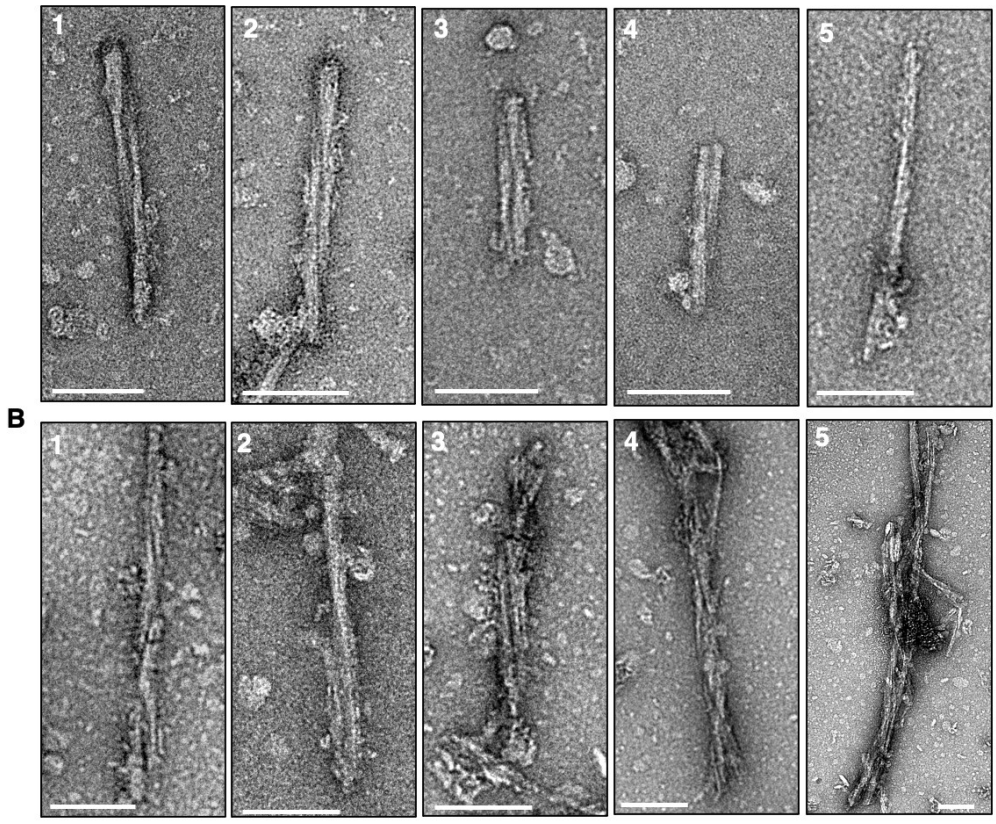
A
1
2
3
4
5
B
1
2
3
4
5

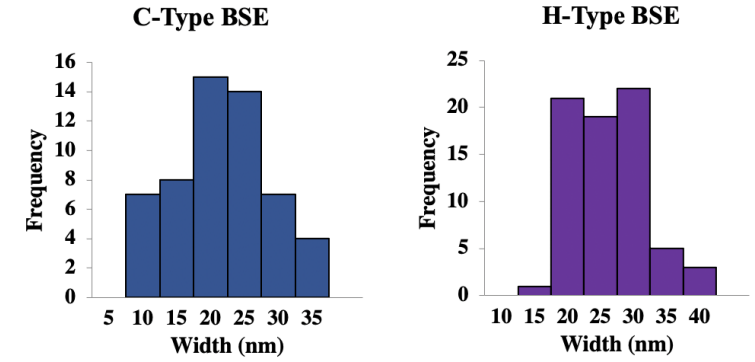
C
C-Type BSE
Frequency
16
14
12
10
8
6
4
2
0
5 10 15 20 25 30 35
Width (nm)
H-Type BSE
Frequency
25
20
15
10
5
0
10 15 20 25 30 35 40
Width (nm)

Figure 3. 3 Visualization of brain-derived C-type and H-type BSE fibrils using electron microscopy.

(**A**) Representative negative staining TEM images of fibrils from C-type BSE purified pellet showing helical morphology. Micrographs 1-4 show two protofilaments, and image 5 represents a fibril containing a single protofilament. Scale bar = 100 nm. (**B**) Representative negative staining TEM images of fibrils from H-type BSE final pellet showing a helical twist. The fibrils appear to consist of two or more protofilaments. Scale bar = 100 nm. (**C**) Width distribution of BSE fibrils. Histogram of the width measurement of C-, and H-type BSE fibrils. The maximum width from a total of 55 C-type and 72 H-type BSE fibrils was measured using EMAN's boxer software.

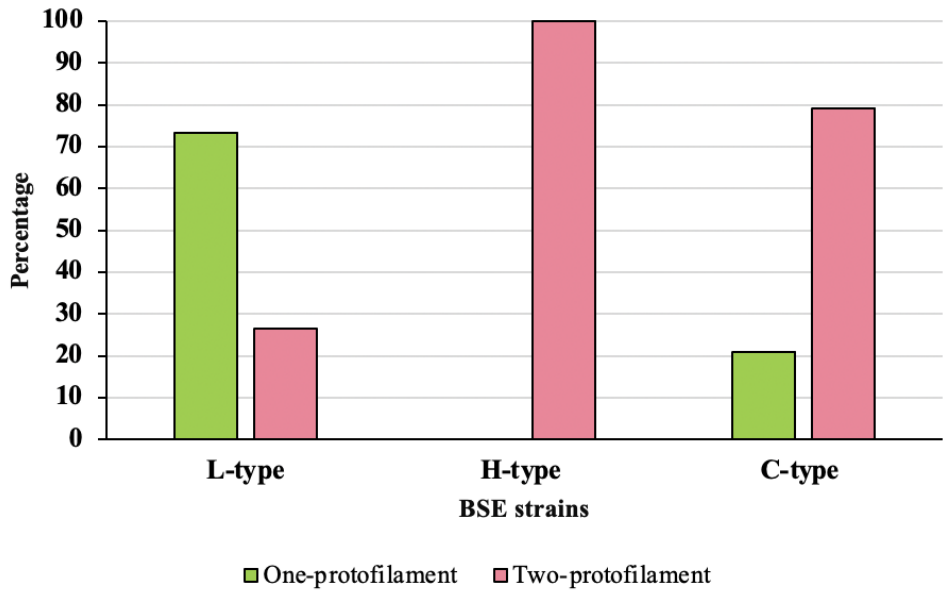

Figure 3. 4 Relative proportions of one- and two-protofilament fibrils in three BSE strains. The bar chart indicates the percentage of C-, H-, and L-type BSE fibrils containing one (green) or two (pink) protofilaments. Compared to L-type BSE fibrils, which contained 73% one-protofilament fibrils (N= 867), only 21% of C-type fibrils (N= 55) were composed of one protofilament and none of the H-type fibrils (N= 66). The L-type BSE preparation contained a significantly higher number of fibrils compared to H- and C-type BSE samples.

BSE Strain	Number of Fibrils	Width Mean ± SD (nm)	Helical Pitch Mean ± SD (nm)	Length Mean ± SD (nm)
C-type	55	20.3 ± 6.8	158.8 ± 43.1	193.3 ± 72.0
H-type	72	24.5 ± 4.8	137 ± 33.2	315.1 ± 169.1

Table 3. 1 Dimensions of negatively stained brain-derived C-type and L-type BSE fibrils.

The measurements were performed using EMAN's boxer image software.

3.3.4 Image processing

After detecting suitable C- and H-type BSE fibrils in the purified samples, we employed image processing approaches on selected micrographs to create reliable three-dimensional (3D) reconstructions of C- and H-type BSE fibrils. Towards this goal, the samples were imaged at a magnification of 29,000x to 50,000x using a Tecnai G2 electron microscope. The step-by-step procedure of the 3D reconstruction method on individual BSE fibrils is depicted in Figure 3.5.

The 3D maps were generated, based on the helical reconstruction technique, from isolated non-overlapping fibrils showing an apparent helical twist. Several 3D models were created using various independently isolated fibrils. In an extended reconstruction approach, the initial 3D models were subjected to further refinements to eliminate the contribution of the unwanted densities corresponding to the background of the images. Figure 3.6 shows representative 3D volumes of individual C-type and H-type two-protofilament BSE fibrils, each presenting a fibrillar structure composed of two intertwined protofilaments winding around each other with a central gap. The overall architecture of both reconstructions resembles the previous helical reconstructions of the cryo-EM micrographs of an anchorless RML prion strain in terms of the number of protofilaments and the overall helical twist (Vazquez-Fernandez, Vos et al. 2016). Contour maps were generated from the cross-section areas of C-type and H-type reconstructions (Figure 3.6A-6 and 3.6B-6). The overlay of the 3D maps with 2D projections of the cross-section of the reconstructions indicated higher densities in the middle of each cross-section (Figure 3.6A-7 and 3.6B-7).

Several EM micrographs were used to generate further 3D reconstructions of different C-type and H-type BSE fibrils. Figure 3.7 presents three representative helical reconstructions of each

BSE strain, showing heterogeneous conformations. Despite the apparent morphological variations, all reconstructed fibrils display a helical twist. Consistent with our TEM analysis, the 3D reconstructions of C-type fibrils exhibited two main polymorphs: two-protofilament fibrils, accounting for the major fibrils' population, and fewer one-protofilament fibrils (Figure 3.7A-B). The same reconstruction approach on isolated H-type BSE fibrils yielded helical fibrils containing two protofilaments twisting around each other with heterogeneous morphology (Figure 3.7D-E). The 2D projections of the cross-section regions of the 3D maps of C-type and H-type BSE fibrils agree well with the densities corresponding to each protofilament (Figure 3.7C and F). Despite the heterogeneity, the cross-sections of all C- and H-type BSE reconstructions appeared to have an oval or circular shape. Averaging the cross-section slices of the 3D maps of one- and two-protofilament fibrils yielded densities confirming the number of protofilaments in each fibril (figure 3.8). For both H-type and C-type BSE strains, comparing the 2D reprojections of the reconstructions with the raw images showed good correspondence, indicating that the reconstructions are consistent with the data (Figure 3.9).

By morphological examination of the EM images, interestingly, some fibrils of classical BSE fibrils were found to have visible subunit repeats; thus, we performed two-dimensional (2D) classification using the fibrils exhibiting such characteristics. As shown in Figure 3.10B, the averaging of hundreds of particles from the selected C-type BSE images provided better visualization of the amplified subunit repeats by increasing the signal-to-noise ratio. The distance between the two densities was measured 36 Å to 40 Å, perhaps corresponding to the height of 8 cross-beta structures (8 x 4.8 Å). Considering the 19.2 Å height of each PrP^{Sc} monomer, as identified in the previous X-ray fiber diffraction study (Wille, Bian et al. 2009), the observed repeating distances could be indicative of the size of a stacked PrP 27-30 dimer.

Overall, given that the resolution limits of the negative staining method (Ohi, Li et al. 2004), we could not resolve secondary structure elements in our 3D maps. However, the high-contrast quality of the images, plus the advanced image processing tools, allowed us to gain insights into the quaternary structure of C- and H-type BSE prions. These data enabled us to establish the morphological differences between the two strains at this level.

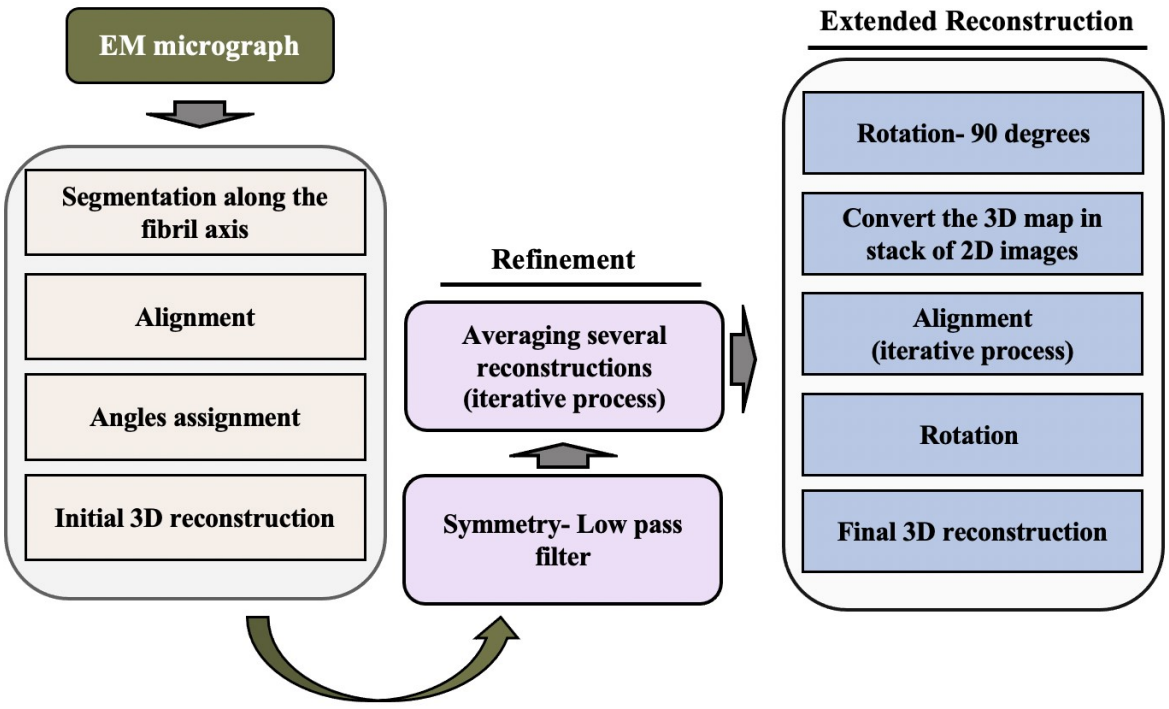

Figure 3. 5 Flow diagram of the helical reconstruction process.

For this process, appropriate EM micrographs of the fibrils showing clear helical pattern were selected. The image processing procedure started with segmentation along the individual fibril's axis with overlapping boxes, and rotation angles were assigned to the boxed particles. Next, initial 3D reconstructions were generated by back projection. In the averaging process, several refined initial 3D reconstructions of the same fibrils were subjected to iterative rounds of averaging and alignment. This stage was followed by an extended helical reconstruction process, in which the average 3D volume was rotated 90 degrees, and the sliced images of the cross-section of the 3D map were obtained. Subsequently, the 2D images of the fibril cross-sections were aligned, averaged and symmetrized. After rotation of the 2D particles, the final 3D volume was created using IMAGIC software.

A

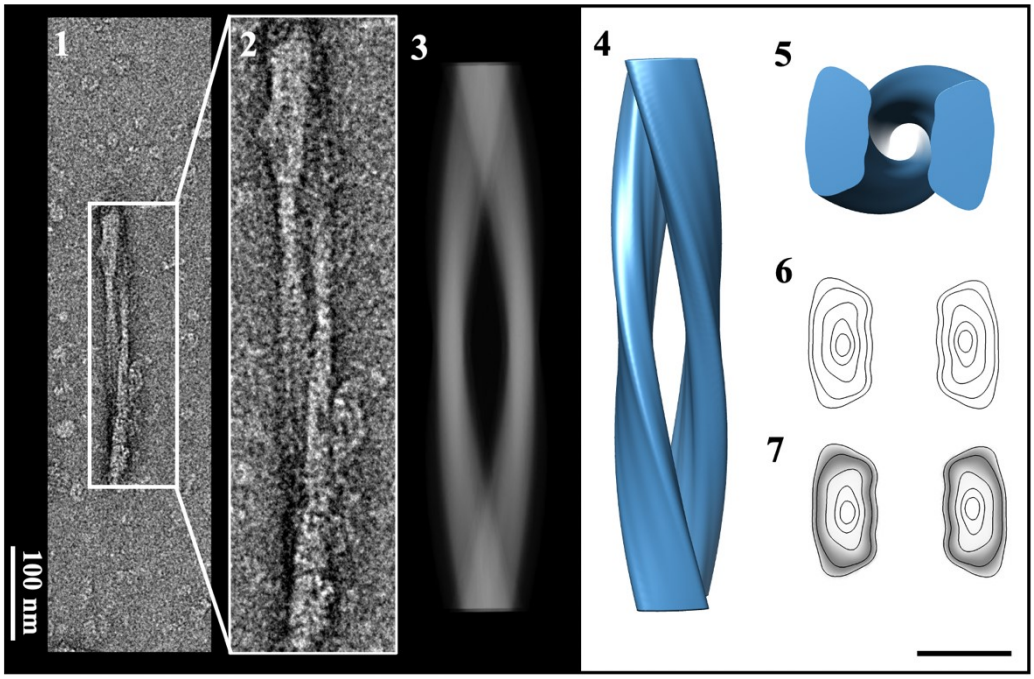

B

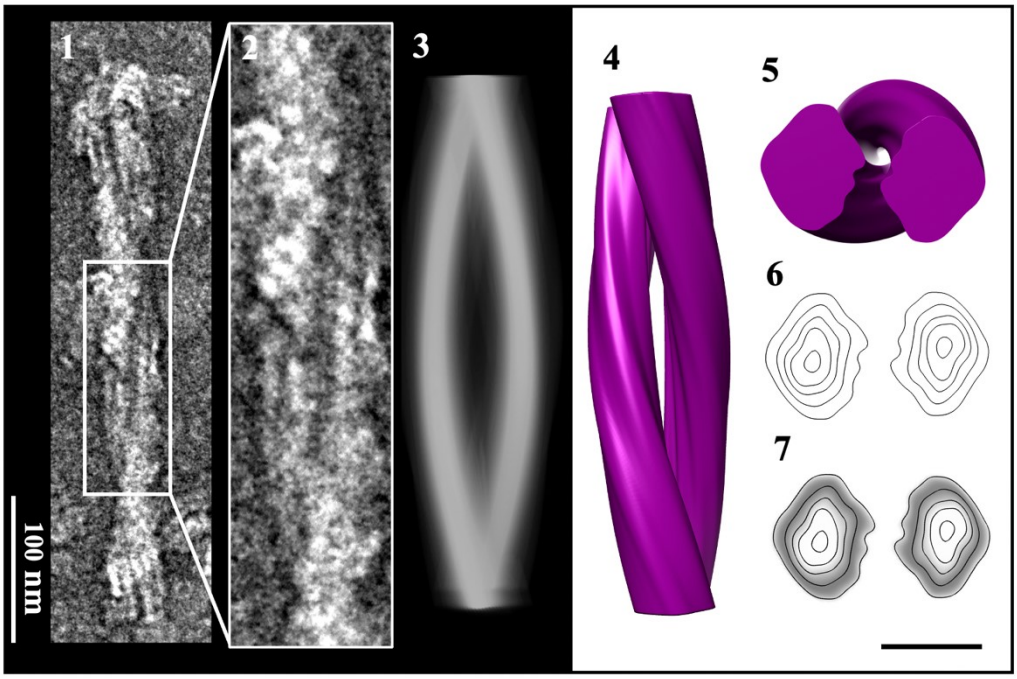

Figure 3. 6 Three-dimensional reconstructions of brain-derived C- and H-type BSE fibrils. (**A**) 3D reconstruction of an individual fibril purified from C-type BSE-infected Tg4092 mice brains. (**1**) Negative-stain EM micrographs of an individual C-type BSE fibril, and (**2**) enlarged view of the same fibril showing helical twist. (**3**) Reprojection of the reconstructed volume. (**4**) Side view of the 3D reconstruction displaying helical fibril with two intertwined protofilaments twisting around each other. (**5**) Cross-section view of the reconstructed model. (**6**) Contour map of the cross-section. (**7**) The cross-section's contour density plot was obtained by the superimposition of the contour map with the cross-section of the 3D volume. (**B**) 3D reconstruction of an individual H-type BSE fibril. (**1**) Negative stain image of an H-type BSE fibril, and (**2**) magnified view of the same fibril. (**3**) Reprojection of the 3D map of the fibril. The reprojections of C- and H-type BSE fibrils agree with the EM images, showing the consistency of the reconstructions with the original data. (**4**) Side view of the 3D reconstruction of the H-type BSE fibril. (**5**) Cross-section view of the reconstructed volume. (**6**) Contour map of the cross-section. (**7**) Contour density plot of the cross-section. 3D structures were low pass filtered to 20 Å resolution. Scale bar = 10 nm.

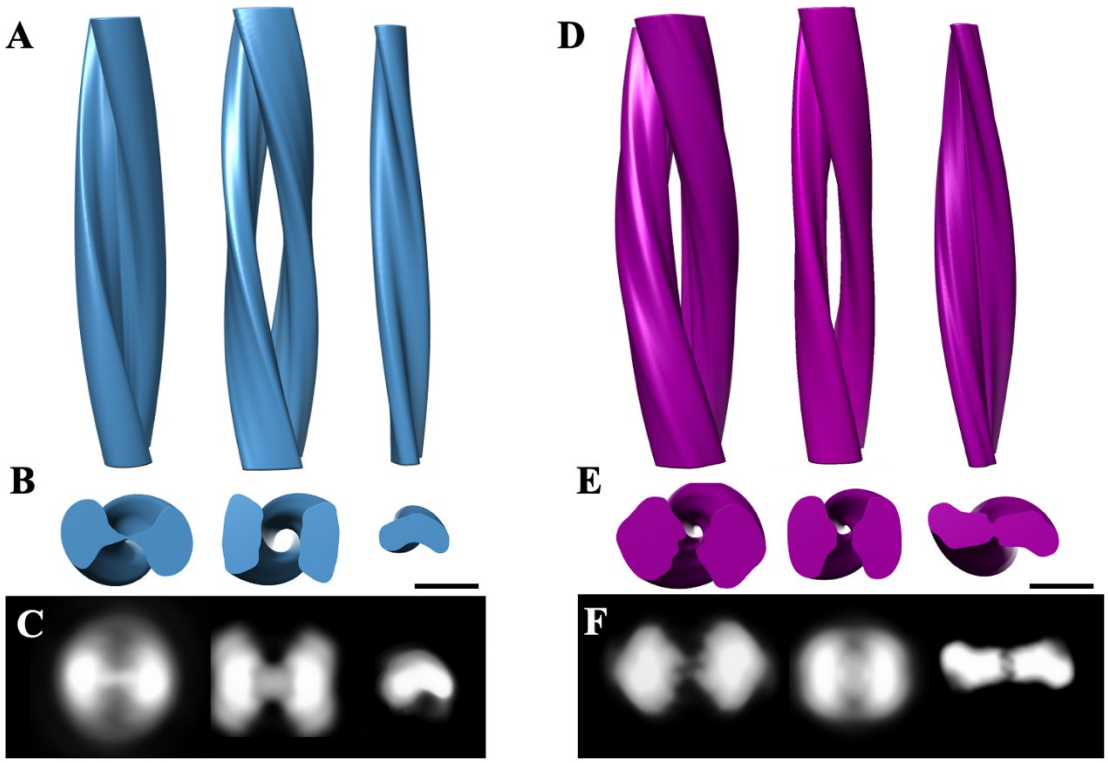

Figure 3. 7 Three-dimensional reconstructions of negatively stained C-type and H-type BSE fibrils, showing morphological heterogeneity.

(**A**) Three representative 3D maps of individual C-type BSE fibrils exhibiting helical patterns. Two fibrils (left and middle) are composed of two intertwined protofilaments, and one contains a single protofilament (right) (**B**) Cross-section views of the helical reconstructions of C-type BSE fibrils. (**C**) 2D projections of the fibril cross-sections exhibiting two densities for the two-protofilament C-type BSE fibrils (left) and one density for the one-protofilament fibril (right). (**D**) Three representative 3D maps of three independent H-type BSE fibrils. The reconstructed fibrils show helical features, and all are composed of two protofilaments. (**E**) Cross-section views of the 3D volumes of H-type BSE fibrils. (**F**) 2D projections of the cross-section of the reconstructions presenting two densities consistent with the cross-section view of the 3D maps. Scale bar = 10 nm.

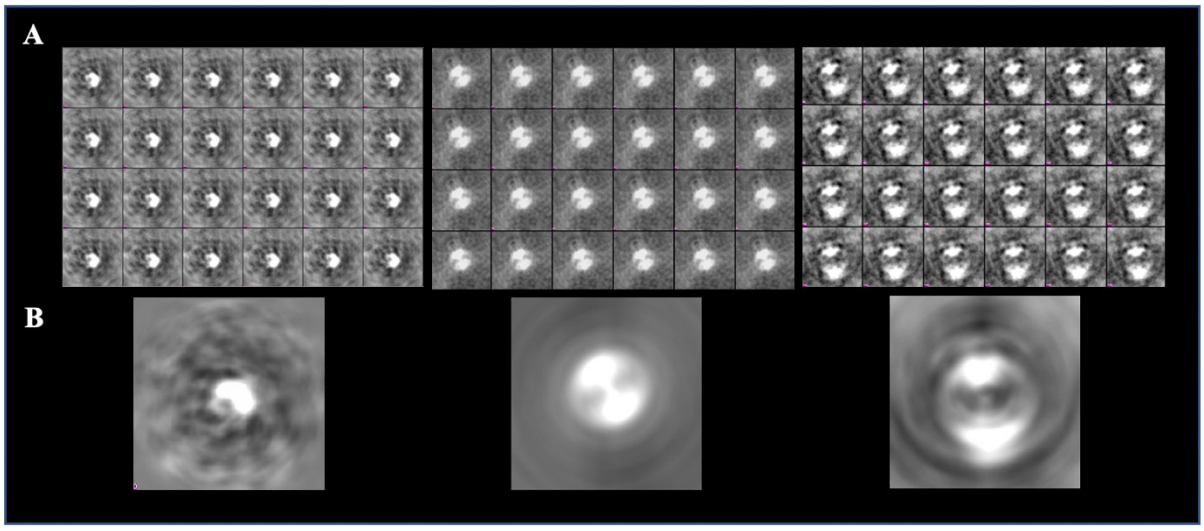

Figure 3. 8 Cross-sectional projections of the helical reconstructions.

(**A**) 2D projections of cross-sections from one- (**Left**) and two-protofilament C-type BSE (**middle**) and H-type BSE (**Right**) 3D reconstructions. (**B**) 2D projections of the averaged cross-section of single-protofilament C-type BSE (**Left**) showing one density. The averaged views of the 2D projections of the cross-sections of two-protofilament C-type BSE (**middle**), and H-type BSE (**Right**) present two apparent densities. The averaged images were used to generate the final 3D reconstruction volumes of the fibrils.

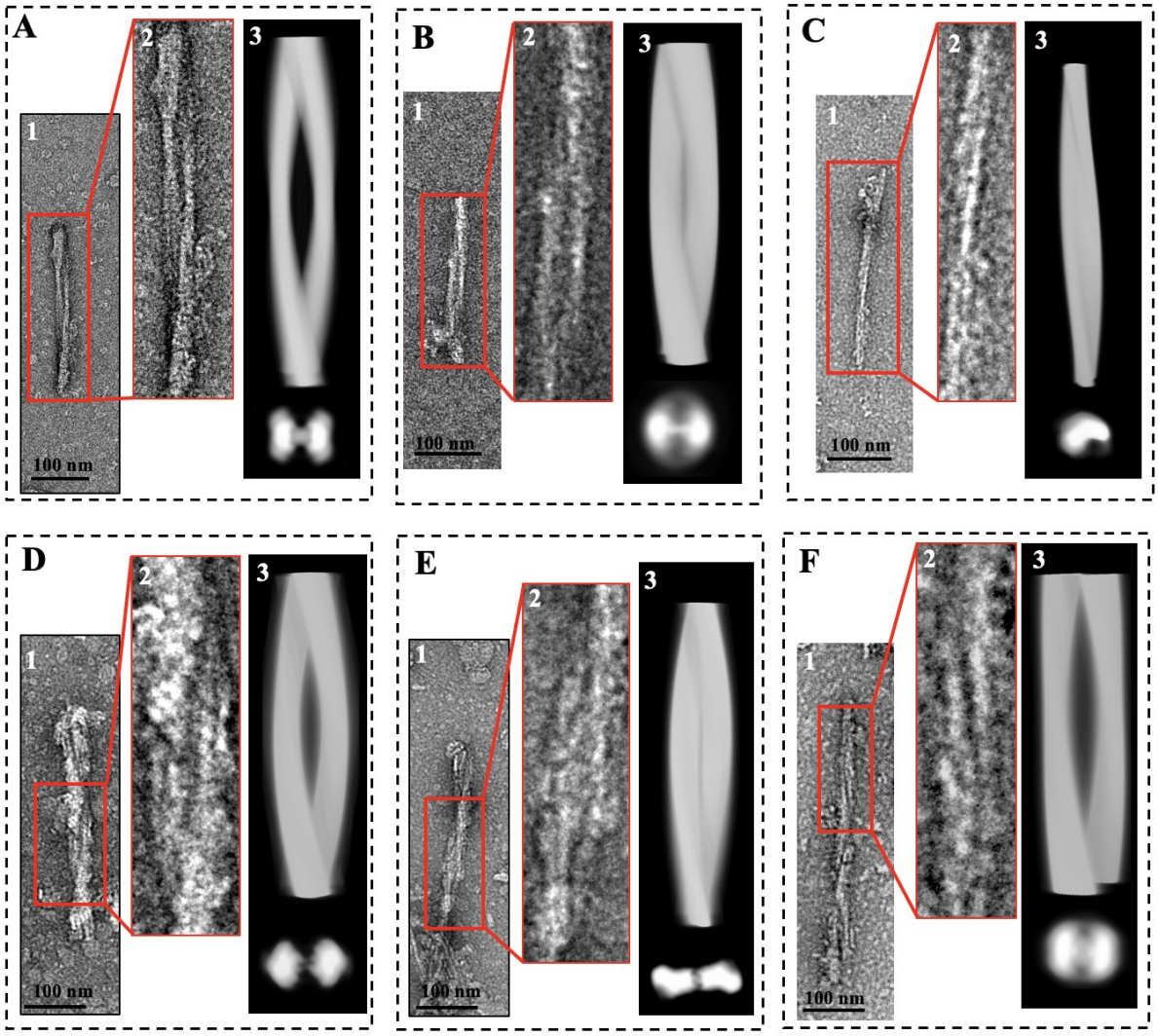

Figure 3. 9 2D projections of the three-dimensional maps.

Two-dimensional projections of the 3D maps of (**A-C**) C-type and (**D-F**) H-type BSE fibrils. Images **1** and **2** show representative EM micrographs of C-type (top) and H-type (bottom) BSE fibrils that were used to generate 3D reconstructions and enlarged views of the same fibrils. (**3**) reprojections of the reconstructions.

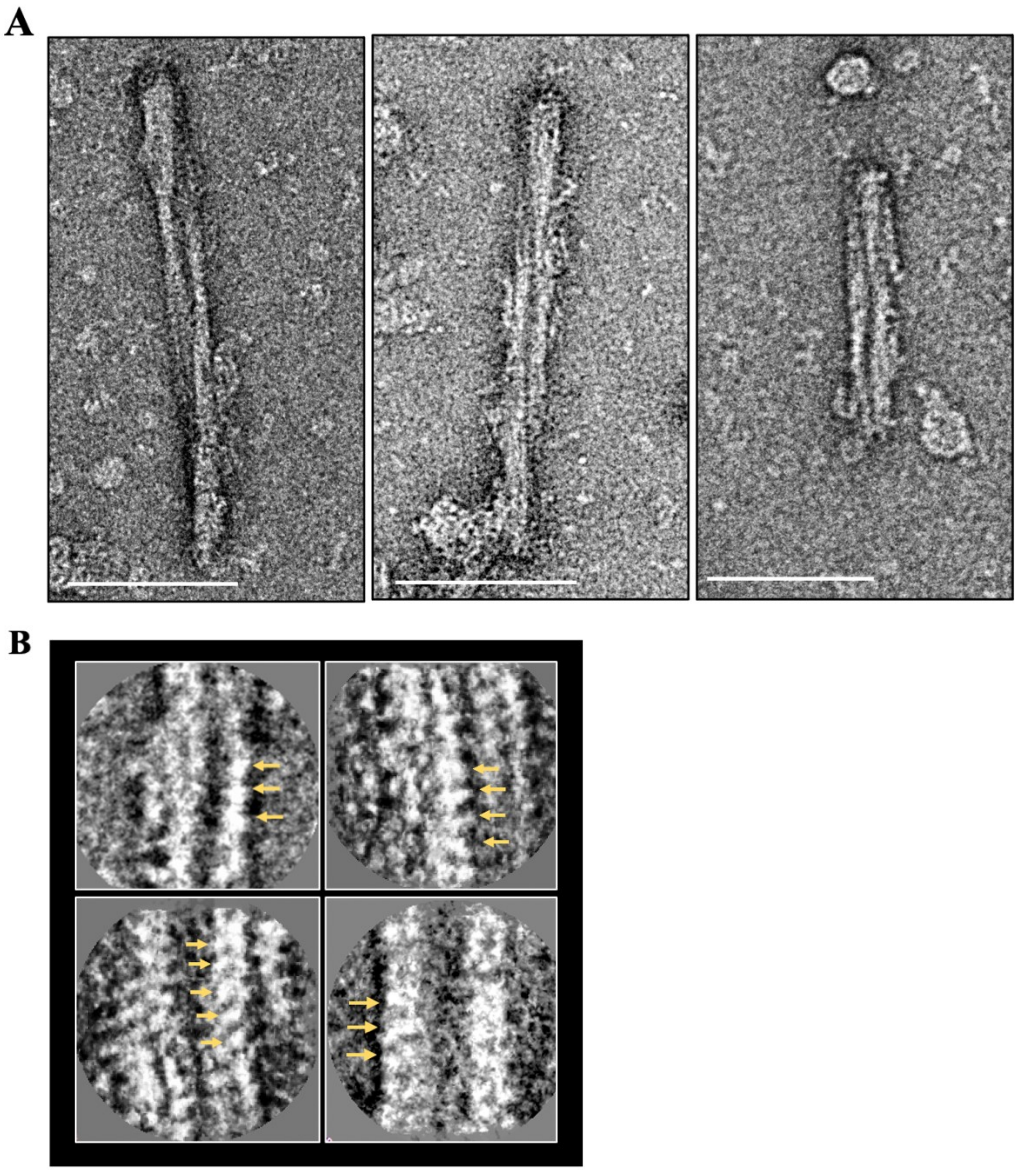

Figure 3. 10 Class averages of repeating structures of C-type BSE fibrils.

(A) Electron microscopy micrographs of three C-type BSE fibrils showing repeating units. Scale bar = 100 nm. **(B)** Images from reference-free 2D class average of the C-type BSE fibril segments showing the repeating features more clearly (yellow arrows). The repeating units were measured ~36 Å on the EM micrographs. The 2D class average was performed using 200 by 200-pixel size boxes, with a 50% overlap along the fibril axis.

3.3.5 Ultrastructural analysis using immunogold labeling

Next, we employed the immunogold labeling technique to verify the presence of PrP^{Sc} in the fibrillar assemblies at the ultrastructural level. Immunogold labeling experiments were carried out using purified pellet samples of C-type and H-type BSE. The PrP-specific labeling was visualized using a gold-conjugated tertiary detection system combined with anti-PrP monoclonal Fab, Fab 69, which recognizes residues within the N-terminal region (100-110) of bovine prion protein. Immunogold labeling examination of both C- and H-type BSE isolates revealed significant densities of gold particles associated with Fab 69 deposited around the fibrils, confirming the PrP27-30 content of these fibrils (Figure 3.11A and C). The control tests for both groups carried out simultaneously without using the primary anti-PrP Fab exhibited no or rare gold particles corresponding to non-specific background labeling (Figure 3.11B and D).

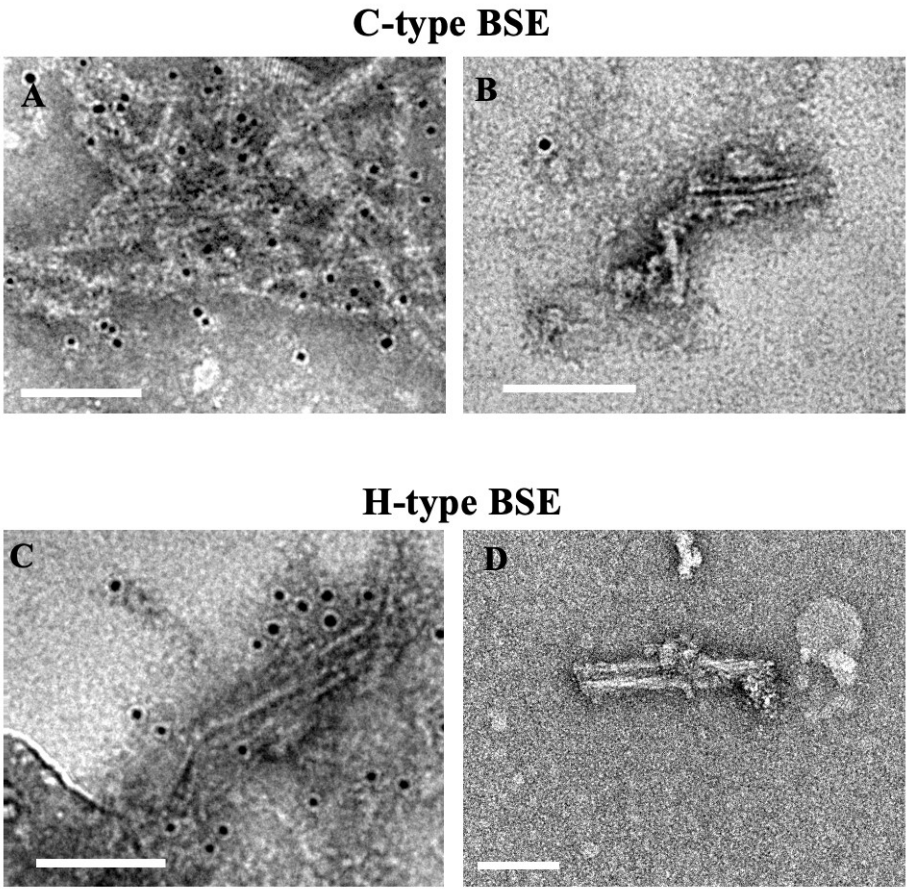

Figure 3. 11 Immunogold electron microscopy of purified BSE fibrils.

(A) Representative electron micrograph of the EM grids indicating brain-derived C-type BSE fibrils labeled with gold-conjugated Fab 69. (**B**) The control grids incubated without the primary antibody showed no or rare gold labeling. (**C**) Gold-labeled H-type BSE fibrils. Gold conjugated Fab 69 anti-PrP antibody was used for immunodetection. (**D**) A representative H-type BSE fibril from the control immunogold labeling grids, showing no specific labeling. Scale bar = 100 nm.

3.3.6 Infectivity of the purified BSE prions

To determine whether the purified C-type and H-type BSE prions contain infectivity, we conducted bioassay experiments using Tg4092 transgenic mice expressing bovine PrP. Animals were inoculated intracerebrally with final purified pellet samples and brain homogenates obtained from C- and H-type BSE-infected mice. The group inoculated with C-type BSE brain homogenate all developed clinical manifestations of prion disease such as ataxia, scruffy coat, loss of appetite, and dyspnea in 303 d.p.i (days post-infection), and the group which received C-type BSE purified pellet presented clinical signs in 299.7 ± 58.7 d.p.i. Two groups of five mice received H-type BSE-infected brain homogenate and pellet sample each, which all developed the prion disease clinical signs after 273 and 255.6 ± 33.6 d.p.i, respectively. By using a standard curve that relates incubation period to prion titer we were able to calculate the $LogID_{50}$/ml units for each of these samples (Safar, Scott et al. 2002) (Table 3.2).

Mouse Line	Sick/Total	BSE Strain	Inoculum	Incubation Time (Days ± SEM)	Prion Titers ($LogID_{50}$/ml)
Tg4092	5/5	C-type	Brain homogenate	303	5.5
Tg4092	10/10	C-type	Pellet	299.7 ± 58.7	5.61
Tg4092	5/5	H-type	Brain homogenate	273	6.12
Tg4092	5/5	H-type	Pellet	255.6 ± 33.6	6.51

Table 3. 2 Infectivity of C-type and H-type BSE purified samples.

Intracerebral inoculation of transgenic mice with the BSE prion samples obtained during purification experiments. For both BSE strains, the comparison of the incubation times between the groups inoculated with the brain homogenate samples and the final pellet samples did not show significant differences. However, the purified samples showed higher infectivity titers than the brain homogenate in both cases. The infectivity titers in $LogID_{50}$/ml units were calculated from a standard curve relating incubation time to prion dose that was obtained using a C-type BSE isolate (Safar, Scott et al. 2002).

3.4 Discussion

In this study, we demonstrated the detection of fibrils in brain-derived, infectious C-type and H-type BSE isolates and generated, for the first time, 3D reconstructions of fibrils from these transmissible agents. Both C- and H-type BSE purified samples contained slightly heterogeneous fibrils with an apparent helical twist, consistent with our previous findings of BASE fibrils (Kamali-Jamil et al., unpublished manuscript). In this investigation, we established that classical and H-type atypical BSE strains have distinct ultrastructures.

Purification of C-type and H-type BSE strains yielded positive PrP27-30 signals using Western blot detection. As expected, based on previous reports (Biacabe, Laplanche et al. 2004), the two BSE strains exhibited distinct electrophoretic profiles (PrP^{Sc}) in Western blot analysis following treatment with PK. Remarkably, the TEM examination of the purified samples revealed that the two BSE strains contain morphologically distinguishable helical fibrils. EM immunogold labeling experiment using gold-conjugated anti-PrP monoclonal Fab, Fab 69, detecting residues 100-110 of the bovine prion protein, confirmed the presence of prion proteins as the building blocks of amyloid fibrils of the classical and H-type BSE samples.

Morphological evaluation of the negatively stained purified samples revealed that C-type BSE isolates contain low-abundant and scattered fibrils mainly composed of two intertwined protofilaments. In comparison, about 19% of the H-type BSE fibrils were often observed to stick together laterally and form fibrils with multiple filaments, perhaps indicating their strain-specific nature. One significant feature of C-type BSE preparations was the presence of two apparent morphologies of one- and two-protofilament fibrils, akin to our recent observation in L-type BSE samples. The observation of both morphologies confirms our previous conclusion that infectious

PrP^{Sc} molecules may assemble into one- or two-protofilament fibrils in the course of infection (Kamali-Jamil et al., unpublished manuscript). However, in contrast to L-type BSE fibrils, a small percentage of C-type BSE fibrils contained one protofilament, while the majority consisted of two protofilaments. The observation of two-protofilament morphology of C-type and H-type BSE fibrils was compared favorably with the findings of the previous cryo-EM and image processing study on GPI-anchorless RML prion rods, in which each PrP 27-30 fibril was comprised of a pair of twisting intertwined protofilaments (Vazquez-Fernandez, Vos et al. 2016). The same conclusion was also drawn from previous negative staining and cryo-EM studies of other infectious strains, such as ME7, 22L, and RML, indicating the isolation of two-protofilament fibrils (Sim and Caughey 2009, Wille, Bian et al. 2009, Terry, Wenborn et al. 2016, Terry, Harniman et al. 2019). Identification of one-protofilament morphology in C-type BSE micrographs is significant because it has not been reported as the conformational assembly of infectious prions elsewhere. Our helical reconstruction approaches allowed better visualization of the quaternary organization of the two-dimensional EM micrographs of C-type and H-type BSE amyloid fibrils. Projections of the reconstructions corresponded well with image averages of the raw data, confirming the validity of the reconstructions.

Bioassay experiments using bovinized transgenic mice have been commonly used instead of bovine bioassay, which is expensive and challenging (Buschmann and Groschup 2005). According to previous findings, BSE-infected transgenic mice expressing bovine PrP^{C} with a PrP ablated background show clinical signs between 230 and 340 d.p.i (Scott, Safar et al. 1997). Comparable to these observations, transgenic mice bioassay using C-type and H-type BSE isolates led to the development of prion disease symptoms in less than 303 days post-incubation, confirming the presence of BSE infectivity in these samples.

Based on our structural analysis and the results from our recent work on L-type BSE (Kamali-Jamil et al., unpublished manuscript), it is possible to conclude that variations in biochemical and pathological properties of different BSE strains are due to the, possibly slight, structural differences between these strains. The observation of both single and two-protofilament fibrils, as the two distinct polymorphs of C-type BSE prions, further supported our recent view regarding the structural architecture of infectious BSE prions. Consistent with our study on the BASE strain, our current data excludes the possibility of in-register stacking of PrP^{Sc} monomers due to discovering both one and two-protofilament fibrils; instead, our findings of L-type BSE strain are in agreement with the four-rung beta-solenoid model for the structure of infectious PrP^{Sc} (Wille, Bian et al. 2009, Requena and Wille 2014). Besides, the repeating subunits of approximately 36 Å to 40 Å in size along the fibrils in the negative stain EM images of some C-type BSE fibrils appear to be in accordance with the four-rung beta-solenoid organization. Based on the 4RβS structure, the observed repeat units along the C-type BSE fibrils' axis could reflect two PrP^{Sc} monomers (19.2 Å x 2 = 38.4 Å) (Wille, Bian et al. 2009). Also, the size of these substructures is consistent with the ~ 40 Å signal observed using Fourier- transform analysis in the above-mentioned cryo-EM study on an anchorless mammalian prion strain, in which the 40 Å signal was attributed to two PrP^{Sc} monomers (Vazquez-Fernandez, Vos et al. 2016).

3.4.1 Conclusion

The results presented in this study, in concert with our recent data on native L-type BSE strain, for the first time, provide evidence regarding the morphological architecture of fibrils from infectious classical and atypical BSE strains at the quaternary structure level. Our reconstructed C-type and H-type BSE models, although with low-resolution, provide a description of the ultrastructural organization and polymorphism in the fibrils of brain-derived infectious BSE

strains. Our data reinforce the growing belief that the biological properties of prion proteins correlate with their unique structures, meaning that the morphological differences that we observed between C-, H-, and L-type BSE strains could be responsible for the different clinical phenotypes in these strains. Future investigations using cryo-electron microscopy would be essential to provide further details about the structure of different BSE prions.

Overall, the present study could provide new constraints on the structure of infectious BSE amyloid fibrils and the mechanisms underlying self-propagation and fibril growth in different prion strains. It also may provide a basis for elucidating the high-resolution structure of infectious prion proteins of different strains.

Chapter 4: Conclusions and future directions

Structural remodeling of host-encoded proteins is the hallmark event in a group of neurodegenerative conditions, including prion diseases, Alzheimer's disease (AD), and Parkinson's disease (Dearborn, Wall et al. 2016, Fitzpatrick, Falcon et al. 2017, Wille and Requena 2018). This conformational difference is believed to play a substantial role in neurodegenerative diseases and their public health impacts. As a case in point, bovine spongiform encephalopathy (BSE), a prion disease in cattle, was first reported in Alberta in 2003 (Dudas, Yang et al. 2010). The beef industry in North America suffered an economic loss of about $ 11 billion due to the BSE impact (Coffey, Mintert et al. 2005, Le Roy, Klein et al. 2006). Differences between clinical phenotypes and electrophoretic profiles for typical and atypical BSE prion strains have been previously described (Biacabe, Laplanche et al. 2004), but little is known about their structural properties at high resolution. Therefore, a detailed understanding of the structure of these agents would be necessary to control these diseases based on their molecular properties and blunt their related economic impacts.

In my PhD research project, I investigated the molecular and structural characteristics of classical and atypical H- and L-type BSE prions, employing a combination of biochemical, biophysical, immunological, and computational techniques. My research work involved purification and biochemical analyses of classical and atypical BSE prions from brain tissues. I conducted a structural characterization of the fibrils from these BSE strains, which revealed distinct polymorphs of these agents. Moreover, I generated the first 3D reconstruction maps of the three native BSE strains, which provided further details into the distinct ultrastructure of BSE prions.

4.1 Distinct ultrastructural morphologies of classical and atypical BSE prions

I presented a detailed structural and biochemical evaluation of infectious natively glycosylated L-type BSE in Chapter 2 of this dissertation. According to previous histopathological observations, L-type BSE strain is characterized by the deposition of amyloidotic plaques in the brain tissue of the affected host (Casalone, Zanusso et al. 2004), as acknowledged in its alternative name, bovine amyloidotic spongiform encephalopathy, BASE. Chapter 3 presented the purification of C-type and H-type BSE, the two other BSE strains, from BSE-infected Tg4092 mice brains (Scott, Safar et al. 1997). Classical and atypical BSE prions were provided by the primary transmission of brain tissues from the Canadian C-, H-, and L-type BSE-affected cattle (Dudas, Yang et al. 2010) into transgenic mice that overexpress bovine PrP, Tg4092 (Scott, Safar et al. 1997). I purified BSE prions from Tg4092 mice brains and assessed the sample preparation quality using immunoblotting experiments. The results of biochemical comparison of the three BSE strains were consistent with previous publications (Jacobs, Langeveld et al. 2007), indicating the differences in the migration pattern of classical and atypical BSE strains in Western blot (Figure 3.2). Our preliminary data using a polyclonal anti-PrP antibody that detects shed PrP indicated the presence of some GPI-less prion protein in the purified samples of C-type and L-type BSE strains (unpublished data).

I used the Tecnai G20 transmission electron microscopy (TEM) facility, equipped with a second-generation direct electron detector, at the Centre for Prions and Protein Folding Diseases (CPPFD) to explore the presence of BSE fibrils in the purified samples. Negative stain electron microscopy evaluation of L-type BSE strain presented in Chapter 2, and C-type and H-type BSE isolates, as discussed in Chapter 3, revealed the existence of fibrils in the purified samples of the three BSE strains (Figure 2.3 & Figure 3.3). Immunogold labeling technique using anti-PrP

monoclonal antibodies established the presence of PrP 27-30 molecules as the structural units of the isolated BSE fibrils.

The fibrils from the three BSE groups, while all presented a helical twist (Figure 4.1), were distinguishable in their overall morphologies. For example, L-type BSE samples had a high yield of fibrils as compared to C- and H-type samples, further confirming the amyloidogenicity of this specific strain (Casalone, Zanusso et al. 2004). Overall, the C-type BSE preparation contained a low yield of BSE fibrils than the two other BSE strains. However, the strong Western blot signal of this sample could suggest that a lower proportion of C-type BSE prions contribute to fibril formation, relative to the atypical BSE strains.

The fibrils from this amyloidic BSE strain were found to have two main morphologies, including one-protofilament fibrils, accounting for major fibrils' population (~ 73%), and two protofilament fibrils (Figure 2.4). However, C- and H-type BSE isolates predominantly comprised of thicker two-protofilament fibrils (Figure 3.4). The observation of the single protofilament morphology was a novel finding of this study and has not been reported in previous studies for any infectious mammalian prion strains. As will be discussed later, the observation of these two morphologies is in favor of the four-rung beta-solenoid (4RβS) model for the structure of infectious prion molecules (Wille, Bian et al. 2009, Vazquez-Fernandez, Vos et al. 2016). The dimensions of the fibrillar structure from C-, H-, and L-type BSE strains in this dissertation, as well as the reports from previous investigations on other infectious and non-infectious prion strains, are summarized in Table 4.1. As shown in Table 4.1, in all three BSE strains, the average width of the two protofilament fibrils ranged from 20 nm to 24 nm (Table 4.1), which is consistent with the widths of double-protofilament fibrils in other investigations.

The width differences between the two-protofilament fibrils of C-, H-, and L-type BSE, as calculated based on a three-way ANOVA test, indicated that the differences between the fibril widths between the three BSE strains are significantly different ($p=0.0000012$). It is notable that in the studies on in vitro-generated and GPI-anchorless brain-derived prion fibrils, the diameter of the fibrils (between 10 and 14 nm) is lower than the fully glycosylated ones, mainly due to the lack of posttranslational modifications (Table 4.1).

Although structural diversity is strongly accepted to exist in different prion strains (Diaz-Espinoza and Soto 2012), there is experimental evidence indicating heterogeneity in the assembly of PrP^{Sc} even within particular prion strain isolates (Igel-Egalon, Bohl et al. 2019). Morphological evaluation of the fibrils from C-, H-, and L-type BSE strains in my PhD study revealed heterogeneous morphologies of PrP^{Sc} assemblies within each strain population in terms of helical pitch distance, width, and fibrils' length. No such morphological examinations have been performed previously on native BSE strains to provide an opportunity for comparison with the samples in this study. However, several investigations on mouse and ovine PrP^{Sc} reported heterogeneity in tertiary and quaternary structures of PrP^{Sc} molecules (Tzaban, Friedlander et al. 2002, Laferrière, Tixador et al. 2013, Vazquez-Fernandez, Vos et al. 2016, Igel-Egalon, Bohl et al. 2019). The observed structural differences between the three BSE strains observed in this dissertation may also be responsible for their distinct biochemical and phenotypic features. The link between specific disease phenotypes and structure has also been described in Alzheimer's disease. Similar morphology of tau fibrils was found in a group of AD patients with similar tauopathies, while different polymorphs were reported to exist in cases with distinct tauopathies (Fitzpatrick, Falcon et al. 2017, Falcon, Zhang et al. 2018, Falcon, Zhang et al. 2018).

4.2 The infectivity of amyloid fibrils

Our bioassay experiments showed that the purified C-, H-, and L-type BSE prions are capable of causing prion disease in Tg4092 transgenic mice; therefore, the fibrillar structures existed in the inoculums could be representative of the intrinsically infectious material. The infectivity titers of the purified pellet samples of C-type, H-type, and L-type BSE were calculated 5.61, 6.51, and 8.06 $LogID_{50}$/ml, respectively. The calculation of the prion titers was performed using a standard curve relating incubation time to prion titer (Safar, Scott et al. 2002). Our immunogold labeling study on the isolated L-type BSE samples utilizing YEG mAb Sc-G1 antibody (Fang et al., manuscript in preparation) showed successful decoration of the L-type BSE fibrils (Chapter 2). Since this antibody only recognizes native PrP^{Sc}, this experiment could further confirm the infectivity of the purified BSE fibrils.

Prion fibrils were initially suggested to be an artefactual conformer of prions generated during the purification process using both detergents and protease treatment of PrP^{Sc} (McKinley, Meyer et al. 1991). However, a later investigation using cell culture assay identified that the prion rods purified from brain tissues have intrinsic infectivity. An earlier idea considering a role of detergents in generating fibrils (McKinley, Meyer et al. 1991) was excluded as these repeating structures were isolated from the brain tissues with no detergent addition, as performed by Terry et al (Terry, Wenborn et al. 2016). In this experiment, it was identified that without using detergents, the heterogeneous nature of crude brain homogenates limits the observation of prion rods with EM and applying detergents could allow better visualization of the pre-existing fibrils in the purified samples. Besides, changing the exposure condition to detergents and protease had no noticeable effect on the conformation and dimensions of the isolated fibrils (Terry, Wenborn

et al. 2016). Moreover, in a recent study, prion purification from brain tissues was conducted without using Sarkosyl or other detergent. In this investigation, purification of infectious prions from rodent brains with the use of styrene maleic acid (SMA) polymers revealed prion fibrils in the isolated samples when examined by electron microscopy (Esmaili, Tancowny et al. 2020).

4.3 Generating 3D maps using 2D electron micrographs

Transmission electron microscopy is a powerful tool for resolving the structure of helical assemblies (Egelman 2007). Negative stain electron microscopy, first demonstrated by Brenner and Horne (1959) (Brenner and Horne 1959), has been used extensively in structural characterization of amyloid fibrils of prion and other proteins, such as AD and Parkinson's disease (Zweckstetter, Requena et al. 2017). The high contrast of negatively stained EM micrographs allows the investigation of distinct conformations and structural characteristics of biomolecules (Whittaker, Wilson-Kubalek et al. 1995). This technique was first used to visualize brain-derived scrapie fibrillar structures, termed "scrapie-associated fibrils" (SAFs) (Merz, Somerville et al. 1981) and prion rods of scrapie agents isolated from brain tissues (Prusiner, McKinley et al. 1983) about four decades ago. Although the two fibrillar structures in the studies mentioned above were similar entities, they were designated differently at the time of their discovery (Diener 1987).

Although this technique provides various structural details, the resolution of the negative stain 3D reconstructions is limited to ~ 20 Å (Ohi, Li et al. 2004). To overcome this limitation and retrieve further information, negative staining can be combined with 2D averaging and 3D reconstruction techniques (Ohi, Li et al. 2004). In further attempts to gain insights into the quaternary structure of BSE fibrils, I conducted a 2D classification and averaging technique,

which revealed finer details of the fibrils of the three BSE strains. For example, the 2D averages performed on hundreds of EM micrographs of BASE prion fibrils confirmed the existence of both polymorphs of two- and one-protofilament fibrils. I identified repeating units of about 36 Å in some C-type BSE fibrils (Figure 3.10). These repeating substructures were revealed more clearly following the generation of class averages from the micrographs presenting this characteristic. It is noteworthy that in a previous cryo-EM study, which supported a 4RβS model for PrP^{Sc} structure, Fourier-transform analysis of the cryo-EM images of GPI-anchorless PrP^{Sc} revealed ~ 40 Å signal, corresponding to the size of two PrP^{Sc} monomers. The observed 40 Å spacing also indicated the possibility of a head-to-head or tail-to-tail stacking of PrP^{Sc} molecules in the fibrillar assembly (Wille and Requena 2018). Thus, the 36 Å to 40 Å repeating structures observed in the C-type BSE fibrils, compatible with the previous cryo-EM study, corresponds well with the size of PrP^{Sc} dimers (in a 4RβS arrangement), possibly interacting in a head-to-head/tail-to-tail fashion.

A transmission electron microscopy image is a 2D projection of a 3D object (Egelman 2007). The repeating nature in amyloid filaments provides an advantage in generating 3D structures from EM micrographs (Egelman 2000). Helical filaments were the first structures to be reconstructed in three dimensions from electron microscopic images. A 3D map of a bacteriophage tail was the first helical object to be reconstructed employing this technique (De Rosier and Klug 1968). In this method, a set of two-dimensional EM micrographs are used to build a three-dimensional model. Theoretically, a single projection of a 2D image of a helical fibril includes a range of views, which provides ample information for generating a 3D reconstruction (Miyazawa, Fujiyoshi et al. 1999). In other words, the Fourier transform of a

helical object has a series of amplitudes and phases that can be used to generate a 3D map of the helical object.

Cryo-EM and negative stain images of recombinant and brain-derived fibrils of prions and other neurodegenerative diseases have been exploited in several investigations to generate 3D models (Terry, Wenborn et al. 2016, Vazquez-Fernandez, Vos et al. 2016, Terry, Harniman et al. 2019, Terry and Wadsworth 2019, Wang, Zhao et al. 2020). For example, very recently, a cryo-EM study on recombinant human prion protein revealed amyloid fibrils consisting of two protofibrils and described that in these fibrils, the C-terminal α-helices of PrP^{C} structure are replaced by β-strands (Wang, Zhao et al. 2020). Other cryo-EM investigation on an infectious GPI-anchorless mouse prion protein, consistent with the above-mentioned study, identified two-protofilament amyloid fibrils. Besides, this study provided supporting evidence for the 4RβS as the core structure of PrP^{Sc} (Vazquez-Fernandez, Vos et al. 2016). A 3D model based on negative stain electron microscopy of infectious RML prions revealed double-helical amyloid fibrils (Terry, Wenborn et al. 2016).

In Chapters 2 and 3, I presented the 3D reconstructions using several independent individual EM micrographs of three BSE strains, providing many details regarding the ultrastructure of these infectious agents. The 3D reconstructions' results indicated structural differences between the studied BSE strains at the quaternary structure level. The results of the 3D reconstruction techniques on typical and atypical BSE fibrils yielded 3D maps showing helical periodicity while slight heterogeneity existed between the individual models. These data were consistent with our negative stain morphological examination and 2D averaging.

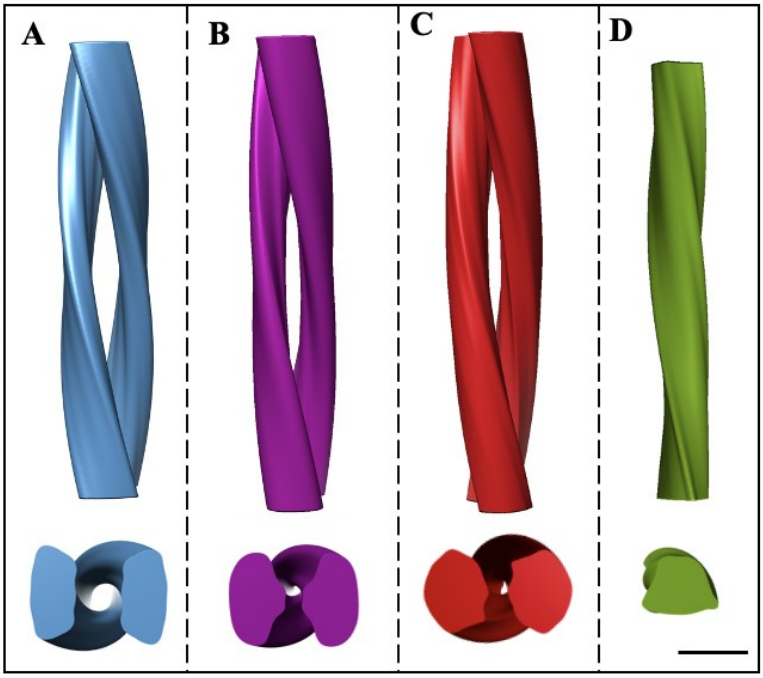

Figure 4. 1 Representative three-dimensional reconstructions of classical and atypical BSE fibrils.

3D maps of (A) C-type, (B) H-type, (C) two-protofilament L-type, and (D) one-protofilament L-type BSE fibrils

Prion strain	Width mean ± SD (nm)	Helical Pitch mean ± SD (nm)	Length mean ±SD (nm)	Protein source	Structural method	Reference
L-type BSE (one protofilament)	10.6 ± 1.7	89.3 ± 15	387.5 ± 155	Brain-derived	Negative stain EM	Chapter 2 of the dissertation
L-type BSE (Two protofilaments)	22.5± 3.4	102.3 ± 16.9	598 ± 268			
H-type BSE	24.5 ± 4.8	137 ± 33.2	315.1 ± 169	Brain-derived	Negative stain EM	Chapter 3 of the dissertation
C-type BSE	20.3 ± 6.8	158.8 ± 43.1	193.3 ± 72	Brain-derived	Negative stain EM	Chapter 3 of the dissertation
263K	16-20	-	98-188	Brain-derived	Cryo-EM	(Kraus, et al. 2021)
Full-length human PrP	~ 14	78.5	-	Recombinant (In vitro)	Cryo-EM	(Wang, Zhao et al. 2020)
Full-length mouse PrP	~ 10	-	> 700	Recombinant (In vitro)	Negative stain- Cryo-EM- AFM	(Terry, Harniman et al. 2019)
RML prion	19.4 - 26.5	-	111.5 - 127.5	Brain-derived	Negative stain- Cryo-EM- AFM	(Terry, Harniman et al. 2019)
GPI-anchorless PrP^{Sc} fibrils of RML prion	~ 10	76 - 98	-	Brain-derived	Cryo-EM	(Vazquez-Fernandez, Vos et al. 2016)
RML prion	~ 21	-	100 - 200	Brain-derived	Negative stain EM	(Terry, Wenborn et al. 2016)

Table 4. 1 Dimensions of infectious brain-derived C-, H-, and L-type BSE fibrils, and infectious and in vitro-generated prion fibrils from other strains.

The maximum widths of the two-protofilaments fibrils of C-, H-, and L-type BSE strains was measured between 20 nm and 24.5 nm, which are in range with those of other prion strains reported in previous publications. The width differences between the two-protofilaments fibrils of the three BSE strains was found to be significant ($p=0.0000012$). The differences may also be significant with regard to the diameters of two-protofilament fibrils in other publications; however, this could not be determined due to the lack of the original data from those investigations.

4.4 The folding and polymerization of PrP^{Sc}

Currently, the exact mechanisms underlying the conformational transition from PrP^{C} to PrP^{Sc} is not fully determined, mainly due to the absence of a high-resolution structure of highly infectious preparations of PrP^{Sc} and possible intermediate conformers. The obvious event in PrP^{C} to PrP^{Sc} transition is a change from an alpha-helical structure to a structure including beta-strands connected by short loops and /or turns (Wille and Requena 2018).

Based on several structural experiments, the core structure of PrP^{Sc} is believed to have a four-rung β-solenoid architecture, (Wille and Requena 2018). Initially, electron crystallography experiments of two-dimensional crystals of an N-terminally truncated prion protein (PrP 27-30) and a miniprion (PrP^{Sc}106) suggested a β-solenoid core for the structure of PrP^{Sc} molecules (Wille, Michelitsch et al. 2002, Govaerts, Wille et al. 2004). Further investigation using an X-ray fiber diffraction experiment of brain-derived PrP 27-30 prions identified a 19.2 Å signal, this being indicative of the height of each PrP^{Sc} monomer (Wille, Bian et al. 2009). The results of a following cryo-EM study on a GPI-anchorless mammalian prion protein further strengthened the 4RβS hypothesis (Vazquez-Fernandez, Vos et al. 2016). Later, a molecular dynamics simulation study, carried out based on the available structural data, presented that the 4RβS model is a physically possible arrangement for prion molecules (Spagnolli, Rigoli et al. 2019).

A Parallel In-Register Intermolecular Beta-Sheet (PIRIBS) model was an alternative model for the PrP^{Sc} structure. This model was defined based on an NMR study of the recombinant murine prion protein, indicating in-register stacking of PrP^{Sc} monomers, and therefore, 4.8 Å intermolecular height of each monomer (Groveman, Dolan et al. 2014). Very recently, using a high resolution cryo-EM study on brain derived 263K prion strain, a PIRIBS-based structure was determined for this prion strain (Kraus, Hoyt et al. 2021). Due to the size proposed for each PrP^{Sc}

molecule, this model does not appear to be compatible with the 19.2 Å height observed in the X-ray fiber diffraction and cryo-EM experiments (Wille, Bian et al. 2009, Vazquez-Fernandez, Vos et al. 2016).

The results of the structural investigation of L-type and possibly C-type BSE strain presented in this dissertation are in good agreement with the 4RβS as the basic structure of infectious PrP^{Sc} molecules. First, the presence of both one- and two-protofilament BSE fibrils seems to be in line with the above-mentioned cryo-EM study on mouse prion protein, which identified amyloid fibrils containing two intertwined protofilaments. Second, the observation of ~ 36 Å to 40 Å repeat units in some C-type BSE fibrils appears to be compatible with the previous X-ray fiber diffraction investigation (Wille, Bian et al. 2009), as the value is double the height measurement by X-ray fiber diffraction (19.2 Å). This could indicate that each repeating unit is a PrP 27-30 dimer, perhaps assembled in a head-to-head or tail-to-tail arrangement (Vazquez-Fernandez, Vos et al. 2016). Third, the reconstructions of BSE amyloid fibrils in our study presented triangular or oval shape cross-sections, a common characteristic of β-helical proteins (Kajava and Steven 2006). Furthermore, the superimposition of the cross-sections of single- and two-protofilament L-type BSE reconstructions with the surface view of the 4RβS model, generated by Spagnolli et al. 2019, showed good correspondence (Figure 2.10).

By contrast, our data, especially from experiments on L-type BSE strain, are not compatible with the PIRIBS model. However, regarding the H-type BSE strain, it needs to be determined if the monomers from this strain adopt a 4RβS, PIRIBS, or another configuration. In this model, due to the 4.8 Å distance between two PrP^{Sc} monomers, each monomer would have to cover both protofilaments. Therefore, according to this model, PrP^{Sc} amyloid fibrils contain only one protofilament, and the authors who proposed this model attribute the density observed in the

middle of amyloid fibrils in negative stain images to stain artifacts (Groveman, Dolan et al. 2014). In my PhD study, however, we observed both one- and two-protofilament fibrils in the purified samples of L-type and C-type BSE strains. Interestingly, a thorough examination of hundreds of EM micrographs revealed some L-type BSE fibrils showing both morphologies on separate ends. I noticed that these fibrils are broken in the middle and present a two-protofilament fibril at one end and two single filaments at another end of the fibril (Figure 2.4). This observation strongly indicates that prion fibrils are not solely composed of one protofilament. A previous study on RML prions also provided evidence that the central gap in the middle of fibrils contains biological material and is not due to the staining procedure (Terry, Harniman et al. 2019). In addition, it was proposed by Baskakov et al. that the four-rung beta-solenoid arrangement, with 4 × 4.8 Å distance between rungs, would provide more space for the two bulky N-linked carbohydrate adducts on PrP^{Sc}, as compared to the PIRIBS model with 4.8 Å distance between adjacent PrP^{Sc} molecules (Baskakov and Katorcha 2016, Artikis, Roy et al. 2020).

Considering the data from the recent cryo-EM study (Kraus, Hoyt et al. 2021) and some previous research evidence (Wille, Bian et al. 2009, Vazquez-Fernandez, Vos et al. 2016), including the data from this dissertation, supporting the 4RβS model, it seems possible that these alternative structures exist in the brain. The heterogeneity that has been observed in PrP protein organization may also suggest more than one PrP^{Sc} structure that co-exist in the brain in one host, as observed in fungal prions. Some fungal prions have been identified to adopt a β-solenoid (two-rung β-solenoid) assembly (Wasmer, Lange et al. 2008) while others have in-register parallel beta-sheet architecture (Wasmer, Lange et al. 2008, Wickner, Edskes et al. 2018, Baskakov, Caughey et al. 2019).

4.5 Does four-rung beta solenoid allow efficient prion replication?

The beta-strands in the upper and lowermost rungs of a beta-solenoid protein can act as templates when encountering other amyloidogenic proteins (Richardson and Richardson 2002). The recent MD simulation study provided evidence that in PrP^{Sc} amyloid fibrils with 4RβS structure, the β-solenoid rungs at the ends of each protofilament, as a templating surface, can participate in converting the incoming PrP^{C} monomers (Martín-Pastor, Codeseira et al. 2020). This event follows by a chain of conformational transition events leading to the complete transformation of the incoming PrP^{C} molecule into its disease-causing counterpart with 4RβS architecture. (Vazquez-Fernandez, Young et al. 2017, Spagnolli, Rigoli et al. 2019, Spagnolli, Rigoli et al. 2020). Therefore, as a structural intermediate, amyloid fibrils can have an essential role in prion propagation (Wille and Requena 2018).

4.6 Conclusions and Future directions

My thesis research involved the structural investigation of fully glycosylated brain-derived, infectious bovine spongiform encephalopathy prions. I established that fibrils from C-, H-, and L-type BSE prions have different morphologies. Our work revealed distinct quaternary structures of classical and atypical H-type and L-type BSE strains, which could be attributed to their strain-specific features. Besides, our data from L-type BSE provide additional support for the four-rung β-solenoid arrangement proposed for the structure of infectious PrP^{Sc} molecules. Therefore, the findings of this dissertation could have implications for prion replication and a better understanding of the species barrier mechanism.

Altogether, the presented findings provide a framework for a future cryo-electron microscopy study to obtain higher-resolution structural details of infectious BSE prions. One advantage of

this method is that the sample is preserved in a frozen-hydrated state, closer to the native form. It will also be essential to compare the 3D reconstructed models of different BSE strains we obtained in this study with the 3D models generated from cryo-EM micrographs.

Bibliography:

Aguzzi, A. and A. M. Calella (2009). "Prions: protein aggregation and infectious diseases." Physiol Rev **89**(4): 1105-1152.

Aguzzi, A. and M. Polymenidou (2004). "Mammalian prion biology: one century of evolving concepts." Cell **116**(2): 313-327.

Aguzzi, A., C. Sigurdson and M. Heikenwaelder (2008). "Molecular mechanisms of prion pathogenesis." Annu Rev Pathol **3**: 11-40.

Alper, T., W. A. Cramp, D. A. Haig and M. C. Clarke (1967). "Does the Agent of Scrapie Replicate without Nucleic Acid ?" Nature **214**(5090): 764-766.

Angers, R. C., H. E. Kang, D. Napier, S. Browning, T. Seward, C. Mathiason, A. Balachandran, D. McKenzie, J. Castilla, C. Soto, J. Jewell, C. Graham, E. A. Hoover and G. C. Telling (2010). "Prion strain mutation determined by prion protein conformational compatibility and primary structure." Science **328**(5982): 1154-1158.

Artikis, E., A. Roy, H. Verli, Y. Cordeiro and B. Caughey (2020). "Accommodation of In-Register N-Linked Glycans on Prion Protein Amyloid Cores." ACS Chemical Neuroscience.

Balkema-Buschmann, A., C. Fast, M. Kaatz, M. Eiden, U. Ziegler, L. McIntyre, M. Keller, B. Hills and M. H. Groschup (2011). "Pathogenesis of classical and atypical BSE in cattle." Prev Vet Med **102**(2): 112-117.

Barlow, R. M. (1972). "Transmissible mink encephalopathy: pathogenesis and nature of the aetiological agent." J Clin Pathol Suppl (R Coll Pathol) **6**: 102-109.

Baron, T., A. Bencsik, A. G. Biacabe, E. Morignat and R. A. Bessen (2007). "Phenotypic similarity of transmissible mink encephalopathy in cattle and L-type bovine spongiform encephalopathy in a mouse model." Emerg Infect Dis **13**(12): 1887-1894.

Baron, T., A. G. Biacabe, J. N. Arsac, S. Benestad and M. H. Groschup (2007). "Atypical transmissible spongiform encephalopathies (TSEs) in ruminants." Vaccine **25**(30): 5625-5630.

Baron, T., C. Crozet, A. G. Biacabe, S. Philippe, J. Verchere, A. Bencsik, J. Y. Madec, D. Calavas and J. Samarut (2004). "Molecular analysis of the protease-resistant prion protein in scrapie and bovine spongiform encephalopathy transmitted to ovine transgenic and wild-type mice." J Virol **78**(12): 6243-6251.

Baron, T., J. Vulin, A. G. Biacabe, L. Lakhdar, J. Verchere, J. M. Torres and A. Bencsik (2011). "Emergence of classical BSE strain properties during serial passages of H-BSE in wild-type mice." PLoS One **6**(1): e15839.

Baron, T. G. and A. G. Biacabe (2001). "Molecular analysis of the abnormal prion protein during coinfection of mice by bovine spongiform encephalopathy and a scrapie agent." J Virol **75**(1): 107-114.

Barria, M. A., A. Balachandran, M. Morita, T. Kitamoto, R. Barron, J. Manson, R. Knight, J. W. Ironside and M. W. Head (2014). "Molecular barriers to zoonotic transmission of prions." Emerging infectious diseases **20**(1): 88.

Bartz, J. C., R. F. Marsh, D. I. McKenzie and J. M. Aiken (1998). "The host range of chronic wasting disease is altered on passage in ferrets." Virology **251**(2): 297-301.

Baskakov, I. V., B. Caughey, J. R. Requena, A. M. Sevillano, W. K. Surewicz and H. Wille (2019). "The prion 2018 round tables (I): the structure of PrP(Sc)." Prion **13**(1): 46-52.

Baskakov, I. V. and E. Katorcha (2016). "Multifaceted Role of Sialylation in Prion Diseases." Front Neurosci **10**: 358.

Belay, E. D., R. A. Maddox, E. S. Williams, M. W. Miller, P. Gambetti and L. B. Schonberger (2004). "Chronic wasting disease and potential transmission to humans." Emerg Infect Dis **10**(6): 977-984.

Bencsik, A., S. Debeer, T. Petit and T. Baron (2009). "Possible case of maternal transmission of feline spongiform encephalopathy in a captive cheetah." PLoS One **4**(9): e6929.

Beringue, V., J. L. Vilotte and H. Laude (2008). "Prion agent diversity and species barrier." Vet Res **39**(4): 47.

Bessen, R. A. and R. F. Marsh (1992). "Biochemical and physical properties of the prion protein from two strains of the transmissible mink encephalopathy agent." Journal of virology **66**(4): 2096-2101.

Bessen, R. A. and R. F. Marsh (1992). "Identification of two biologically distinct strains of transmissible mink encephalopathy in hamsters." Journal of General Virology **73**(2): 329-334.

Bessen, R. A. and R. F. Marsh (1994). "Distinct PrP properties suggest the molecular basis of strain variation in transmissible mink encephalopathy." J Virol **68**(12): 7859-7868.

Biacabe, A. G., J. G. Jacobs, A. Bencsik, J. P. Langeveld and T. G. Baron (2007). "H-type bovine spongiform encephalopathy: complex molecular features and similarities with human prion diseases." Prion **1**(1): 61-68.

Biacabe, A. G., J. L. Laplanche, S. Ryder and T. Baron (2004). "Distinct molecular phenotypes in bovine prion diseases." EMBO Rep **5**(1): 110-115.

Biacabe, A. G., E. Morignat, J. Vulin, D. Calavas and T. G. Baron (2008). "Atypical bovine spongiform encephalopathies, France, 2001-2007." Emerg Infect Dis **14**(2): 298-300.

Bolton, D. C., M. P. McKinley and S. B. Prusiner (1982). "Identification of a protein that purifies with the scrapie prion." Science **218**(4579): 1309-1311.

Brandel, J. P., M. B. Vlaicu, A. Culeux, M. Belondrade, D. Bougard, K. Grznarova, A. Denouel, I. Plu, E. Bouaziz-Amar, D. Seilhean, M. Levasseur and S. Haik (2020). "Variant Creutzfeldt-Jakob Disease Diagnosed 7.5 Years after Occupational Exposure." N Engl J Med **383**(1): 83-85.

Brenner, S. and R. W. Horne (1959). "A negative staining method for high resolution electron microscopy of viruses." Biochim Biophys Acta **34**: 103-110.

Brockes, J. P. (1999). "Topics in prion cell biology." Curr Opin Neurobiol **9**(5): 571-577.

Brown, P., F. Cathala, R. Raubertas, D. Gajdusek and P. Castaigne (1987). "The epidemiology of Creutzfeldt-Jakob disease: conclusion of a 15-year investigation in France and review of the world literature." Neurology **37**(6): 895-895.

Bruce, M., A. Chree, I. McConnell, J. Foster, G. Pearson and H. Fraser (1994). "Transmission of bovine spongiform encephalopathy and scrapie to mice: strain variation and the species barrier." Philos Trans R Soc Lond B Biol Sci **343**(1306): 405-411.

Bruce, M. E., R. G. Will, J. W. Ironside, I. McConnell, D. Drummond, A. Suttie, L. McCardle, A. Chree, J. Hope, C. Birkett, S. Cousens, H. Fraser and C. J. Bostock (1997). "Transmissions to mice indicate that 'new variant' CJD is caused by the BSE agent." Nature **389**(6650): 498-501.

Bueler, H., A. Aguzzi, A. Sailer, R. A. Greiner, P. Autenried, M. Aguet and C. Weissmann (1993). "Mice devoid of PrP are resistant to scrapie." Cell **73**(7): 1339-1347.

Buschmann, A. and M. H. Groschup (2005). "Highly bovine spongiform encephalopathy–sensitive transgenic mice confirm the essential restriction of infectivity to the nervous system in clinically diseased cattle." The Journal of infectious diseases **192**(5): 934-942.

Capobianco, R., C. Casalone, S. Suardi, M. Mangieri, C. Miccolo, L. Limido, M. Catania, G. Rossi, G. Di Fede, G. Giaccone, M. G. Bruzzone, L. Minati, C. Corona, P. Acutis, D. Gelmetti, G. Lombardi, M. H. Groschup, A. Buschmann, G. Zanusso, S. Monaco, M. Caramelli and F. Tagliavini (2007). "Conversion of the BASE prion strain into the BSE strain: the origin of BSE?" PLoS Pathog **3**(3): e31.

Casalone, C., G. Zanusso, P. Acutis, S. Ferrari, L. Capucci, F. Tagliavini, S. Monaco and M. Caramelli (2004). "Identification of a second bovine amyloidotic spongiform encephalopathy: molecular similarities with sporadic Creutzfeldt-Jakob disease." Proc Natl Acad Sci U S A **101**(9): 3065-3070.

Castilla, J., R. Morales, P. Saa, M. Barria, P. Gambetti and C. Soto (2008). "Cell-free propagation of prion strains." EMBO J **27**(19): 2557-2566.

Castle, A. R. and A. C. Gill (2017). "Physiological Functions of the Cellular Prion Protein." Front Mol Biosci **4**: 19.

Caughey, B., G. J. Raymond and R. A. Bessen (1998). "Strain-dependent differences in beta-sheet conformations of abnormal prion protein." J Biol Chem **273**(48): 32230-32235.

Caughey, B. W., A. Dong, K. S. Bhat, D. Ernst, S. F. Hayes and W. S. Caughey (1991). "Secondary structure analysis of the scrapie-associated protein PrP 27-30 in water by infrared spectroscopy." Biochemistry **30**(31): 7672-7680.

Chesebro, B., R. Race, K. Wehrly, J. Nishio, M. Bloom, D. Lechner, S. Bergstrom, K. Robbins, L. Mayer, J. M. Keith and et al. (1985). "Identification of scrapie prion protein-specific mRNA in scrapie-infected and uninfected brain." Nature **315**(6017): 331-333.

Chesebro, B., M. Trifilo, R. Race, K. Meade-White, C. Teng, R. LaCasse, L. Raymond, C. Favara, G. Baron, S. Priola, B. Caughey, E. Masliah and M. Oldstone (2005). "Anchorless prion protein results in infectious amyloid disease without clinical scrapie." Science **308**(5727): 1435-1439.

Cobb, N. J., F. D. Sonnichsen, H. McHaourab and W. K. Surewicz (2007). "Molecular architecture of human prion protein amyloid: a parallel, in-register beta-structure." Proc Natl Acad Sci U S A **104**(48): 18946-18951.

Coffey, B., J. Mintert, J. A. Fox, T. C. Schroeder and L. Valentin (2005). "The economic impact of BSE on the US beef industry: Product value losses, regulatory costs, and consumer reactions."

Cohen, F. E., K. M. Pan, Z. Huang, M. Baldwin, R. J. Fletterick and S. B. Prusiner (1994). "Structural clues to prion replication." Science **264**(5158): 530-531.

Colby, D. W. and S. B. Prusiner (2011). "Prions." Cold Spring Harb Perspect Biol **3**(1): a006833.

Collinge, J. (2001). "Prion diseases of humans and animals: their causes and molecular basis." Annu Rev Neurosci **24**: 519-550.

Collinge, J. (2016). "Mammalian prions and their wider relevance in neurodegenerative diseases." Nature **539**(7628): 217-226.

Collinge, J. and A. R. Clarke (2007). "A general model of prion strains and their pathogenicity." Science **318**(5852): 930-936.

Collinge, J., M. S. Palmer and A. J. Dryden (1991). "Genetic predisposition to iatrogenic Creutzfeldt-Jakob disease." Lancet **337**(8755): 1441-1442.

Collinge, J., K. C. Sidle, J. Meads, J. Ironside and A. F. Hill (1996). "Molecular analysis of prion strain variation and the aetiology of'new variant'CJD." Nature **383**(6602): 685-690.

Collinge, J., J. Whitfield, E. McKintosh, J. Beck, S. Mead, D. J. Thomas and M. P. Alpers (2006). "Kuru in the 21st century--an acquired human prion disease with very long incubation periods." Lancet **367**(9528): 2068-2074.

Collins, S., C. A. McLean and C. L. Masters (2001). "Gerstmann-Sträussler-Scheinker syndrome,fatal familial insomnia, and kuru: a review of these less common human transmissible spongiform encephalopathies." J Clin Neurosci **8**(5): 387-397.

Come, J. H., P. E. Fraser and P. T. Lansbury, Jr. (1993). "A kinetic model for amyloid formation in the prion diseases: importance of seeding." Proc Natl Acad Sci U S A **90**(13): 5959-5963.

Comoy, E. E., C. Casalone, N. Lescoutra-Etchegaray, G. Zanusso, S. Freire, D. Marce, F. Auvre, M. M. Ruchoux, S. Ferrari, S. Monaco, N. Sales, M. Caramelli, P. Leboulch, P. Brown, C. I. Lasmezas and J. P. Deslys (2008). "Atypical BSE (BASE) transmitted from asymptomatic aging cattle to a primate." PLoS One **3**(8): e3017.

Costassa, E. V., B. Iulini, M. Mazza, P. Acutis, C. Maurella, D. Meloni, A. Pautasso, L. Capucci, E. Bozzetta, M. M. Simmons, G. Zanusso, M. Pocchiari, C. Corona and C. Casalone (2016). "Pathogenesis and Transmission of Classical and Atypical BSE in Cattle." Food Saf (Tokyo) **4**(4): 130-134.

Creutzfeldt, H. G. (1989). "On a particular focal disease of the central nervous system (preliminary communication), 1920." Alzheimer Dis Assoc Disord **3**(1-2): 3-25.

De Rosier, D. and A. Klug (1968). "Reconstruction of three dimensional structures from electron micrographs." Nature **217**(5124): 130-134.

Dearborn, A. D., J. S. Wall, N. Cheng, J. B. Heymann, A. V. Kajava, J. Varkey, R. Langen and A. C. Steven (2016). "alpha-Synuclein Amyloid Fibrils with Two Entwined, Asymmetrically Associated Protofibrils." J Biol Chem **291**(5): 2310-2318.

Diaz-Espinoza, R. and C. Soto (2012). "High-resolution structure of infectious prion protein: the final frontier." Nat Struct Mol Biol **19**(4): 370-377.

Diener, T. O. (1987). "PrP and the nature of the scrapie agent." Cell **49**(6): 719-721.

Ducrot, C., M. Arnold, A. de Koeijer, D. Heim and D. Calavas (2008). "Review on the epidemiology and dynamics of BSE epidemics." Vet Res **39**(4): 15.

Dudas, S., J. Yang, C. Graham, M. Czub, T. A. McAllister, M. B. Coulthart and S. Czub (2010). "Molecular, biochemical and genetic characteristics of BSE in Canada." PLoS One **5**(5): e10638.

Eckroade, R. J., G. M. ZuRhein and R. P. Hanson (1973). "Transmissible mink encephalopathy in carnivores: clinical, light and electron microscopic studies in raccons, skunks and ferrets." J Wildl Dis **9**(3): 229-240.

Egelman, E. H. (2000). "A robust algorithm for the reconstruction of helical filaments using single-particle methods." Ultramicroscopy **85**(4): 225-234.

Egelman, E. H. (2007). "Single-particle reconstruction from EM images of helical filaments." Curr Opin Struct Biol **17**(5): 556-561.

Eklund, C., R. C. Kennedy and W. Hadlow (1967). "Pathogenesis of scrapie virus infection in the mouse." The Journal of infectious diseases: 15-22.

Eloit, M., K. Adjou, M. Coulpier, J. J. Fontaine, R. Hamel, T. Lilin, S. Messiaen, O. Andreoletti, T. Baron, A. Bencsik, A. G. Biacabe, V. Beringue, H. Laude, A. Le Dur, J. L. Vilotte, E. Comoy, J. P. Deslys, J. Grassi, S. Simon, F. Lantier and P. Sarradin (2005). "BSE agent signatures in a goat." Vet Rec **156**(16): 523-524.

Esmaili, M., B. P. Tancowny, X. Wang, A. Moses, L. M. Cortez, V. L. Sim, H. Wille and M. Overduin (2020). "Native nanodiscs formed by styrene maleic acid copolymer derivatives help recover infectious prion multimers bound to brain-derived lipids." J Biol Chem **295**(25): 8460-8469.

Falcon, B., W. Zhang, A. G. Murzin, G. Murshudov, H. J. Garringer, R. Vidal, R. A. Crowther, B. Ghetti, S. H. W. Scheres and M. Goedert (2018). "Structures of filaments from Pick's disease reveal a novel tau protein fold." Nature **561**(7721): 137-140.

Falcon, B., W. Zhang, M. Schweighauser, A. G. Murzin, R. Vidal, H. J. Garringer, B. Ghetti, S. H. W. Scheres and M. Goedert (2018). "Tau filaments from multiple cases of sporadic and inherited Alzheimer's disease adopt a common fold." Acta Neuropathol **136**(5): 699-708.

Fast, C., M. Keller, A. Balkema-Buschmann, B. Hills and M. H. Groschup (2013). "Complementary studies detecting classical bovine spongiform encephalopathy infectivity in jejunum, ileum and ileocaecal junction in incubating cattle." Vet Res **44**: 123.

Fitzpatrick, A. W. P., B. Falcon, S. He, A. G. Murzin, G. Murshudov, H. J. Garringer, R. A. Crowther, B. Ghetti, M. Goedert and S. H. W. Scheres (2017). "Cryo-EM structures of tau filaments from Alzheimer's disease." Nature **547**(7662): 185-190.

Flores-Fernández, J. M., V. Rathod and H. Wille (2018). "Comparing the Folds of Prions and Other Pathogenic Amyloids." Pathogens **7**(2).

Frank, J., M. Radermacher, P. Penczek, J. Zhu, Y. Li, M. Ladjadj and A. Leith (1996). "SPIDER and WEB: processing and visualization of images in 3D electron microscopy and related fields." J Struct Biol **116**(1): 190-199.

Franz, M., M. Eiden, A. Balkema-Buschmann, J. Greenlee, H. Schatzl, C. Fast, J. Richt, J.-P. Hildebrandt and M. H. Groschup (2012). "Detection of PrPSc in peripheral tissues of clinically

affected cattle after oral challenge with bovine spongiform encephalopathy." Journal of General Virology **93**(12): 2740-2748.

Fukuda, S., Y. Iwamaru, M. Imamura, K. Masujin, Y. Shimizu, Y. Matsuura, Y. Shu, M. Kurachi, K. Kasai, Y. Murayama, S. Onoe, K. Hagiwara, T. Sata, S. Mohri, T. Yokoyama and H. Okada (2009). "Intraspecies transmission of L-type-like Bovine Spongiform Encephalopathy detected in Japan." Microbiol Immunol **53**(12): 704-707.

Gajdusek, D. C. (1965). Slow, Latent, and Temperate Virus Infections: Ed. by D. Carleton Gajdusek [et Al, National Institute of Neurological Diseases and Blindness.

Gajdusek, D. C. (1988). "Transmissible and non-transmissible amyloidoses: autocatalytic post-translational conversion of host precursor proteins to beta-pleated sheet configurations." J Neuroimmunol **20**(2-3): 95-110.

Gajdusek, D. C., C. J. Gibbs and M. Alpers (1966). "Experimental transmission of a Kuru-like syndrome to chimpanzees." Nature **209**(5025): 794-796.

Gajdusek, D. C. and V. Zigas (1957). "Degenerative disease of the central nervous system in New Guinea; the endemic occurrence of kuru in the native population." N Engl J Med **257**(20): 974-978.

Gambetti, P., P. Parchi, R. B. Petersen, S. G. Chen and E. Lugaresi (1995). "Fatal familial insomnia and familial Creutzfeldt-Jakob disease: clinical, pathological and molecular features." Brain pathology **5 1**: 43-51.

Gibbs, C. J., Jr. and D. C. Gajdusek (1973). "Experimental subacute spongiform virus encephalopathies in primates and other laboratory animals." Science **182**(4107): 67-68.

Gibbs, C. J., Jr., D. C. Gajdusek and R. Latarjet (1978). "Unusual resistance to ionizing radiation of the viruses of kuru, Creutzfeldt-Jakob disease, and scrapie." Proc Natl Acad Sci U S A **75**(12): 6268-6270.

Gilch, S., N. Chitoor, Y. Taguchi, M. Stuart, J. E. Jewell and H. M. Schätzl (2011). "Chronic wasting disease." Top Curr Chem **305**: 51-77.

Glaves, J. P., P. A. Gorski, K. Alier, L. Ma, L. Renault, J. O. Primeau, J. H. Jhamandas and H. S. Young (2013). "Distinct morphological and electrophysiological properties of an elk prion peptide." Peptides **40**: 49-56.

Glynn, C., M. R. Sawaya, P. Ge, M. Gallagher-Jones, C. W. Short, R. Bowman, M. Apostol, Z. H. Zhou, D. S. Eisenberg and J. A. Rodriguez (2020). "Cryo-EM structure of a human prion fibril with a hydrophobic, protease-resistant core." Nat Struct Mol Biol **27**(5): 417-423.

Goldmann, W., N. Hunter, J. D. Foster, J. M. Salbaum, K. Beyreuther and J. Hope (1990). "Two alleles of a neural protein gene linked to scrapie in sheep." Proc Natl Acad Sci U S A **87**(7): 2476-2480.

Goldmann, W., N. Hunter, T. Martin, M. Dawson and J. Hope (1991). "Different forms of the bovine PrP gene have five or six copies of a short, GC-rich element within the protein-coding exon." Journal of General Virology **72**(1): 201-204.

Goldmann, W., N. Hunter, G. Smith, J. Foster and J. Hope (1994). "PrP genotype and agent effects in scrapie: change in allelic interaction with different isolates of agent in sheep, a natural host of scrapie." J Gen Virol **75 (Pt 5)**: 989-995.

Gordon, W. S. (1946). "Advances in veterinary research." Vet Rec **58**(47): 516-525.

Govaerts, C., H. Wille, S. B. Prusiner and F. E. Cohen (2004). "Evidence for assembly of prions with left-handed beta-helices into trimers." Proc Natl Acad Sci U S A **101**(22): 8342-8347.

Greenlee, J. J. (2019). "Review: Update on Classical and Atypical Scrapie in Sheep and Goats." Vet Pathol **56**(1): 6-16.

Groveman, B. R., M. A. Dolan, L. M. Taubner, A. Kraus, R. B. Wickner and B. Caughey (2014). "Parallel in-register intermolecular beta-sheet architectures for prion-seeded prion protein (PrP) amyloids." J Biol Chem **289**(35): 24129-24142.

Hadlow, W. J. (1959). "Scrapie and kuru." Scrapie and Kuru.: 289-290.

Hamir, A. N., R. C. Cutlip, J. M. Miller, E. S. Williams, M. J. Stack, M. W. Miller, K. I. O'Rourke and M. J. Chaplin (2001). "Preliminary findings on the experimental transmission of chronic wasting disease agent of mule deer to cattle." J Vet Diagn Invest **13**(1): 91-96.

Hamir, A. N., M. E. Kehrli, Jr., R. A. Kunkle, J. J. Greenlee, E. M. Nicholson, J. A. Richt, J. M. Miller and R. C. Cutlip (2011). "Experimental interspecies transmission studies of the transmissible spongiform encephalopathies to cattle: comparison to bovine spongiform encephalopathy in cattle." J Vet Diagn Invest **23**(3): 407-420.

Hamir, A. N., R. A. Kunkle, J. M. Miller, J. C. Bartz and J. A. Richt (2006). "First and second cattle passage of transmissible mink encephalopathy by intracerebral inoculation." Vet Pathol **43**(2): 118-126.

Hamir, A. N., J. M. Miller, K. I. O'Rourke, J. C. Bartz, M. J. Stack and M. J. Chaplin (2004). "Transmission of Transmissible Mink Encephalopathy to Raccoons (Procyon Lotor) by Intracerebral Inoculation." Journal of Veterinary Diagnostic Investigation **16**(1): 57-63.

Hartsough, G. R. and D. Burger (1965). "Encephalopathy of mink*: I. Epizootiologic and clinical observations." The Journal of Infectious Diseases **115**(4): 387-392.

Hill, A. F., M. Desbruslais, S. Joiner, K. C. Sidle, I. Gowland, J. Collinge, L. J. Doey and P. Lantos (1997). "The same prion strain causes vCJD and BSE." Nature **389**(6650): 448-450, 526.

Hoffmann, C., M. Eiden, M. Kaatz, M. Keller, U. Ziegler, R. Rogers, B. Hills, A. Balkema-Buschmann, L. van Keulen, J. G. Jacobs and M. H. Groschup (2011). "BSE infectivity in jejunum, ileum and ileocaecal junction of incubating cattle." Vet Res **42**: 21.

Hoinville, L. J. (1994). "Decline in the incidence of BSE in cattle born after the introduction of the 'feed ban'." Vet Rec **134**(11): 274-275.

Hope, J. (2013). "Bovine spongiform encephalopathy: a tipping point in One Health and Food Safety." Curr Top Microbiol Immunol **366**: 37-47.

Hornemann, S., C. Schorn and K. Wuthrich (2004). "NMR structure of the bovine prion protein isolated from healthy calf brains." EMBO Rep **5**(12): 1159-1164.

Hourrigan, J. (1979). "Epidemiology of scrapie in the United States." Slow transmissible diseases of the nervous system: 331-336.

Houston, F. and O. Andreoletti (2018). "The zoonotic potential of animal prion diseases." Handb Clin Neurol **153**: 447-462.

Hsiao, K., H. F. Baker, T. J. Crow, M. Poulter, F. Owen, J. D. Terwilliger, D. Westaway, J. Ott and S. B. Prusiner (1989). "Linkage of a prion protein missense variant to Gerstmann–Sträussler syndrome." Nature **338**(6213): 342-345.

Hsiao, K., S. R. Dlouhy, M. R. Farlow, C. Cass, M. Da Costa, P. M. Conneally, M. E. Hodes, B. Ghetti and S. B. Prusiner (1992). "Mutant prion proteins in Gerstmann-Straussler-Scheinker disease with neurofibrillary tangles." Nat Genet **1**(1): 68-71.

Hsiao, K. and S. B. Prusiner (1990). "Inherited human prion diseases." Neurology **40**(12): 1820-1827.

Huang, Y., R. A. Forshee, D. Keire, S. Lee, L. Gregori, D. M. Asher, C. Bett, B. Niland, S. A. Brubaker, S. A. Anderson and H. Yang (2020). "Assessment of risk of variant creutzfeldt-Jakob disease (vCJD) from use of bovine heparin." Pharmacoepidemiol Drug Saf **29**(5): 575-581.

Hubbard, S. J. (1998). "The structural aspects of limited proteolysis of native proteins." Biochim Biophys Acta **1382**(2): 191-206.

Hunter, N., J. D. Foster, G. Benson and J. Hope (1991). "Restriction fragment length polymorphisms of the scrapie-associated fibril protein (PrP) gene and their association with susceptibility to natural scrapie in British sheep." J Gen Virol **72 (Pt 6)**: 1287-1292.

Huor, A., J. C. Espinosa, E. Vidal, H. Cassard, J. Y. Douet, S. Lugan, N. Aron, A. Marin-Moreno, P. Lorenzo, P. Aguilar-Calvo, J. Badiola, R. Bolea, M. Pumarola, S. L. Benestad, L. Orge, A. M. Thackray, R. Bujdoso, J. M. Torres and O. Andreoletti (2019). "The emergence of classical BSE from atypical/Nor98 scrapie." Proc Natl Acad Sci U S A.

Igel-Egalon, A., J. Bohl, M. Moudjou, L. Herzog, F. Reine, H. Rezaei and V. Beringue (2019). "Heterogeneity and Architecture of Pathological Prion Protein Assemblies: Time to Revisit the Molecular Basis of the Prion Replication Process?" Viruses **11**(5).

Jacobs, J. G., J. P. Langeveld, A. G. Biacabe, P. L. Acutis, M. P. Polak, D. Gavier-Widen, A. Buschmann, M. Caramelli, C. Casalone, M. Mazza, M. Groschup, J. H. Erkens, A. Davidse, F. G. van Zijderveld and T. Baron (2007). "Molecular discrimination of atypical bovine spongiform encephalopathy strains from a geographical region spanning a wide area in Europe." J Clin Microbiol **45**(6): 1821-1829.

Jarrett, J. T. and P. T. Lansbury, Jr. (1993). "Seeding "one-dimensional crystallization" of amyloid: a pathogenic mechanism in Alzheimer's disease and scrapie?" Cell **73**(6): 1055-1058.

Jeffrey, M., L. González, A. Chong, J. Foster, W. Goldmann, N. Hunter and S. Martin (2006). "Ovine infection with the agents of scrapie (CH1641 isolate) and bovine spongiform encephalopathy: immunochemical similarities can be resolved by immunohistochemistry." J Comp Pathol **134**(1): 17-29.

Kaatz, M., C. Fast, U. Ziegler, A. Balkema-Buschmann, B. Hammerschmidt, M. Keller, A. Oelschlegel, L. McIntyre and M. H. Groschup (2012). "Spread of classic BSE prions from the gut via the peripheral nervous system to the brain." Am J Pathol **181**(2): 515-524.

Kajava, A. V. and A. C. Steven (2006). "Beta-rolls, beta-helices, and other beta-solenoid proteins." Adv Protein Chem **73**: 55-96.

Kimberlin, R. H., S. Cole and C. A. Walker (1986). "Transmissible mink encephalopathy (TME) in Chinese hamsters: identification of two strains of TME and comparisons with scrapie." Neuropathol Appl Neurobiol **12**(2): 197-206.

Knaus, K. J., M. Morillas, W. Swietnicki, M. Malone, W. K. Surewicz and V. C. Yee (2001). "Crystal structure of the human prion protein reveals a mechanism for oligomerization." Nat Struct Biol **8**(9): 770-774.

Kocisko, D. A., P. T. Lansbury, Jr. and B. Caughey (1996). "Partial unfolding and refolding of scrapie-associated prion protein: evidence for a critical 16-kDa C-terminal domain." Biochemistry **35**(41): 13434-13442.

Kong, Q., S. Huang, W. Zou, D. Vanegas, M. Wang, D. Wu, J. Yuan, M. Zheng, H. Bai, H. Deng, K. Chen, A. L. Jenny, K. O'Rourke, E. D. Belay, L. B. Schonberger, R. B. Petersen, M. S. Sy, S. G. Chen and P. Gambetti (2005). "Chronic wasting disease of elk: transmissibility to humans examined by transgenic mouse models." J Neurosci **25**(35): 7944-7949.

Kong, Q., M. Zheng, C. Casalone, L. Qing, S. Huang, B. Chakraborty, P. Wang, F. Chen, I. Cali, C. Corona, F. Martucci, B. Iulini, P. Acutis, L. Wang, J. Liang, M. Wang, X. Li, S. Monaco, G. Zanusso, W. Q. Zou, M. Caramelli and P. Gambetti (2008). "Evaluation of the human transmission risk of an atypical bovine spongiform encephalopathy prion strain." J Virol **82**(7): 3697-3701.

Konold, T., G. E. Bone, D. Clifford, M. J. Chaplin, S. Cawthraw, M. J. Stack and M. M. Simmons (2012). "Experimental H-type and L-type bovine spongiform encephalopathy in cattle: observation of two clinical syndromes and diagnostic challenges." BMC Vet Res **8**: 22.

Kraus, A., F. Hoyt, C. L. Schwartz, B. Hansen, A. G. Hughson, E. Artikis, B. Race and B. Caughey (2021). "Structure of an infectious mammalian prion." bioRxiv: 2021.2002.2014.431014.

Kuczius, T. and M. H. Groschup (1999). "Differences in proteinase K resistance and neuronal deposition of abnormal prion proteins characterize bovine spongiform encephalopathy (BSE) and scrapie strains." Molecular medicine **5**(6): 406-418.

Kuczius, T., I. Haist and M. H. Groschup (1998). "Molecular Analysis of Bovine Spongiform Encephalopathy and Scrapie Strain Variation." The Journal of Infectious Diseases **178**(3): 693-699.

Laferrière, F., P. Tixador, M. Moudjou, J. Chapuis, P. Sibille, L. Herzog, F. Reine, E. Jaumain, H. Laude and H. Rezaei (2013). "Quaternary structure of pathological prion protein as a determining factor of strain-specific prion replication dynamics." PLoS Pathog **9**(10): e1003702.

Laplanche, J. L., J. Chatelain, D. Westaway, S. Thomas, M. Dussaucy, J. Brugere-Picoux and J. M. Launay (1993). "PrP polymorphisms associated with natural scrapie discovered by denaturing gradient gel electrophoresis." Genomics **15**(1): 30-37.

Le Roy, D. G., K. K. Klein and T. Klvacek (2006). The losses in the beef sector in Canada from BSE.

Leffers, K. W., H. Wille, J. Stohr, E. Junger, S. B. Prusiner and D. Riesner (2005). "Assembly of natural and recombinant prion protein into fibrils." Biol Chem **386**(6): 569-580.

Legname, G., I. V. Baskakov, H. O. Nguyen, D. Riesner, F. E. Cohen, S. J. DeArmond and S. B. Prusiner (2004). "Synthetic mammalian prions." Science **305**(5684): 673-676.

Levine, D. J., J. Stohr, L. E. Falese, J. Ollesch, H. Wille, S. B. Prusiner and J. R. Long (2015). "Mechanism of scrapie prion precipitation with phosphotungstate anions." ACS Chem Biol **10**(5): 1269-1277.

Lezmi, S., S. Martin, S. Simon, E. Comoy, A. Bencsik, J. P. Deslys, J. Grassi, M. Jeffrey and T. Baron (2004). "Comparative molecular analysis of the abnormal prion protein in field scrapie cases and experimental bovine spongiform encephalopathy in sheep by use of Western blotting and immunohistochemical methods." J Virol **78**(7): 3654-3662.

Liemann, S. and R. Glockshuber (1999). "Influence of amino acid substitutions related to inherited human prion diseases on the thermodynamic stability of the cellular prion protein." Biochemistry **38**(11): 3258-3267.

Locht, C., B. Chesebro, R. Race and J. M. Keith (1986). "Molecular cloning and complete sequence of prion protein cDNA from mouse brain infected with the scrapie agent." Proc Natl Acad Sci U S A **83**(17): 6372-6376.

Lombardi, G., C. Casalone, D. A. A, D. Gelmetti, G. Torcoli, I. Barbieri, C. Corona, E. Fasoli, A. Farinazzo, M. Fiorini, M. Gelati, B. Iulini, F. Tagliavini, S. Ferrari, M. Caramelli, S. Monaco, L. Capucci and G. Zanusso (2008). "Intraspecies transmission of BASE induces clinical dullness and amyotrophic changes." PLoS Pathog **4**(5): e1000075.

Lopez Garcia, F., R. Zahn, R. Riek and K. Wuthrich (2000). "NMR structure of the bovine prion protein." Proc Natl Acad Sci U S A **97**(15): 8334-8339.

Ludtke, S. J., P. R. Baldwin and W. Chiu (1999). "EMAN: semiautomated software for high-resolution single-particle reconstructions." J Struct Biol **128**(1): 82-97.

Lugaresi, E., R. Medori, P. Montagna, A. Baruzzi, P. Cortelli, A. Lugaresi, P. Tinuper, M. Zucconi and P. Gambetti (1986). "Fatal familial insomnia and dysautonomia with selective degeneration of thalamic nuclei." N Engl J Med **315**(16): 997-1003.

Maddelein, M. L., S. Dos Reis, S. Duvezin-Caubet, B. Coulary-Salin and S. J. Saupe (2002). "Amyloid aggregates of the HET-s prion protein are infectious." Proc Natl Acad Sci U S A **99**(11): 7402-7407.

Manson, J., J. D. West, V. Thomson, P. McBride, M. H. Kaufman and J. Hope (1992). "The prion protein gene: a role in mouse embryogenesis?" Development **115**(1): 117-122.

Marsh, R. and G. Hartsough (1988). Evidence that transmissible mink encephalopathy results from feeding infected cattle. Proceedings of the Fourth International Scientific Congress in Fur Animal Production, Canada Mink Breeders Association, Toronto.

Marsh, R. F., R. A. Bessen, S. Lehmann and G. R. Hartsough (1991). "Epidemiological and experimental studies on a new incident of transmissible mink encephalopathy." The Journal of general virology **72 (Pt 3)**: 589-594.

Marsh, R. F. and R. P. Hanson (1969). "Physical and chemical properties of the transmissible mink encephalopathy agent." J Virol **3**(2): 176-180.

Martín-Pastor, M., Y. B. Codeseira, G. Spagnolli, H. Eraña, L. C. Fernández, S. Bravo, A. Iglesias, R. López-Moreno, S. Veiga, E. Biasini, V. M. Sánchez-Pedregal, J. Castilla and J. R. Requena (2020). "Structural features of an infectious recombinant PrP^{Sc} prion using solid state NMR." bioRxiv: 2020.2004.2008.032839.

Masters, C. L., D. C. Gajdusek and C. J. Gibbs, Jr. (1981). "Creutzfeldt-Jakob disease virus isolations from the Gerstmann-Sträussler syndrome with an analysis of the various forms of amyloid plaque deposition in the virus-induced spongiform encephalopathies." Brain **104**(3): 559-588.

Masujin, K., H. Okada, K. Miyazawa, Y. Matsuura, M. Imamura, Y. Iwamaru, Y. Murayama and T. Yokoyama (2016). "Emergence of a novel bovine spongiform encephalopathy (BSE) prion from an atypical H-type BSE." Sci Rep **6**: 22753.

McKinley, M. P., D. C. Bolton and S. B. Prusiner (1983). "A protease-resistant protein is a structural component of the scrapie prion." Cell **35**(1): 57-62.

McKinley, M. P., R. K. Meyer, L. Kenaga, F. Rahbar, R. Cotter, A. Serban and S. B. Prusiner (1991). "Scrapie prion rod formation in vitro requires both detergent extraction and limited proteolysis." J Virol **65**(3): 1340-1351.

Medori, R., H. J. Tritschler, A. LeBlanc, F. Villare, V. Manetto, H. Y. Chen, R. Xue, S. Leal, P. Montagna, P. Cortelli and et al. (1992). "Fatal familial insomnia, a prion disease with a mutation at codon 178 of the prion protein gene." N Engl J Med **326**(7): 444-449.

Meinhardt, J., C. Sachse, P. Hortschansky, N. Grigorieff and M. Fandrich (2009). "Abeta(1-40) fibril polymorphism implies diverse interaction patterns in amyloid fibrils." J Mol Biol **386**(3): 869-877.

Merril, C. R., M. L. Dunau and D. Goldman (1981). "A rapid sensitive silver stain for polypeptides in polyacrylamide gels." Anal Biochem **110**(1): 201-207.

Merz, P. A., R. A. Somerville, H. M. Wisniewski and K. Iqbal (1981). "Abnormal fibrils from scrapie-infected brain." Acta Neuropathol **54**(1): 63-74.

Miyazawa, A., Y. Fujiyoshi, M. Stowell and N. Unwin (1999). "Nicotinic acetylcholine receptor at 4.6 A resolution: transverse tunnels in the channel wall." J Mol Biol **288**(4): 765-786.

Morales, R. (2017). "Prion strains in mammals: Different conformations leading to disease." PLoS Pathog **13**(7): e1006323.

Morales, R., K. Abid and C. Soto (2007). "The prion strain phenomenon: molecular basis and unprecedented features." Biochim Biophys Acta **1772**(6): 681-691.

Nathanson, N., J. Wilesmith and C. Griot (1997). "Bovine Spongiform Encephalopathy (BSE): Causes and Consequences of a Common Source Epidemic." American Journal of Epidemiology **145**(11): 959-969.

Nguyen, J. T., H. Inouye, M. A. Baldwin, R. J. Fletterick, F. E. Cohen, S. B. Prusiner and D. A. Kirschner (1995). "X-ray diffraction of scrapie prion rods and PrP peptides." J Mol Biol **252**(4): 412-422.

Nicholson, E. M., H. Mo, S. B. Prusiner, F. E. Cohen and S. Marqusee (2002). "Differences between the prion protein and its homolog Doppel: a partially structured state with implications for scrapie formation." J Mol Biol **316**(3): 807-815.

Nicot, S., A. Bencsik, S. Migliore, D. Canal, M. Leboidre, U. Agrimi, R. Nonno and T. Baron (2014). "L-type bovine spongiform encephalopathy in genetically susceptible and resistant sheep: changes in prion strain or phenotypic plasticity of the disease-associated prion protein?" J Infect Dis **209**(6): 950-959.

Oesch, B., D. Westaway, M. Walchli, M. P. McKinley, S. B. Kent, R. Aebersold, R. A. Barry, P. Tempst, D. B. Teplow, L. E. Hood and et al. (1985). "A cellular gene encodes scrapie PrP 27-30 protein." Cell **40**(4): 735-746.

Ohi, M., Y. Li, Y. Cheng and T. Walz (2004). "Negative Staining and Image Classification - Powerful Tools in Modern Electron Microscopy." Biol Proced Online **6**: 23-34.

Okada, H., K. Miyazawa, S. Fukuda, Y. Iwamaru, M. Imamura, K. Masujin, Y. Matsuura, T. Fujii, K. Fujii, S. Kageyama, M. Yoshioka, Y. Murayama and T. Yokoyama (2014). "The presence of disease-associated prion protein in skeletal muscle of cattle infected with classical bovine spongiform encephalopathy." J Vet Med Sci **76**(1): 103-107.

Pan, K. M., M. Baldwin, J. Nguyen, M. Gasset, A. Serban, D. Groth, I. Mehlhorn, Z. Huang, R. J. Fletterick, F. E. Cohen and et al. (1993). "Conversion of alpha-helices into beta-sheets features in the formation of the scrapie prion proteins." Proc Natl Acad Sci U S A **90**(23): 10962-10966.

Pettersen, E. F., T. D. Goddard, C. C. Huang, G. S. Couch, D. M. Greenblatt, E. C. Meng and T. E. Ferrin (2004). "UCSF Chimera--a visualization system for exploratory research and analysis." J Comput Chem **25**(13): 1605-1612.

Priola, S. A. and B. Chesebro (1995). "A single hamster PrP amino acid blocks conversion to protease-resistant PrP in scrapie-infected mouse neuroblastoma cells." J Virol **69**(12): 7754-7758.

Prusiner, S. B. (1982). "Novel proteinaceous infectious particles cause scrapie." Science **216**(4542): 136-144.

Prusiner, S. B. (1991). "Molecular biology of prion diseases." Science **252**(5012): 1515-1522.

Prusiner, S. B. (1998). "Prions." Proc Natl Acad Sci U S A **95**(23): 13363-13383.

Prusiner, S. B. (2004). Prion biology and diseases, Cold Spring Harbor Laboratory Press.

Prusiner, S. B., D. C. Bolton, D. F. Groth, K. A. Bowman, S. P. Cochran and M. P. McKinley (1982). "Further purification and characterization of scrapie prions." Biochemistry **21**(26): 6942-6950.

Prusiner, S. B., D. C. Bolton, D. F. Groth, K. A. Bowman, S. P. Cochran and M. P. McKinley (1982). "Further purification and characterization of scrapie prions." Biochemistry **21**(26): 6942-6950.

Prusiner, S. B. and S. J. DeArmond (1994). "Prion diseases and neurodegeneration." Annu Rev Neurosci **17**: 311-339.

Prusiner, S. B., M. P. McKinley, K. A. Bowman, D. C. Bolton, P. E. Bendheim, D. F. Groth and G. G. Glenner (1983). "Scrapie prions aggregate to form amyloid-like birefringent rods." Cell **35**(2): 349-358.

Prusiner, S. B., M. Scott, D. Foster, K. M. Pan, D. Groth, C. Mirenda, M. Torchia, S. L. Yang, D. Serban, G. A. Carlson and et al. (1990). "Transgenetic studies implicate interactions between homologous PrP isoforms in scrapie prion replication." Cell **63**(4): 673-686.

Puoti, G., A. Bizzi, G. Forloni, J. G. Safar, F. Tagliavini and P. Gambetti (2012). "Sporadic human prion diseases: molecular insights and diagnosis." Lancet Neurol **11**(7): 618-628.

Requena, J. R. (2020). "The protean prion protein." PLoS Biol **18**(6): e3000754.

Requena, J. R. and H. Wille (2014). "The structure of the infectious prion protein: experimental data and molecular models." Prion **8**(1): 60-66.

Richardson, J. S. and D. C. Richardson (2002). "Natural β-sheet proteins use negative design to avoid edge-to-edge aggregation." Proceedings of the National Academy of Sciences **99**(5): 2754-2759.

Richt, J. A. and S. M. Hall (2008). "BSE case associated with prion protein gene mutation." PLoS Pathog **4**(9): e1000156.

Riek, R., S. Hornemann, G. Wider, M. Billeter, R. Glockshuber and K. Wuthrich (1996). "NMR structure of the mouse prion protein domain PrP(121-231)." Nature **382**(6587): 180-182.

Riek, R., S. Hornemann, G. Wider, R. Glockshuber and K. Wuthrich (1997). "NMR characterization of the full-length recombinant murine prion protein, mPrP(23-231)." FEBS Lett **413**(2): 282-288.

Rivera, N. A., A. L. Brandt, J. E. Novakofski and N. E. Mateus-Pinilla (2019). "Chronic Wasting Disease In Cervids: Prevalence, Impact And Management Strategies." Vet Med (Auckl) **10**: 123-139.

Robinson, M. M., W. J. Hadlow, D. P. Knowles, T. P. Huff, P. A. Lacy, R. F. Marsh and J. R. Gorham (1995). "Experimental infection of cattle with the agents of transmissible mink encephalopathy and scrapie." J Comp Pathol **113**(3): 241-251.

Ryder, S., G. Dexter, S. Bellworthy and S. Tongue (2004). "Demonstration of lateral transmission of scrapie between sheep kept under natural conditions using lymphoid tissue biopsy." Research in veterinary science **76**(3): 211-217.

Safar, J., H. Wille, V. Itri, D. Groth, H. Serban, M. Torchia, F. E. Cohen and S. B. Prusiner (1998). "Eight prion strains have PrP(Sc) molecules with different conformations." Nat Med **4**(10): 1157-1165.

Safar, J. G., M. Scott, J. Monaghan, C. Deering, S. Didorenko, J. Vergara, H. Ball, G. Legname, E. Leclerc, L. Solforosi, H. Serban, D. Groth, D. R. Burton, S. B. Prusiner and R. A. Williamson (2002). "Measuring prions causing bovine spongiform encephalopathy or chronic wasting disease by immunoassays and transgenic mice." Nat Biotechnol **20**(11): 1147-1150.

Sajnani, G., M. A. Pastrana, I. Dynin, B. Onisko and J. R. Requena (2008). "Scrapie prion protein structural constraints obtained by limited proteolysis and mass spectrometry." J Mol Biol **382**(1): 88-98.

Saupe, S. J. (2007). "A short history of small s: a prion of the fungus Podospora anserina." Prion **1**(2): 110-115.

Schenkein, J. and P. Montagna (2006). "Self-management of fatal familial insomnia. Part 2: case report." MedGenMed **8**(3): 66.

Scheres, S. H., W. Zhang, B. Falcon and M. Goedert (2020). "Cryo-EM structures of tau filaments." Curr Opin Struct Biol **64**: 17-25.

Scott, M., D. Foster, C. Mirenda, D. Serban, F. Coufal, M. Wälchli, M. Torchia, D. Groth, G. Carlson, S. J. DeArmond, D. Westaway and S. B. Prusiner (1989). "Transgenic mice expressing hamster prion protein produce species-specific scrapie infectivity and amyloid plaques." Cell **59**(5): 847-857.

Scott, M. R., J. Safar, G. Telling, O. Nguyen, D. Groth, M. Torchia, R. Koehler, P. Tremblay, D. Walther, F. E. Cohen, S. J. DeArmond and S. B. Prusiner (1997). "Identification of a prion protein epitope modulating transmission of bovine spongiform encephalopathy prions to transgenic mice." Proc Natl Acad Sci U S A **94**(26): 14279-14284.

Scott, M. R., R. Will, J. Ironside, H. O. Nguyen, P. Tremblay, S. J. DeArmond and S. B. Prusiner (1999). "Compelling transgenetic evidence for transmission of bovine spongiform encephalopathy prions to humans." Proc Natl Acad Sci U S A **96**(26): 15137-15142.

Senatore, A., K. Frontzek, M. Emmenegger, A. Chincisan, M. Losa, R. Reimann, G. Horny, J. Guo, S. Fels, S. Sorce, C. Zhu, N. George, S. Ewert, T. Pietzonka, S. Hornemann and A. Aguzzi (2020). "Protective anti-prion antibodies in human immunoglobulin repertoires." EMBO Mol Med **12**(9): e12739.

Silva, C. J., E. Vázquez-Fernández, B. Onisko and J. R. Requena (2015). "Proteinase K and the structure of PrPSc: The good, the bad and the ugly." Virus Res **207**: 120-126.

Sim, V. L. and B. Caughey (2009). "Ultrastructures and strain comparison of under-glycosylated scrapie prion fibrils." Neurobiol Aging **30**(12): 2031-2042.

Simmons, H. A., M. M. Simmons, Y. I. Spencer, M. J. Chaplin, G. Povey, A. Davis, A. Ortiz-Pelaez, N. Hunter, D. Matthews and A. E. Wrathall (2009). "Atypical scrapie in sheep from a UK research flock which is free from classical scrapie." BMC veterinary research **5**(1): 1-9.

Simonic, T., S. Duga, B. Strumbo, R. Asselta, F. Ceciliani and S. Ronchi (2000). "cDNA cloning of turtle prion protein." FEBS Lett **469**(1): 33-38.

Smirnovas, V., G. S. Baron, D. K. Offerdahl, G. J. Raymond, B. Caughey and W. K. Surewicz (2011). "Structural organization of brain-derived mammalian prions examined by hydrogen-deuterium exchange." Nat Struct Mol Biol **18**(4): 504-506.

Smith, P. G. (2003). "The epidemics of bovine spongiform encephalopathy and variant Creutzfeldt-Jakob disease: current status and future prospects." Bull World Health Organ **81**(2): 123-130.

Spagnolli, G., M. Rigoli, G. Novi Inverardi, Y. B. Codeseira, E. Biasini and J. R. Requena (2020). "Modeling PrP(Sc) Generation Through Deformed Templating." Front Bioeng Biotechnol **8**: 590501.

Spagnolli, G., M. Rigoli, S. Orioli, A. M. Sevillano, P. Faccioli, H. Wille, E. Biasini and J. R. Requena (2019). "Full atomistic model of prion structure and conversion." PLoS Pathog **15**(7): e1007864.

Spencer, M. D., R. S. Knight and R. G. Will (2002). "First hundred cases of variant Creutzfeldt-Jakob disease: retrospective case note review of early psychiatric and neurological features." BMJ **324**(7352): 1479-1482.

Stack, M. J., S. J. Moore, A. Vidal-Diez, M. E. Arnold, E. M. Jones, Y. I. Spencer, P. Webb, J. Spiropoulos, L. Powell, P. Bellerby, L. Thurston, J. Cooper, M. J. Chaplin, L. A. Davis, S. Everitt, R. Focosi-Snyman, S. A. Hawkins, M. M. Simmons and G. A. Wells (2011). "Experimental bovine spongiform encephalopathy: detection of PrP(Sc) in the small intestine relative to exposure dose and age." J Comp Pathol **145**(2-3): 289-301.

Stahl, N., M. A. Baldwin, D. B. Teplow, L. Hood, B. W. Gibson, A. L. Burlingame and S. B. Prusiner (1993). "Structural studies of the scrapie prion protein using mass spectrometry and amino acid sequencing." Biochemistry **32**(8): 1991-2002.

Supattapone, S., P. Bosque, T. Muramoto, H. Wille, C. Aagaard, D. Peretz, H. O. Nguyen, C. Heinrich, M. Torchia, J. Safar, F. E. Cohen, S. J. DeArmond, S. B. Prusiner and M. Scott (1999). "Prion protein of 106 residues creates an artifical transmission barrier for prion replication in transgenic mice." Cell **96**(6): 869-878.

Telling, G., P. Parchi, S. DeArmond, P. Cortelli, P. Montagna, R. Gabizon, J. Mastrianni, E. Lugaresi, P. Gambetti and S. Prusiner (1996). "Evidence for the Conformation of the Pathologic Isoform of the Prion Protein Enciphering and Propagating Prion Diversity." Science **274**: 2079 - 2082.

Terry, C., R. L. Harniman, J. Sells, A. Wenborn, S. Joiner, H. R. Saibil, M. J. Miles, J. Collinge and J. D. F. Wadsworth (2019). "Structural features distinguishing infectious ex vivo mammalian prions from non-infectious fibrillar assemblies generated in vitro." Sci Rep **9**(1): 376.

Terry, C. and J. D. F. Wadsworth (2019). "Recent Advances in Understanding Mammalian Prion Structure: A Mini Review." Front Mol Neurosci **12**: 169.

Terry, C., A. Wenborn, N. Gros, J. Sells, S. Joiner, L. L. Hosszu, M. H. Tattum, S. Panico, D. K. Clare, J. Collinge, H. R. Saibil and J. D. Wadsworth (2016). "Ex vivo mammalian prions are formed of paired double helical prion protein fibrils." Open Biol **6**(5).

Terry, L., S. Marsh, S. Ryder, S. Hawkins, G. Wells and Y. Spencer (2003). "Detection of disease-specific PrP in the distal ileum of cattle exposed orally to the agent of bovine spongiform encephalopathy." Veterinary Record **152**(13): 387-392.

Torres, J. M., O. Andreoletti, C. Lacroux, I. Prieto, P. Lorenzo, M. Larska, T. Baron and J. C. Espinosa (2011). "Classical bovine spongiform encephalopathy by transmission of H-type prion in homologous prion protein context." Emerg Infect Dis **17**(9): 1636-1644.

Touzeau, S., M. E. Chase-Topping, L. Matthews, D. Lajous, F. Eychenne, N. Hunter, J. D. Foster, G. Simm, J. M. Elsen and M. E. Woolhouse (2006). "Modelling the spread of scrapie in a sheep flock: evidence for increased transmission during lambing seasons." Arch Virol **151**(4): 735-751.

Turner, M. L. and C. A. Ludlam (2009). "An update on the assessment and management of the risk of transmission of variant Creutzfeldt-Jakob disease by blood and plasma products." Br J Haematol **144**(1): 14-23.

Tycko, R., R. Savtchenko, V. G. Ostapchenko, N. Makarava and I. V. Baskakov (2010). "The α-helical C-terminal domain of full-length recombinant PrP converts to an in-register parallel β-sheet structure in PrP fibrils: evidence from solid state nuclear magnetic resonance." Biochemistry **49**(44): 9488-9497.

Tzaban, S., G. Friedlander, O. Schonberger, L. Horonchik, Y. Yedidia, G. Shaked, R. Gabizon and A. Taraboulos (2002). "Protease-sensitive scrapie prion protein in aggregates of heterogeneous sizes." Biochemistry **41**(42): 12868-12875.

van Duijn, C. M., N. Delasnerie-Laupretre, C. Masullo, I. Zerr, R. de Silva, D. P. Wientjens, J. P. Brandel, T. Weber, V. Bonavita, M. Zeidler, A. Alperovitch, S. Poser, E. Granieri, A. Hofman and R. G. Will (1998). "Case-control study of risk factors of Creutzfeldt-Jakob disease in Europe during 1993-95. European Union (EU) Collaborative Study Group of Creutzfeldt-Jakob disease (CJD)." Lancet **351**(9109): 1081-1085.

van Heel, M., G. Harauz, E. V. Orlova, R. Schmidt and M. Schatz (1996). "A new generation of the IMAGIC image processing system." J Struct Biol **116**(1): 17-24.

Van Melckebeke, H., C. Wasmer, A. Lange, E. Ab, A. Loquet, A. Bockmann and B. H. Meier (2010). "Atomic-resolution three-dimensional structure of HET-s(218-289) amyloid fibrils by solid-state NMR spectroscopy." J Am Chem Soc **132**(39): 13765-13775.

Vanni, I., L. Pirisinu, C. Acevedo-Morantes, R. Kamali-Jamil, V. Rathod, M. A. Di Bari, C. D'Agostino, S. Marcon, E. Esposito, G. Riccardi, S. Hornemann, A. Senatore, A. Aguzzi, U. Agrimi, H. Wille and R. Nonno (2020). "Isolation of infectious, non-fibrillar and oligomeric prions from a genetic prion disease." Brain **143**(5): 1512-1524.

Vázquez-Fernández, E., J. Alonso, M. A. Pastrana, A. Ramos, L. Stitz, E. Vidal, I. Dynin, B. Petsch, C. J. Silva and J. R. Requena (2012). "Structural organization of mammalian prions as probed by limited proteolysis." PLoS One **7**(11): e50111.

Vazquez-Fernandez, E., M. R. Vos, P. Afanasyev, L. Cebey, A. M. Sevillano, E. Vidal, I. Rosa, L. Renault, A. Ramos, P. J. Peters, J. J. Fernandez, M. van Heel, H. S. Young, J. R. Requena and H. Wille (2016). "The Structural Architecture of an Infectious Mammalian Prion Using Electron Cryomicroscopy." PLoS Pathog **12**(9): e1005835.

Vazquez-Fernandez, E., H. S. Young, J. R. Requena and H. Wille (2017). "The Structure of Mammalian Prions and Their Aggregates." Int Rev Cell Mol Biol **329**: 277-301.

Waddell, L., J. Greig, M. Mascarenhas, A. Otten, T. Corrin and K. Hierlihy (2018). "Current evidence on the transmissibility of chronic wasting disease prions to humans-A systematic review." Transbound Emerg Dis **65**(1): 37-49.

Wadsworth, J. D., A. F. Hill, J. A. Beck and J. Collinge (2003). "Molecular and clinical classification of human prion disease." Br Med Bull **66**: 241-254.

Wan, W. and G. Stubbs (2014). "Heterogeneous seeding of HET-s(218-289) and the mutability of prion structures." Prion **8**(2).

Wan, W., H. Wille, J. Stohr, U. Baxa, S. B. Prusiner and G. Stubbs (2012). "Degradation of fungal prion HET-s(218-289) induces formation of a generic amyloid fold." Biophys J **102**(10): 2339-2344.

Wang, F., X. Wang, R. Abskharon and J. Ma (2018). "Prion infectivity is encoded exclusively within the structure of proteinase K-resistant fragments of synthetically generated recombinant PrP(Sc)." Acta Neuropathol Commun **6**(1): 30.

Wang, F., X. Wang, C. D. Orru, B. R. Groveman, K. Surewicz, R. Abskharon, M. Imamura, T. Yokoyama, Y. S. Kim, K. J. Vander Stel, K. Sinniah, S. A. Priola, W. K. Surewicz, B. Caughey and J. Ma (2017). "Self-propagating, protease-resistant, recombinant prion protein conformers with or without in vivo pathogenicity." PLoS Pathog **13**(7): e1006491.

Wang, L. Q., K. Zhao, H. Y. Yuan, Q. Wang, Z. Guan, J. Tao, X. N. Li, Y. Sun, C. W. Yi, J. Chen, D. Li, D. Zhang, P. Yin, C. Liu and Y. Liang (2020). "Cryo-EM structure of an amyloid fibril formed by full-length human prion protein." Nat Struct Mol Biol **27**(6): 598-602.

Wasmer, C., A. Lange, H. Van Melckebeke, A. B. Siemer, R. Riek and B. H. Meier (2008). "Amyloid fibrils of the HET-s(218-289) prion form a beta solenoid with a triangular hydrophobic core." Science **319**(5869): 1523-1526.

Weissmann, C. (2004). "The state of the prion." Nat Rev Microbiol **2**(11): 861-871.

Wells, G. A., A. Scott, C. Johnson, R. Gunning, R. Hancock, M. Jeffrey, M. Dawson and R. Bradley (1987). "A novel progressive spongiform encephalopathy in cattle." Veterinary Record **121**(18): 419-420.

Wells, G. A., J. Spiropoulos, S. A. Hawkins and S. J. Ryder (2005). "Pathogenesis of experimental bovine spongiform encephalopathy: preclinical infectivity in tonsil and observations on the distribution of lingual tonsil in slaughtered cattle." Vet Rec **156**(13): 401-407.

Westaway, D., V. Zuliani, C. M. Cooper, M. Da Costa, S. Neuman, A. L. Jenny, L. Detwiler and S. B. Prusiner (1994). "Homozygosity for prion protein alleles encoding glutamine-171 renders sheep susceptible to natural scrapie." Genes & development **8**(8): 959-969.

Whittaker, M., E. M. Wilson-Kubalek, J. E. Smith, L. Faust, R. A. Milligan and H. L. Sweeney (1995). "A 35-A movement of smooth muscle myosin on ADP release." Nature **378**(6558): 748-751.

Wickner, R. B., H. K. Edskes, M. Son, E. E. Bezsonov, M. DeWilde and M. Ducatez (2018). "Yeast Prions Compared to Functional Prions and Amyloids." J Mol Biol **430**(20): 3707-3719.

Wilesmith, J. W., J. B. Ryan and M. J. Atkinson (1991). "Bovine spongiform encephalopathy: epidemiological studies on the origin." Vet Rec **128**(9): 199-203.

Wilesmith, J. W., G. A. Wells, M. P. Cranwell and J. B. Ryan (1988). "Bovine spongiform encephalopathy: epidemiological studies." Vet Rec **123**(25): 638-644.

Will, R. G., J. W. Ironside, M. Zeidler, S. N. Cousens, K. Estibeiro, A. Alperovitch, S. Poser, M. Pocchiari, A. Hofman and P. G. Smith (1996). "A new variant of Creutzfeldt-Jakob disease in the UK." Lancet **347**(9006): 921-925.

Will, R. G., M. Zeidler, G. E. Stewart, M. A. Macleod, J. W. Ironside, S. N. Cousens, J. Mackenzie, K. Estibeiro, A. J. Green and R. S. Knight (2000). "Diagnosis of new variant Creutzfeldt-Jakob disease." Ann Neurol **47**(5): 575-582.

Wille, H., W. Bian, M. McDonald, A. Kendall, D. W. Colby, L. Bloch, J. Ollesch, A. L. Borovinskiy, F. E. Cohen, S. B. Prusiner and G. Stubbs (2009). "Natural and synthetic prion structure from X-ray fiber diffraction." Proc Natl Acad Sci U S A **106**(40): 16990-16995.

Wille, H., C. Govaerts, A. Borovinskiy, D. Latawiec, K. H. Downing, F. E. Cohen and S. B. Prusiner (2007). "Electron crystallography of the scrapie prion protein complexed with heavy metals." Arch Biochem Biophys **467**(2): 239-248.

Wille, H., M. D. Michelitsch, V. Guenebaut, S. Supattapone, A. Serban, F. E. Cohen, D. A. Agard and S. B. Prusiner (2002). "Structural studies of the scrapie prion protein by electron crystallography." Proc Natl Acad Sci U S A **99**(6): 3563-3568.

Wille, H. and J. R. Requena (2018). "The Structure of PrP(Sc) Prions." Pathogens **7**(1).

Wille, H., M. Shanmugam, M. Murugesu, J. Ollesch, G. Stubbs, J. R. Long, J. G. Safar and S. B. Prusiner (2009). "Surface charge of polyoxometalates modulates polymerization of the scrapie prion protein." Proc Natl Acad Sci U S A **106**(10): 3740-3745.

Williams, E. S. and S. Young (1980). "Chronic wasting disease of captive mule deer: a spongiform encephalopathy." J Wildl Dis **16**(1): 89-98.

Won, S. Y., Y. C. Kim and B. H. Jeong (2020). "First Report of the Potential Bovine Spongiform Encephalopathy (BSE)-Related Somatic Mutation E211K of the Prion Protein Gene (PRNP) in Cattle." Int J Mol Sci **21**(12).

Wroe, S. J., S. Pal, D. Siddique, H. Hyare, R. Macfarlane, S. Joiner, J. M. Linehan, S. Brandner, J. D. Wadsworth, P. Hewitt and J. Collinge (2006). "Clinical presentation and pre-mortem diagnosis of variant Creutzfeldt-Jakob disease associated with blood transfusion: a case report." Lancet **368**(9552): 2061-2067.

Yoshimoto, J., T. Iinuma, N. Ishiguro, M. Horiuchi, M. Imamura and M. Shinagawa (1992). "Comparative sequence analysis and expression of bovine PrP gene in mouse L-929 cells." Virus Genes **6**(4): 343-356.

Zabel, M. D. and C. Reid (2015). "A brief history of prions." Pathog Dis **73**(9): ftv087.

Zahn, R., A. Liu, T. Luhrs, R. Riek, C. von Schroetter, F. Lopez Garcia, M. Billeter, L. Calzolai, G. Wider and K. Wuthrich (2000). "NMR solution structure of the human prion protein." Proc Natl Acad Sci U S A **97**(1): 145-150.

Zanusso, G., A. Farinazzo, F. Prelli, M. Fiorini, M. Gelati, S. Ferrari, P. G. Righetti, N. Rizzuto, B. Frangione and S. Monaco (2004). "Identification of distinct N-terminal truncated forms of prion protein in different Creutzfeldt-Jakob disease subtypes." J Biol Chem **279**(37): 38936-38942.

Zou, W. Q., S. Capellari, P. Parchi, M. S. Sy, P. Gambetti and S. G. Chen (2003). "Identification of novel proteinase K-resistant C-terminal fragments of PrP in Creutzfeldt-Jakob disease." J Biol Chem **278**(42): 40429-40436.

Zweckstetter, M., J. R. Requena and H. Wille (2017). "Elucidating the structure of an infectious protein." PLoS Pathog **13**(4): e1006229.

Appendix A

Purification of L-type bovine spongiform encephalopathy prions from transgenic mice brains using Pronase E

Introduction

Partial resistance of infectious prion proteins has been commonly used as a molecular diagnostic tool to distinguish infectious PrP^{Sc} from PrP^{C}. Of the different proteases used for this purpose, Pronase E (PE) is known to keep the full-length disease-causing prion protein (PrP^{Sc}) intact while removing cellular prion protein (PrP^{C}) (D'Castro, Wenborn et al. 2010). To preserve the full-length PrP^{Sc}, here we isolated L-type BSE prions from brains of transgenic mice that overexpress bovine prion protein (Tg4092) using Pronase E. The purification protocol included PTA precipitation and sucrose gradient centrifugation. Successful isolation of L-type BSE fibrils was confirmed using Western blot and electron microscopy negative stain experiments.

Material & Methods

Isolation of L-type BSE prions

Brains from terminally sick Tg4092 mice (Scott, Safar et al. 1997) were used to make 10% (w/v) brain homogenate in PBS. 500 µl aliquots of the brain homogenates were mixed with 100 µg/ml Pronase E (Sigma) and incubated for 30 minutes. The digestion reaction was stopped using 0.5 M EDTA pH 8.0 and 0.1 M PMSF. Next, the samples were incubated with 4% (w/v) Sarkosyl in PBS for 1 hour before adding Phosphotungstic acid (PTA). After one-hour incubation at 37 °C, the samples were centrifuged at 18,000 x g for 30 minutes, and the pellets were resuspended using 0.2% Sarkosyl in PBS. The resulting pellet sample (pellet 1) was then loaded onto a sucrose-step gradient of 40% and 80% sucrose and centrifuged at 115,000 × g at 4 °C for 16 hours. Finally, fractions A to G were collected from the centrifugation tube. Sample H (pellet wash) was obtained by washing the tube with 100 µl of sucrose buffer (10 mM Tris HCl pH 7,

1mM NaN_3, 0.2% Sarkosyl) to recover pelleted proteins. Samples were stored at -80 °C for immunoblotting and EM experiments.

Immunoblotting

Western blot and silver stain experiments were carried out according to a previous protocol (Chapter 2). D15.15 anti-PrP monoclonal antibody was used for immunodetection.

Negative staining

Negative stain electron microscopy was carried out as described previously (Chapter 2).

Results and Discussion

To detect PrP^{Sc} signals, samples obtained in different steps of the purification procedure were examined using Silver stain SDS PAGE and Western blot experiments. As presented in Figure A.1A, Western blot analysis using D15.15 anti-PrP monoclonal antibody detected PrP^{Sc} in the pellet 1 sample. WB of the sucrose gradient fractions utilizing D15.15 anti-PrP antibody indicated PrP^{Sc} signals in the top fractions, including fractions A-C and weak or faint bands in the middle to bottom fractions (D-G). The Pellet wash fraction (H) also presented PrP^{Sc} signals, which could be due to the combination of prion aggregates with PTA with a density of 1.4 g/ml (Levine, Stohr et al. 2015). It is noteworthy to mention that, compared to **the** sucrose gradient experiment of the PK-digested L-type BSE prions (Figure 2.1), which contained a stronger PrP 27-30 signals in the middle fraction, WB of the Pronase E-treated samples showed slightly higher intensity of PrP^{Sc} signal in the top fractions of the sucrose gradient tube. Consistent with the WB study, the Silver stain experiment of the purified L-type BSE samples showed a strong signal of the semi-pure pellet 1 sample (Figure A.1B).

To evaluate the presence of BSE fibrils, the brain-derived L-type BSE isolates were negatively stained using 2% uranyl acetate and examined with EM. EM analysis of the PE-purified L-type BSE samples revealed relatively long, unbranched fibrils (Figure A.2), similar to the fibrils from PK-digested L-type BSE samples (Figure 2.3) (Chapter 2). Both semi-purified pellet 1 and the final pellet from sucrose gradient centrifugation contained fibrils. The fibrils seemed to be thicker and fuzzier compared to the PK-digested L-type BSE fibrils, described in Chapter 2. In PE-treated L-type BSE purified sample we could discern single and two-protofilament L-type BSE fibrils with diameters of ~13 nm and ~30 nm, respectively.

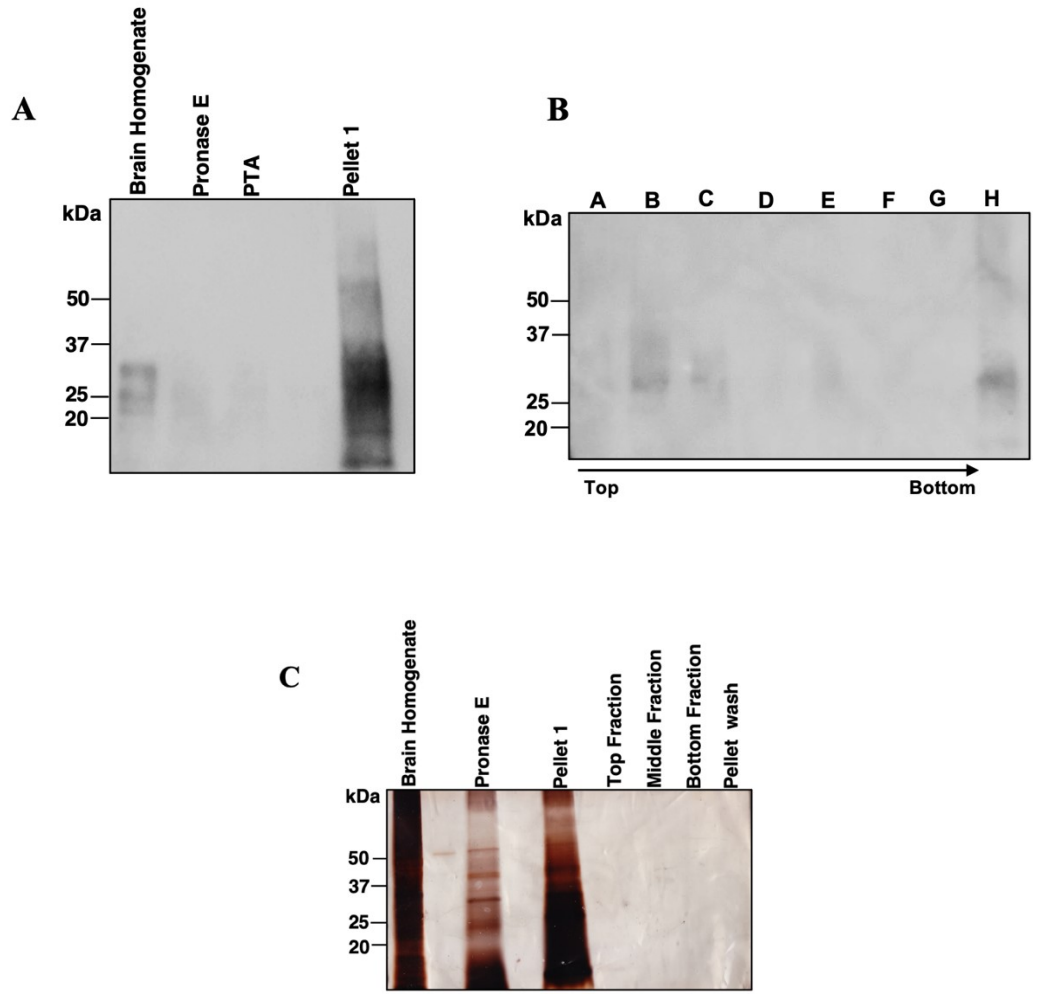

Figure A. 1 Biochemical characterization of L-type BSE prions purified using Pronase E. (**A**) Western blot of the L-type BSE prion samples isolated using PE and PTA. D15.15 anti-prion monoclonal antibody was used for immunodetection. Western blotting of the PE-digested pellet 1 revealed a strong PrP^{Sc} signal. (**B**) PE-treated semi-purified pellet 1 sample underwent two-step (40% and 80%) sucrose gradient ultracentrifugation. Lanes A to G represent fractions from the top to the bottom of the sucrose gradient tube. Lane H represents pellet wash fraction. The fractions obtained from the sucrose gradient tube were examined with Western blot using D15.15 antibody. The top fractions (A-C) and the pellet wash (H) sample showed stronger PrP^{Sc} signals comparing to the other fractions. (**C**) Silver stain SDS-PAGE gel of samples taken at different steps of the PTA purification.

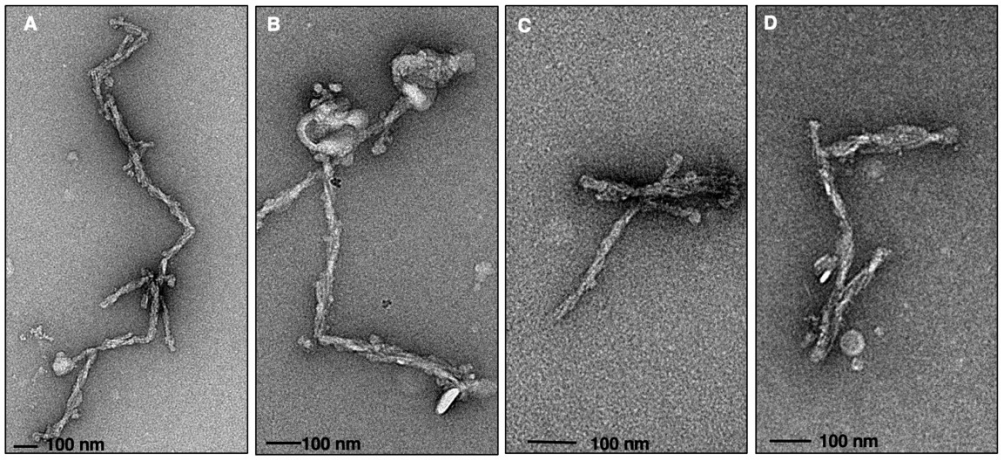

Figure A. 2 Electron microscopy micrographs of L-type BSE fibrils isolated using Pronase E treatment.

Negative staining of the L-type BSE samples, performed using 2% uranyl acetate, showed relatively long L-type BSE fibrils.

Bibliography:

D'Castro, L., A. Wenborn, N. Gros, S. Joiner, S. Cronier, J. Collinge and J. D. Wadsworth (2010). "Isolation of proteinase K-sensitive prions using pronase E and phosphotungstic acid." PLoS One **5**(12): e15679.

Levine, D. J., J. Stohr, L. E. Falese, J. Ollesch, H. Wille, S. B. Prusiner and J. R. Long (2015). "Mechanism of scrapie prion precipitation with phosphotungstate anions." ACS Chem Biol **10**(5): 1269-1277.

Scott, M. R., J. Safar, G. Telling, O. Nguyen, D. Groth, M. Torchia, R. Koehler, P. Tremblay, D. Walther, F. E. Cohen, S. J. DeArmond and S. B. Prusiner (1997). "Identification of a prion protein epitope modulating transmission of bovine spongiform encephalopathy prions to transgenic mice." Proc Natl Acad Sci U S A **94**(26): 14279-14284.